

# ABSTRACT

Title of Document: DEVELOPMENT, ENHANCEMENT, AND  
EVALUATION OF AIRCRAFT  
MEASUREMENT TECHNIQUES FOR  
CRITERIA AIR POLLUTANTS

Lacey Cluff Brent, Doctor of Philosophy, 2014

Directed By: Professor Russell R. Dickerson,  
Department of Atmospheric and Oceanic  
Sciences and Department of Chemistry and  
Biochemistry

The atmospheric contaminants most harmful to human health are designated Criteria Pollutants. To help Maryland attain the national ambient air quality standards (NAAQS) for Criteria Pollutants, and to improve our fundamental understanding of atmospheric chemistry, I conducted aircraft measurements in the Regional Atmospheric Measurement Modeling Prediction Program (RAMMPP). These data are used to evaluate model simulations and satellite observations. I developed techniques for improving airborne observation of two NAAQS pollutants, particulate matter (PM) and nitrogen dioxide (NO<sub>2</sub>). While structure and composition of organic aerosol are important for understanding PM formation, the molecular speciation of organic ambient aerosol remains largely unknown. The spatial distribution of reactive nitrogen is likewise poorly constrained. To examine water-soluble organic aerosol (WSOA) during an air pollution episode, I designed and implemented a

shrouded aerosol inlet system to collect PM onto quartz fiber filters from a Cessna 402 research aircraft. Inlet evaluation conducted during a side-by-side flight with the NASA P3 demonstrated agreement to within 30%. An ion chromatographic mass spectrometric method developed using the NIST Standard Reference Material (SRM) 1649b Urban Dust, as a surrogate material resulted in acidic class separation and resolution of at least 34 organic acids; detection limits approach pg/g concentrations. Analysis of aircraft filter samples resulted in detection of 8 inorganic species and 16 organic acids of which 12 were quantified. Aged, re-circulated metropolitan air showed a greater number of dicarboxylic acids compared to air recently transported from the west. While the NAAQS for NO<sub>2</sub> is rarely exceeded, it is a precursor molecule for ozone, America's most recalcitrant pollutant. Using cavity ringdown spectroscopy employing a light emitting diode (LED), I measured vertical profiles of NO<sub>2</sub> (surface to 2.5 km) west (upwind) of the Baltimore/Washington, area in the morning, and east (downwind) in the afternoon. Column contents (altitude integrals of concentration) were remarkably similar ( $\approx 3 \times 10^{15}$  molecules cm<sup>-2</sup>). These measurements indicate that NO<sub>2</sub> is widely distributed over the eastern US and help quantify the regional nature of smog events and prove extensive interstate transport of pollutants. These results were used to help shape air pollution control policy based on solid science.

DEVELOPMENT, ENHANCEMENT, AND EVALUATION OF AIRCRAFT  
MEASUREMENT TECHNIQUES FOR NATIONAL AMBIENT AIR QUALITY  
STANDARD CRITERIA POLLUTANTS

By

Lacey Cluff Brent

Dissertation submitted to the Faculty of the Graduate School of the  
University of Maryland, College Park, in partial fulfillment  
of the requirements for the degree of  
Doctor of Philosophy  
2014

Advisory Committee:  
Professor Russell R. Dickerson, Chair  
Professor Neil V. Blough  
Professor Michael R. Zachariah  
Doctor Lane C. Sander  
Doctor Jessica L. Reiner  
Professor Sheryl H. Ehrman, Dean's Representative

© Copyright by  
Lacey Cluff Brent  
2014

## Dedication

To Peter, because you are you!

## Acknowledgements

First, I'd like to acknowledge my advisor, Russell Dickerson. Thanks to the countless hours spent in the lab, at the white board, and reading (and re-reading) my material, I've become a fine Engineer. I have truly enjoyed my journey to becoming a scientist as a member of the RAMMPP program and I look forward to future collaboration as fellow scientists. From the University of Maryland I'd also like to acknowledge Jeff Stehr, the PI of the aircraft program, for always making time to teach, for answering the phone after business hours to answer questions when we got stuck in the lab, and for feeding both the mind and body by maintaining an endless supply of snacks at the airport. From UMD I'd like to thank my lab mates particularly, Patti Castellanos, Hao, He and Heather Arkinson with whom I worked closely and Allison Ring, Christina Liaskos, Dan Anderson, and Dan Goldberg. You've been a great group of people to work with.

As a teacher and a mentor, I'd also like to thank Bill Thorn from NIST who taught me all of the little things that a good laboratory scientist ought to know and for teaching me to slow down (a lot) to get the right answer the first time.

I'd like to especially acknowledge Tom Gorman from Tipton Airport Service and Bray Besse from the University Research Foundation for their help with the aerosol inlet installation. I appreciate you as both colleagues and friends.

I'd like to thank the wonderful team of people at NIST who provided invaluable mentorship and training throughout the years. Thanks to Lane Sander and Jessica Reiner for acting as members of my committee, for their input on my

experimental design and analysis, and for co-authoring papers with me. Thanks to Karen Phinney, who brought me in the door and provided me with the opportunity to obtain a Ph.D. under a student appointment at NIST. Thanks to Joe Conny who provided guidance, mentorship and equipment for making carbon measurements. Thanks to Jim Norris who taught me to better understand nuances in the calibration process and always made time for our instruments. I'd like to thank Katrice Lipka for always having her door open and being my "go to" person when professional (and sometimes personal) guidance was needed. I thank Dave Duewer who has read everything I've written and for making me a better, "NISTer" by teaching statistics and improving written communication. I'd like to thank my office mate Lyn Gameson, who politely tolerated my incessant muttering over data and formatting and answered countless random scientific questions on demand. Lastly, from NIST, I'd like to thank Frank Guenther for bringing me into the gas group and providing me with future opportunities at NIST.

I must also acknowledge my little sister, Lyette Brown, Wendy Young, and Nikki Schneck for their enduring friendship and for getting me through the last mile of the dissertation process. I thank my parents for their continued support over the years and for raising me to believe that I can do anything I put my mind to.

Without the input and support of the community of scientists around me, this work would never have been accomplished.

This research was supported by NIST, the Maryland Department of the Environment through the RAMMPP program, by the NASA DISCOVER-AQ program, and the NASA AURA Science Team and ACAST.

# Table of Contents

|   |      |
|---|------|
| Dedication .....  | ii   |
| Acknowledgements .....  | iii  |
| Table of Contents .....   | v    |
| List of Tables .....  | viii |
| List of Figures .....   | ix   |
| List of Abbreviations .....   | xi   |
| CHAPTER 1: OVERVIEW .....   | 1    |
| CHAPTER 2: BACKGROUND .....   | 6    |
| 2.1 Background part A, water soluble organic carbon aerosols .....                                    | 6    |
| 2.1.1 Introduction to organic aerosols .....  | 6    |
| 2.1.2 Health effects .....  | 10   |
| 2.1.3 Measurement approaches .....  | 11   |
| 2.1.4 Dissertation aerosol analysis objectives .....  | 17   |
| 2.2 Background part B, Introduction to inlet design for aircraft collection .....                     | 18   |
| 2.2.1 Introduction to aircraft aerosol inlets .....   | 18   |
| 2.2.2 Description of the Cessna 402 aerosol inlet .....   | 21   |
| 2.2.3 Dissertation aerosol inlet objectives .....   | 22   |
| 2.3 Background part C, Introduction to ambient NO <sub>2</sub> and NO <sub>2</sub> measurements ..... | 23   |
| CHAPTER 3: METHODS .....  | 24   |
| 3.1 Materials and methods part A, WSOC IC/MS/MS method development .....                              | 25   |
| 3.1.1 Chemicals .....   | 25   |
| 3.1.2 Sample collection and extraction .....  | 25   |
| 3.1.3 Standard solutions .....  | 26   |
| 3.1.4 Analysis .....  | 27   |
| 3.2 WSOC aircraft collection and analysis .....   | 29   |
| 3.2.1 In Situ optical and trace gas aircraft measurements .....                                       | 29   |
| 3.2.2 Filters .....   | 29   |
| 3.2.3 Calibration standards .....   | 31   |
| 3.2.4 Filter sample analysis .....  | 31   |
| 3.3 Materials and Methods part B, Inlet materials, design and comparison .....                        | 32   |



|  |    |
|--|----|
| 3.3.1 Materials.....   | 32 |
| 3.3.1.1 Hardware .....   | 32 |
| 3.3.1.2 Inlet and Tubing .....   | 32 |
| 3.3.1.3 Support .....  | 33 |
| 3.3.2 Installation configuration .....   | 33 |
| 3.3.3 Note on aircraft modification FAA regulations .....  | 34 |
| 3.3.4 Instruments .....  | 34 |
| 3.3.4.1 Light Scattering .....   | 34 |
| 3.3.4.2 Meteorological Data .....  | 35 |
| 3.3.4.3 Data processing .....  | 35 |
| <br>   |    |
| CHAPTER 4: RESULTS AND DISCUSSION (part A) on a method for characterization<br>of low molecular weight organic acids using IC/MS/MS.....           | 37 |
| 4.1 Introduction .....   | 37 |
| 4.2 Results and discussion .....   | 37 |
| 4.2.1 Optimization of separation conditions .....  | 37 |
| 4.2.2 Mass spectral identification of compounds .....  | 42 |
| 4.2.3 SRM 1649b .....  | 48 |
| 4.2.3.1 Qualitative analysis .....   | 50 |
| 4.2.3.2 Quantitative results .....   | 52 |
| 4.3 Conclusions .....  | 55 |
| <br>   |    |
| CHAPTER 5: RESULTS AND DISCUSSION (part A continued) on the correlation of<br>particulate matter size and density to aerosol composition .....     | 57 |
| 5.1 Introduction .....   | 57 |
| 5.1.1 Flight description and sampling conditions .....   | 58 |
| 5.2. Results .....   | 64 |
| 5.2.1 <i>In Situ</i> optical measurements.....   | 64 |
| 5.2.2 Filter sample analysis .....   | 68 |
| 5.3 Discussion .....   | 72 |
| 5.4 Conclusion .....   | 74 |
| <br>   |    |
| CHAPTER 6: RESULTS AND DISCUSSION (part B) on the evaluation of a newly<br>installed inlet for particulate matter sampling on the Cessna 402. .... | 76 |
| 6.1 Introduction .....   | 76 |
| 6.2 Results and discussion .....   | 77 |
| 6.2.1 Cessna 402 and P3-Binlet comparison.....   | 78 |
| 6.2.2 Cessna 402 and Piper Aztec inlet comparison .....  | 84 |
| 6.3 Conclusions .....  | 86 |

|  |     |
|--|-----|
| CHAPTER 7: Evaluation of the use of a commercially available cavity ringdown absorption spectrometer for measuring NO <sub>2</sub> in flight, and observations over the Mid-Atlantic States, during DISCOVER-AQ..... | 88  |
| 7.1 Abstract .....   | 88  |
| 7.2 Introduction .....   | 89  |
| 7.3 Instrument description and calibration methods .....   | 93  |
| 7.3.1 Cavity ringdown instrument description .....   | 93  |
| 7.3.2 Calibration procedures .....   | 96  |
| 7.3.2.1 Standard addition.....   | 96  |
| 7.3.2.2 Gas phase titration .....  | 99  |
| 7.3.3 Instruments used for flight intercomparison .....  | 100 |
| 7.3.3.1 Photolysis followed by chemiluminescence (P-CL) .....  | 100 |
| 7.3.3.2 Laser Induced Fluorescence .....   | 101 |
| 7.4 Aircraft and flight patterns .....   | 102 |
| 7.4.1 Side-by-side flight plan .....   | 102 |
| 7.4.2 Westerly transport flight plan.....  | 102 |
| 7.5 Results and Discussion.....  | 106 |
| 7.5.1 Calibration and stability .....  | 106 |
| 7.5.2 Detector limit, residence and response time.....   | 107 |
| 7.5.3 NASA P3-B and Cessna 402 side-by-side flight data comparison .....   | 108 |
| 7.5.4 Summary of summer 2011 NO <sub>2</sub> measurements .....  | 111 |
| 7.5.4.1 NO <sub>2</sub> column content .....   | 111 |
| 7.5.4.2 Regional observations .....  | 114 |
| 7.6 Conclusions .....  | 117 |
| CHAPTER 8: CONCLUSIONS .....   | 120 |
| CHAPTER 9: FUTURE WORK .....   | 123 |
| 9.1 Molecular characterization of particulate matter .....   | 123 |
| 9.2 Continued evaluation of the aerosol sampling system.....   | 125 |
| 9.3 Measurements of NO <sub>2</sub> by a commercially available CRD instrument .....   | 126 |
| Appendix.....  | 127 |
| Appendix A - Aerosol inlet and sampling specifications.....  | 127 |
| Appendix B - Aerosol inlet installation – Extended instructions and pictures ....  | 142 |
| Bibliography .....   | 150 |

## List of Tables

**Table 1.1** Relationship between NAAQS and AQI

**Table 2.1** A summary of suggested global SOA concentrations

**Table 2.2** Literature review of aerosol molecular species observations

**Table 4.1** Precursor and product ion MRM transitions monitored for the inorganic ions

**Table 4.2** Precursor and production ion MRM transitions monitored for the organic ions

**Table 4.3** Measurements of 6  $m/z$ s in SRM 1649b

**Table 5.1** Collection parameters and average meteorological conditions across the sampling region

**Table 5.2** *In situ* trace gas and aerosol size data

**Table 5.3** Molecular constituents of aerosol measured at 1 km over western Maryland on the third and sixth day of an air quality episode in July 2011

**Table 6.1** Description of NASA P3-B and UMD Cessna 402 sampling configurations

**Table 6.2** Ratios of  $\sigma_{sp}Ces/\sigma_{sp}P3-B$

**Table 7.1** Equations relating cavity ringdown extensive and intensive properties

**Table 7.2** Intercomparison instrument uncertainties and averaging times

**Table 7.3** RAMMPP AM/PM vertical profile information

**Table 7.4** Calibration curve data

**Table 7.5** A comparison between 1 s, 10 s, and 60 s NO<sub>2</sub> scatter plots

## List of Figures

**Figure 1.** Maryland PM<sub>2.5</sub> and O<sub>3</sub> air quality overview, 2007 to 2013

**Figure 2.1** Change in OC mass versus total aerosol mass with increasing altitude over the Atlantic Ocean

**Figure 2.2** Change in OC mass fraction as a function of altitude over two oceans

**Figure 2.3** Low turbulence inlet

**Figure 2.4** Community aerosol inlet

**Figure 2.5** Shrouded double diffuser inlet

**Figure 4.1** Chromatographic separations of 25 compounds

**Figure 4.2** Retention of organic and inorganic species

**Figure 4.3** Site of SRM 1649b collection in Washington D.C.

**Figure 4.4** Baghouses used for SRM 1649b Urban Dust collection

**Figure 4.5** MRM transitions for  $m/z$  191 in stock solution and SRM 1649b

**Figure 4.6** IC/QQQ analysis of acids selected for quantitation

**Figure 5.1** Flight tracks

**Figure 5.2** Vertical profiles of particle number density over Cumberland, MD, 2011

**Figure 5.3** NOAA HYSPLIT 24 hour forward and backward trajectories

**Figure 5.4** *in situ*, trace gas and particles measured across the collection period

**Figure 5.5** IC separation of aerosol collected onto filters during flight

**Figure 6.1** Piper Aztec roof mounted aerosol inlet

**Figure 6.2** Shrouded inlet diffuser on Cessna 402

**Figure 6.3** NASA P3-B and UMD Cessna 402 side-by-side aerosol inlet evaluation

**Figure 6.4** Plots of  $\sigma_{sp}CES/\sigma_{sp}P3B$  versus time

**Figure 6.5** Scattering comparison of aerosols sampled from the Cessna 402 and Piper Aztec

**Figure 6.6** Plots of  $\sigma_{sp}Ces/\sigma_{sp}Azt$  for each point in time

**Figure 7.1** RAMMPP westerly transport flight path and side-by-side flight tracks

**Figure 7.2** Results from the NIST calibration and periodic calibration verifications

**Figure 7.3** Side-by-side trace gas measurements

**Figure 7.4** Correlation plots between UMD, and P-CL and LIF from side-by-side flight

**Figure 7.5** Vertical variability of  $NO_2$  in BL and LFT reservoirs

**Figure 7.6** AM/PM  $NO_2$  quartile analysis

**Figure 7.7** Average vertical  $NO_2$  distribution for the metropolitan region

**Figure 7.8**  $NO_2$  hourly column content

## List of Abbreviations

|             |   |
|-------------|---|
| AGASP       | arctic gas and aerosol sampling program   |
| AMS         | aerosol mass spectrometer   |
| AQI         | air quality index   |
| BC          | black carbon  |
| BL          | boundary layer  |
| BRACE       | Bay Regional Atmospheric Chemistry Experiment   |
| CAA         | Clean Air Act   |
| CAI         | community aerosol inlet   |
| CARBIC      | civil aircraft for regular investigation of the atmosphere based on an instrument container |
| CD          | conductivity detection  |
| CIRPA       | center for Interdisciplinary Remotely Piloted Aircraft                                      |
| CMAQ        | chemical mechanism air quality  |
| CRD         | cavity ringdown   |
| DICE        | CD-8 Inlet Characterization Experiment  |
| DYCOMS      | dynamics and chemistry of the marine stratocumulus  |
| EC          | elemental carbon  |
| EPA         | environmental Protection Agency   |
| ESI         | electrospray ionization   |
| FIRE        | first ISCCP regional experiment   |
| FTIR        | Fourier transform infrared  |
| GCMS        | gas chromatography mass spectrometry  |
| GTE/ABLE 3A | global tropospheric experiment / arctic boundary layer expedition                           |
| HR          | high resolution   |
| IC          | ion chromatography  |
| INDOEX      | Indian Ocean Experiment   |
| LC          | liquid chromatography   |
| LCNMR       | liquid chromatography with nuclear magnetic resonance                                       |
| LCUV        | liquid chromatography with ultraviolet detection  |
| LFT         | lower free troposphere  |
| LTI         | low turbulence inlet  |
| MBL         | marine boundary layer   |
| MDE         | Maryland Department of Environment  |

|                   |  |
|-------------------|--|
| MS                | mass spectrometry  |
| NAAQS             | National Ambient Air Quality Standards                                   |
| NASA              | National Aviation and Space Administration                               |
| NCAR              | National Center for Atmospheric Research                                 |
| NIST              | National Institute of Standards and Technology                           |
| NMR               | nuclear magnetic resonance imaging                                       |
| OA                | organic aerosols   |
| OC                | organic carbon   |
| PAH               | polycyclic aromatic hydrocarbon  |
| PASIN             | particulate matter airborne sampling inlet experiment                    |
| PCB               | polychlorinated biphenyl   |
| PELTI             | passing efficiency of a low turbulence inlet                             |
| PILS-IC           | particle into liquid sampler-ion chromatography                          |
| PM                | particulate matter   |
| PM <sub>2.5</sub> | PM with aerodynamic diameters 2.5 µm or less                             |
| POA               | primary organic aerosol  |
| QQQ               | triple quadrupole MS mass analyzer<br>regional atmospheric measurements, |
| RAMMPP            | modeling and prediction program  |
| SD                | shrouded diffuser  |
| SIP               | state implementation plan  |
| SOA               | secondary organic aerosol  |
| SRM               | Standard Reference Material  |
| SRS               | self-regenerating suppressor   |
| SVOC              | semi-volatile organic compound<br>tropospheric aerosol radiative forcing |
| TARFOX            | observational experiment   |
| TOF               | time of flight   |
| UMD               | University of Maryland   |
| USG               | unhealthy for sensitive groups   |
| UV                | ultraviolet  |
| VOC               | volatile organic compound  |
| WSOC              | water soluble organic carbon   |

## CHAPTER 1: OVERVIEW

Energy and emissions related issues touch every facet of human existence. A major consideration in the evolution of U.S. national energy policy is the need to balance increasing emissions, resulting from growing economic demand, with the atmosphere's ability to counterbalance these emissions through positive and negative feedback loops. To assess emission's impact, well-characterized measurement tools are needed to accurately characterize and quantify changes in the Earth's atmosphere and then relate those observations to emissions inventories. The Regional Atmospheric Measurement, Modeling and Prediction Program (RAMMPP) employs optical methods for the observation of national ambient air quality standard (NAAQS) criteria pollutants for the state of Maryland [[P Castellanos et al., 2011](#); [Hains et al., 2007](#); [Hains et al., 2008a](#); [Marufu et al., 2004](#); [2005](#); [Taubman B.F., 2004](#); [B. F. Taubman, 2004](#); [B. F. Taubman et al., 2006](#); [B. F. Taubman et al., 2004a](#); [B. F. Taubman et al., 2004b](#); [Thompson et al., 2007](#); [Vant-Hull et al., 2005](#)]. Discussed in this work are measurement techniques added to the RAMMPP platform effectively enhancing RAMMPP measurement and modeling capabilities.

The NAAQS, directed by the Environmental Protection Agency (EPA), are authorized by the Federal Clean Air Act (CAA) originally enacted in 1970 [[Clean Air Act, 1970](#)]. This act requires the EPA to regulate pollutants that are both ubiquitous across the United States and known to harm human health. Areas not in compliance with the NAAQS are designated as areas of nonattainment and must develop state implementation plans (SIP) detailing how compliance with the federal regulation will be



achieved. A challenge to policy makers in the northeastern U.S. is the regional (multi-state) nature of air pollution episodes. The CAA designates a good neighbor provision requiring SIPs to prohibit emissions that significantly contribute to the nonattainment of downwind states (42.U.S.C. 7410(a)(s)(D)(i)(I)). Attempts to equally distribute multiple upwind emitter responsibilities make this provision difficult to regulate [[Hubertz, 2013](#)]. EPA attempts to regulate the good neighbor provision by the Cross-State Air Pollution Rule have resulted in a Supreme Court level dispute [, 2014 #643].

Since the 1980s, violations of NAAQS pollutants PM<sub>2.5</sub> and ozone have decreased remarkably [[H. He et al., 2013b](#)]. The number of Maryland PM<sub>2.5</sub> and ozone exceedance days since 2007 is shown in Figure 1.1A. The snapshot of exceedances is limited to the last five years because it is more reflective of current considerations. Since 2007, PM<sub>2.5</sub> has steadily declined, including a year with only one exceedance day. The recent annual ozone trend, on the other hand, is more complicated due to its dependence on precursor molecule transport [[P Castellanos, Ehrman, S.H., Dickerson, R.R., Stehr, J.W., 2009](#); [H. He et al., 2013b](#)]. Tropospheric ozone is a secondary pollutant whose accumulation is a function of both current meteorological conditions and the availability of chemical precursors. Ozone abundance depends on temperature, sunlight and the availability of NO<sub>2</sub> and hydrocarbons [[EPA, 2006; 2013](#)][[Kleinman et al., 2005](#)]. While Figure 1.1A reflects NAAQS exceedances, it does not fully capture an overall, generalized assessment of local air quality. To assess air quality, days are labeled according to the air quality index (AQI). Days coded orange are designated as unhealthy for sensitive groups (USG). Code orange (as shown in Figure 1.1A) is assigned whenever just one of the six criteria pollutants exceeds the NAAQS. Drivers for code orange days in the state of Maryland

are O<sub>3</sub> and PM<sub>2.5</sub>. Table 1.1 shows the relationship between the color coded Air Quality Index and ambient 8 and 24-hour average O<sub>3</sub> and PM<sub>2.5</sub> levels. Figure 1.1B shows that the number of O<sub>3</sub> days in the moderate (or code yellow) range is similar to the number of ozone exceedance (orange) days. When comparing PM<sub>2.5</sub> between Figures 1A and 1B we see that while very few exceedances occurred there are many days with PM<sub>2.5</sub> in the moderate range. Maryland air quality is code green or “good” approximately half of the year. For the other half of the year, local air quality is only moderate with a few USG days. Although the number of NAAQS exceedances is decreasing, Maryland air quality can still be improved.

Local air quality can be partially understood through comparison of surface monitoring to inventoried local emissions, but this understanding remains limited without also including the contributions of regional emissions transported to a local area [[Hains et al., 2008b](#)]. The ability to estimate the additional impact of regional emissions on local air quality is necessary for the development of policy that effectively limits adverse human health, maintains visibility allowing transport for commerce, and limits contributions to global radiative forcing. As the primary transportation and industrial fuel sources change, both nationally and globally, so will the resulting emissions. The conceptual framework of models used to manage air quality must be capable of capturing the impacts of these changes. This can be achieved only with a thorough understanding of the source, fate and transport of atmospheric pollutants. This dissertation presents a combination of techniques developed, enhanced, and/or validated for the improvement of airborne data measurements of NAAQS criteria pollutants and pollutant production pathways for PM<sub>2.5</sub>, NO<sub>2</sub>, and O<sub>3</sub>.

After a background in chapter 2 and a description of methods in chapter 3, chapter 4 presents the results of the IC-MS/MS method I developed at NIST using SRM 1649b Urban Dust. Presented in chapter 5 is the application of the IC-MS/MS method to samples of ambient particulate matter collected onto quartz fiber filters during a flight beginning near Baltimore to western Maryland. Chapter 6 contains information on the aerosol inlet installation and shows the results of aerosol scattering data from a side-by-side flight with the NASA P3. Lastly, Chapter seven reports the modifications made to a commercially available cavity ringdown spectrometer and discusses regional NO<sub>2</sub> measurements made upwind and downwind of the Baltimore / Washington D.C. metropolitan area.

*Table 1.1. Relationship between NAAQS and AQI*

| Category                                    | O <sub>3</sub> 8-hr avg (ppb) | PM <sub>2.5</sub> 24-hr avg (µg/m <sup>3</sup> ) |
|---|-------------------------------|--|
| <b>Good</b>                                 | 0-59                          | 0-12.0   |
| <b>Moderate</b>                             | 60-75                         | 12.1-35.4  |
| <b>Unhealthy for sensitive groups (USG)</b> | 76-95                         | 35.5-55.4  |
| <b>Unhealthy</b>                            | 96-115                        | 55.5-150.4                                       |
| <b>Very unhealthy</b>                       | 116-374                       | 150.5-250.4                                      |
| <b>hazardous</b>                            | ≥ 375                         | ≥ 250.4  |

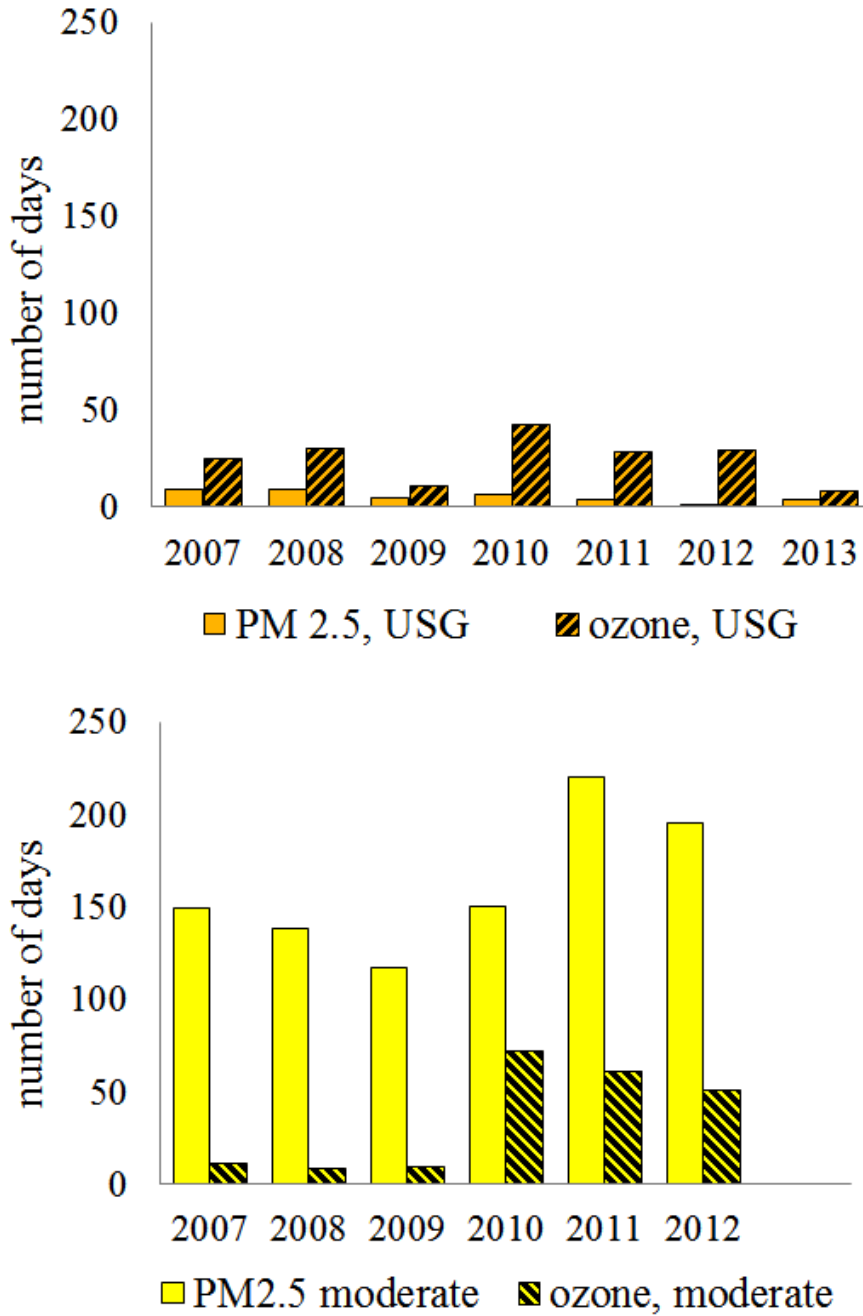


*Figure 1.1 Maryland O<sub>3</sub> and PM<sub>2.5</sub> air quality indicators Figure 1.1A Number of USG days due to NAAQS exceedances PM<sub>2.5</sub> and O<sub>3</sub>. Figure 1.1B Number of moderate air quality days.*

## CHAPTER 2: BACKGROUND

### 2.1 Background part A, water soluble organic carbon aerosols

#### 2.1.1 Introduction to organic aerosols

Knowledge of aerosol concentrations, mechanisms of formation, and the ability to model their fate and transport are important for determining aerosol effects on human health and their role in the environment. Organic aerosols (OA) are a significant component of atmospheric aerosols but their origin, mechanisms of formation, and fate are poorly understood [[Henze and Seinfeld, 2006](#); [Jacobson et al., 2000](#); [Maria et al., 2004](#); [Robinson et al., 2007](#)]). Aerosols, defined as solid or liquid particles suspended in a gas [[Hinds, 1999](#)], are composed of a variety of substances from a variety of sources.

To study aerosols, they are typically broken down into various categories such as:

1. Fog, haze, cloud, dust, smog, and fumes [[Hinds, 1999](#)]
2. Anthropogenic, biogenic, and marine [[Carlton et al., 2007](#)]
3. Primary vs. secondary [[Claeys, 2004](#)]
4. Carbonaceous or inorganic [[Novakov et al., 1997](#)]
5. Optical properties such as absorber or scatterer of solar radiation [[Claeys, 2004](#)]

The focus of this research is on the carbonaceous category of aerosols, and narrowed further to the polar, oxidized fraction.

Although aerosols can be broken down by various sources, their route into the atmosphere must always fall into either the primary aerosol or secondary aerosol category. Primary aerosols are emitted directly into the atmosphere while secondary

aerosols are formed *in situ*. The contributions to each fraction will be a result of the local precursor sources and the current meteorological conditions [[Blando et al., 1998](#); [Chang, 2005](#); [Jacobson et al., 2000](#); [Maria et al., 2004](#)].

As early as 1972, it was thought that the primary component contains mainly alkanes, polycyclic aromatics, and substituted phenols, while the secondary component contains acids, aldehydes, alcohols, chlorides and nitrates [[Schuetzle, 1975](#)]. Typical sources of primary organic aerosols (POA) are internal combustion engines, fires, and mineral dust [[Maria et al., 2004](#); [Robinson et al., 2007](#)]. Attempts to quantify POA emitted from combustion engines are conducted through emission inventories of fossil fuel supply and consumption. Emissions due to biomass burning, on the other hand, can be complex due to the variety of sources (rainforest vs. grasslands) and local conditions [[Jacobson et al., 2000](#)].

Secondary Organic Aerosols (SOA) are atmospheric particles formed *in situ* through the photooxidation of volatile and semivolatile organic (VOC, SVOC) species yielding oxygenated and nitrated compounds that condense into new particles, condense onto existing particles, or adsorb onto existing particles [[Baron, 2005](#); [Librando and Tringali, 2005](#); [Turpin et al., 2000](#)]. The dominant source of SOA is the vegetative emission of isoprene, the base molecular unit of terpenes, monoterpenes and sesquiterpenes. Still, anthropogenic sources are indicated by observation of molecular products resultant of gas-phase photochemical reactions between hydrocarbons, ozone, and oxides of nitrogen suggesting that these sources are significant [[Baron, 2005](#); [Forstner et al., 1997](#); [Inuma, 2004](#); [Librando and Tringali, 2005](#); [Seinfeld, 2006](#)]. The principal anthropogenic precursors to atmospheric SOA concentrations are aromatic hydrocarbons, alkanes, and

alkenes with at least seven carbons, carbonyls and sulfates emitted into the troposphere from diesel exhaust, jet aircraft, gasoline vapors, and power plant emissions [[Odum et al., 1997](#); [Seinfeld, 2006](#)]. Table 2.1, a summary of model estimated global SOA concentrations, demonstrates that global concentrations are a widely debated topic. The global impact of SOA with regard to health and climate is, likewise, largely unknown. Table 2.2 provides a brief list of aerosol molecular species reported in the literature. A review of chemical structures and the laboratory techniques used to report these compounds was used to determine the aerosol fraction chosen to be the focus of this research. Because many reports useful for targeting the nonpolar fraction present in primary and/or newly formed SOA already exist [[Forstner et al., 1997](#); [Kawamura et al., 1985](#); [Nocun and Schantz, 2013](#)], I chose to focus on the less well-understood fraction of aged, water-soluble organic aerosols. The need for enhancement of methods used to identify the less well-understood molecular species comprising SOA aligns well with RAMMPP priorities of studying atmospheric composition and the fate of transport of pollutants.

**Table 2.1** A summary of estimated global SOA emissions

| Compounds   | Concentration (Tg C yr <sup>-1</sup> ) | Reference                    |
|---|--|------------------------------|
| Biogenic SOAs   | 13-24                                  | Griffin et al., 1999         |
| Biogenic SOAs   | 270                                    | Andrea, Crutzen et al., 1997 |
| Global biogenic emissions                               | 491 – 1150                             | Guenther et al., 1995        |
| Annual biogenic SOA formation                           | 61-79                                  | Kanakidou et al 2000         |
| VOCs isoprene and terpenes                              | 12-70                                  | Kanakidou et al., 2005       |
| Isoprene  | 2                                      | Claeys et al., 2004          |
| Isoprene  | ~500                                   | Guenther et al., 1995        |
| Isoprene  | 10-120                                 | Matsunaga et al., 2005       |
| SOA formation by cloud processing of isoprene oxidation | 1.6                                    | Lim et al., 2005             |
| Terpenes  | 725                                    | Lathi re et al., 2006        |

**Table 2.2** Literature review of aerosol molecular species observations

| Product                         | Precursor  | Mechanistic route to becoming a SOA                              | Primary or secondary | Location observed           | ref                     |
|---------------------------------|--|--|----------------------|-----------------------------|-------------------------|
| Methyl-tetrol                   | Isoprene   | Gas to particle conversion, condensation onto existing particles | 2°                   | Amazon                      | Claeys 2004             |
| Methyl-glyceric acid            | Isoprene   | Photochemical oxidation  | 2°                   | Smog chamber, NC, MD, PA    | Edney 2005              |
| Methyl-gloxal                   | Isoprene   | Photochemical oxidation  | 2°                   | Smog chamber                | Carlton 2006            |
| Pyruvic acid                    | methylglyoxal  | Photochemical oxidation  | 2°                   | Smog chamber                | Carlton 2006            |
| Oxalic acid                     | Pyruvic acid   | Photochemical oxidation  | 2°                   | Smog chamber                | Carlton 2006            |
| Tartaric acid                   | Fatty acids, <i>n</i> -alkanes emitted by biogenic sources | Photochemical oxidation  | 2°                   | Amazon                      | Claeys 2004             |
| Malic acid                      | Fatty acids, <i>n</i> -alkanes emitted by biogenic sources | Photochemical oxidation  | 2°                   | Amazon                      | Claeys 2004             |
| Hydroxy-glutaric acid           | Fatty acids, <i>n</i> -alkanes emitted by biogenic sources | Photochemical oxidation  | 2°                   | Amazon                      | Claeys 2004, Stone 2009 |
| Levo-glucosan                   | Biomass  | Burning  | 1°                   | Amazon                      | Claeys 2004, Stone 2009 |
| Arabitol                        | Biomass, fungal spores                                     | Biomass burning  | 1°                   | Amazon                      | Claeys 2004             |
| Manitol                         | Biomass, fungal spores                                     | Biomass burning  | 1°                   | Amazon                      | Claeys 2004             |
| glucose                         | biomass pollen   | Biomass burning  | 1°                   | Amazon                      | Claeys 2004             |
| Methoxy phenols                 | Lignin (guaiacyl compounds)                                | Burning of soft wood   | 1°                   | Laboratory, controlled burn | Hoffmann 2007           |
|                                 | Vanillin   | Oxidation  | 2°                   |                             |                         |
| 4-hydroxy-3,5-dimethoxy-phenols | Lignin (syringyl compounds)                                | Burning of hard wood   | 1°                   |                             |                         |



|                             |   |                         |    |                             |                               |
|-----------------------------|---|-------------------------|----|-----------------------------|-------------------------------|
| 4-hydroxy-cinnamic acid     | Savannah grass                                  | Burning                 |    | Laboratory, controlled burn | Hoffmann 2007                 |
| Methyl-glyoxal              | Polluted fox                                    |                         |    |                             | Chang 2005                    |
| Lactate                     | Biomass   | Burning                 |    | Greenland                   | Jaffrezo 1998                 |
| Glyoxalate / glyoxalic acid | Biomass<br>Pyruvic acid                         | OH                      | 2° | Greenland<br>Glass vessel   | Jaffrezo 1998<br>Carlton 2006 |
| Azaleic acid                | Unsaturated fatty acid with double bond and C-9 | Photochemical oxidation | 2° | Antarctic                   | Kawamura 1996                 |
| Glutaric acid               | Cyclohexene                                     | Ozonolysis in the dark  |    | Smog chamber                | Hamilton 2006                 |

This table is a summary of aerosols that have been identified in different locations. Stars mean the compound is considered a molecular marker. Some of the compounds have been collected onto filters at various locations around the globe and some have been produced in smog chamber experiments.

### 2.1.2 Health effects

Clinical studies have shown that exposure to particulate matter and particularly the fraction with aerodynamic diameters  $\leq 2.5 \mu\text{m}$  ( $\text{PM}_{2.5}$ ) can be linked to lung cancer and cardiopulmonary mortality [[Brook et al., 2010](#); [C A Pope, Burnett, R., Thun, M., Calle, E., Krewski, D., Ito, K., Thurston, G., 2002](#); [Samet, 2000](#)]. Pope *et al.* analyzed statistics compiled in a national database and saw a correlation between fine particulate air pollution and incidence of lung cancer and heart disease in urban areas [[C A Pope et al., 1995](#)]. Fine particulate matter is also thought to play a role in child mortality in India where an estimated 270,000 children under age 5 die each year of acute respiratory infections caused by particulate air pollution [[Hansen and Sato, 2001](#); [Smith, 2000](#)]. The ease with which aerosols can enter the blood stream or interact with lung tissue is evidenced by the fact that this is also a common method employed for drug delivery.

Baron and Willeke point out that, “To estimate the toxicity of an aerosol entering the lung, one need know the size-dependent diffusion, gravitational settling, impaction, and interception properties of the particles to determine the deposition rate within the lung. In addition, the chemistry, surface area, and fibrosity of the particle may indicate their interactions with the lung tissues once they are deposited,” [\[Baron, 2005\]](#). The impact of PM<sub>2.5</sub> on respiratory health across a region cannot be fully realized until the molecular structure of the species composing PM<sub>2.5</sub> is known.

Two organic aerosols, polycyclic aromatic hydrocarbons (PAHs) and polychlorinated biphenyls (PCBs) exist in a variety of terrestrial matrices. Dispersed most often as pesticides, evidence of their fate and widespread transport was observed when they were discovered in the tissue of arctic animals [\[Hinckley et al., 1991\]](#). The presence of molecules belonging to these molecular classes have been certified in the National Institute of Standards and Technology (NIST) Standard Reference Material (SRM) 1649b Urban Dust (a 12+ month collection of PM in Washington, D.C.) and are a wide area of concern for indoor pollution [SRM Cert, \[Rudel, 2003\]](#). Unlike the situation with PAHs and PCBs, much less is known about emission sources, molecular structure, or the fate and transport of anthropogenic, polar organic compounds [\[Patton et al., 1991\]](#).

### 2.1.3 Measurement approaches

Aerosol composition, number concentration and optical properties play an important role in air quality and pollution events [\[Anderson et al., 2003; Bates et al., 1998; Petzold et al., 2002\]](#). Instrument requirements plus sample preparation and processing pose significant challenges to both field and laboratory methods for molecular

determination. Numerical simulations of atmospheric behavior are designed to overcome the impossibility of knowing the chemical composition and physical properties for individual aerosols. By the computational approach, challenges to including chemical and physical properties specific to individual aerosol masses are overcome by applying well-known chemical and physical phenomena in an effort to predict the amounts and effects of aerosol bulk properties [[Donahue et al., 2013](#); [Hänel, 1976](#); [Henze and Seinfeld, 2006](#); [Maria et al., 2004](#)]. Experimental approaches include optical methods for measuring the extensive properties used to derive aerosol intensive properties [[Anderson et al., 2003](#); [Bahreini et al., 2003](#); [Gassó, 2000](#); [Heintzenberg, 2006](#); [Öström, 2000](#)]. The bulk atmospheric properties derived from sizing, absorption, and scattering measurements are hemispheric backscatter, single scattering albedo, aerosol optical depth and Ångström exponent. The ability to predict these features based on shifting meteorological and chemical conditions is constantly being evaluated by modelers, and is important to successful remote sensing from ground and space [[Clarisse et al., 2013](#); [Gassó, 2000](#); [Hoff, 2009](#); [Levy et al., 2013](#); [Levy et al., 2005](#); [Remer et al., 2005](#); [P J Sheridan et al., 2012](#); [Yoon et al., 2012](#)].

Routine monitoring of PM chemical composition typically includes analysis of organic carbon (OC), black carbon (BC) also called elemental carbon (EC) and inorganic salts. Analytical techniques such as Fourier transform infrared spectroscopy (FTIR), liquid chromatography with ultraviolet detection (LCUV) or nuclear magnetic resonance (LCNMR), and aerosol mass spectrometry (AMS) measurements have independently indicated at different locations around the globe that water soluble organic carbon (WSOC) is often dominated by the presence of carboxylic acids [[Chang, 2005](#); [Decesari](#)

[et al., 2001](#); [Jimenez et al., 2009](#); [Russell et al., 2011](#); [Topping D., 2004](#)]. Compositional analysis by these methods frequently ends with bulk property characterization.

The last decade has produced numerous improvements in methods and instruments allowing for more specific measurements of molecular constituents. Field sampling techniques analyze the end state of aerosol atmospheric processing while smog chamber experiments are useful for following specific reaction pathways. Study of molecular composition is often divided into molecular classes based on polarity. Gas chromatography coupled to mass spectrometry detection (GCMS) methods have demonstrated reliable structural identification of water insoluble aromatic compounds and soluble hydroxylated and alkoxyated aliphatic compounds [[Carvalho et al., 2003](#); [Kleindienst et al., 2009](#); [Nocun and Schantz, 2013](#); [Schantz et al., 2012](#)]. GCMS has also been used for the molecular determination of organic acids, but the procedure requires labor intensive derivitization [[Balducci, 2010](#); [Kawamura et al., 2012](#)].

Numerous LC and LCMS methods have been used for WSOC characterization in both smog chamber and field experiments. A LC method developed by Decesari et al., (2000) used anion exchange chromatography to separate water soluble filter sample extract into classes of neutral compounds, combined mono- and dicarboxylates, and lastly polycarboxylates. Structural determination was performed by NMR. Chang et al (2005) applied Decesari's LCNMR method to aerosol in mountainous and desert locations using a similar anion exchange chromatography separation method. In the latter case molecular assignment was performed by retention time and comparison to standards using UV detection [[Chang, 2005](#)]. Ion chromatographic (IC) methods are most often limited to measurements of inorganic ions and the simplest diacid, oxalic acid, but have also been

used to suggest the presence of mono- and dicarboxylates in Brazil, Taiwan and Germany [[Domingos et al., 2012](#); [Rohrl and Lammel, 2002](#); [Tsai, 2008](#)]. Confirmation of organic acids by IC with conductivity detection (CD) can only be tentative because of the inability to determine coeluting compounds [[Fisseha et al., 2004](#)]. Procedures to elucidate the molecular composition of ambient aerosol have accounted for only 5 to 30% of the total organic aerosol mass indicating that this effort still requires much method development [[Forstner et al., 1997](#); [Rogge et al., 1993](#)].

The greatest advances in chemical characterization have been achieved through developments in MS, particularly with respect to sources for sample ionization and mass analyzer accuracy and resolution. MS techniques for characterizing aerosol content break down into two main categories, elemental analysis and molecular characterization. MS used for *in situ* continuous monitoring targets elemental and small molecule analysis. *In situ* AMSs frequently use laser ablation or electron impact sources to estimate oxygen, carbon, hydrogen, nitrogen and sulfur, the ratios of which are used to predict the likelihood of molecular saturation and water solubility [[Topping D., 2004](#)]. These instruments are typically coupled with a laser for submicrometer particle sizing. More recent advances have led to high resolution (HR) MS. High resolution aerosol time of flight aerosol mass spectrometers (HR-TOF-AMS) are capable of distinguishing organic from inorganic ions of the same nominal mass and of predicting the number of rings and double bonds associated with a mass fragment [[DeCarlo et al., 2006](#)].

Analysis targeted for the molecular determination of small, polar molecules has largely shifted to LC electrospray ionization mass spectrometry (ESI-MS) [[Hamilton et al., 2008](#); [Winterhalter, 2003](#); [Wozniak et al., 2008](#)]. ESI has the advantage of being

compatible with polar mobile phases and soft ionization leaving a largely intact molecular ion as the dominant ionization product. A high-resolution instrument for laboratory use is the electrospray ionization Fourier transform ion cyclotron resonance mass spectrometer. With the advantage of soft ionization, this instrument has been used to characterize the bulk properties of intact SOA species in filter extract in the Northeast and from smog chambers [[Bateman et al., 2010](#); [Surratt et al., 2007](#); [Wozniak et al., 2008](#)]. Ultimate determination of the molecular structures composing an aerosol mass relies upon reference against known standards. Preceding MS analysis with chromatographic separation adds a dimension to molecular confirmation through assignment of retention time based on molecular properties such as size, polarity and charge.

In this work, molecular determination of water soluble organic aerosol against known standards is accomplished using IC-ESI/MS/MS. The mass analyzer is a triple quadrupole (QQQ). Instances of incomplete chromatographic resolution are overcome through mass selective ion monitoring. Tables 2.1 and 2.2 above show a collection of published information regarding organic carbon content in aerosol masses at different locations around the globe. While carbonaceous aerosols may not always be the dominant fraction in the boundary layer, aircraft data shown in Figures 2.1 and 2.2 show that the fraction of their contribution to the total aerosol mass increases with altitude. The fractional increase with altitude shows the importance of carbonaceous aerosol with challenges related to transport and regional air quality questions.

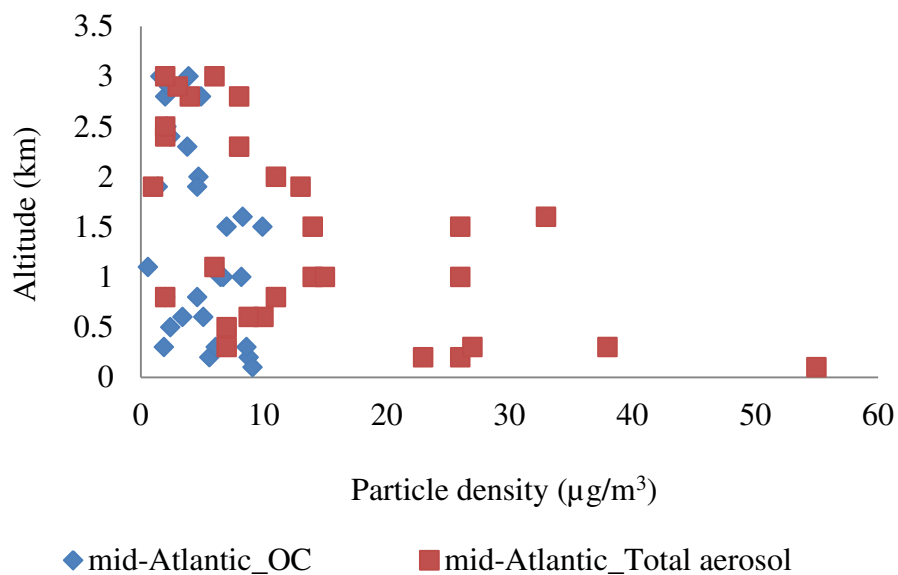


**Figure 2.1** Change in organic carbon mass versus total aerosol mass with increasing altitude During TARFOX aerosol samples were collected over the mid-Atlantic off the coast of Virginia. The density of total aerosol decreased with altitude, but the fraction of organic aerosol particles did not change proportionately. TARFOX is the tropospheric aerosol radiative forcing observational experiment targeting in situ measurements of marine aerosol influenced with continental air over the mid-Atlantic Ocean [\[Novakov et al., 1997\]](#)

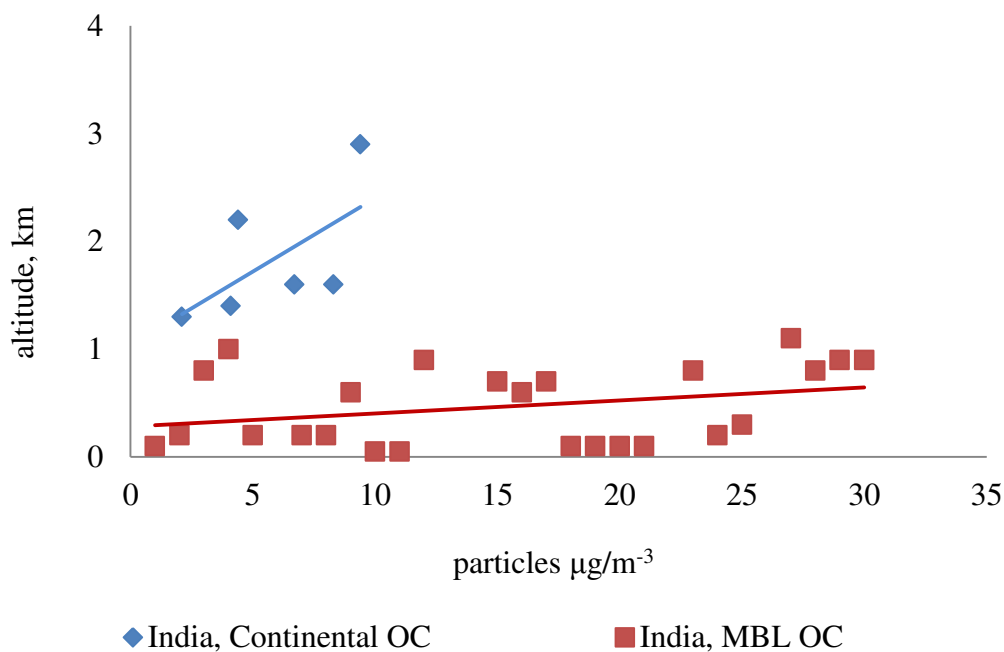


**Figure 2.2** Change in OC mass fraction as a function of altitude over the Indian peninsula and the Indian Ocean. Over Indian land and the Indian Ocean the OC particle mass per volume air increased. Sulfate concentration decreased slightly with altitude over the Indian Ocean [Mayol-Bracero et al., 2002; Novakov et al., 1997]

#### 2.1.4 Dissertation aerosol analysis objectives

Routine, light aircraft monitoring as conducted under RAMMPP, a joint University of Maryland (UMD) and the Maryland Department of Environment (MDE) program, provides insight into photochemical processing with altitude, and chemical behavior in two different reservoirs. In this collaborative research project involving the UMD, MDE and NIST, I present results of aerosols collected onto quartz fiber filters through a shrouded inlet diffuser on board a Cessna 402 at ~ 1 km altitude. Collection occurred on the peak day and dissipation day of an air quality episode. All laboratory work was conducted at the NIST. This work demonstrates application of an IC/MS/MS method suitable for routine quantitative and qualitative aerosol molecular determination.



Also shown in this work is an observed correlation between particle size and chemical composition with respect to air mass.

## 2.2 Background part B, Introduction to inlet design for aircraft collection

### 2.2.1 Introduction to aircraft aerosol inlets

Before addressing the effects of OA on human health and global climate it is necessary to first tackle the challenge of efficient aerosol collection on an aircraft platform. A major measurement challenge involves efficient sampling of particles collected with high speed intake. Particles collected at flows of 50-200 m/s must be slowed to a few meters per second to match the sampling flow rate capability of the instruments or filter packs [[Huebert et al., 2004](#)]. In a review by N.A. Fuchs, 1975, general conditions for aerosol sampling observed during the preceding decades were summarized and published [[Fuchs, 1975](#)]. Over time and with further sampling experience these conditions have been adapted to high speed sampling from aircraft and have evolved into general aircraft sampling guidelines recognized and followed by many. These guidelines were summarized by Huebert *et. al.* in 1990 and again by Bloomquist *et. al.* in 2001 [[Blomquist et al., 2001](#); [Huebert et al., 1990](#)]. The guidelines state that:

1. Inlet positioning should be outside of the boundary layer of the plane
2. Inlet positioning should be isoaxial to the streamlined flow of air around the plane
3. Sampling should be isokinetic; the velocity of particle flow into the inlet should match the true air speed.

Over the years, a variety of inlet designs (sharp edges [[Jonsson, 1995](#)], blunt edges [[P J Sheridan and Zoller, 1989](#)], thin walls [[Andrea, 1998; Talbot et al., 1992](#)]) have been evaluated for their sampling efficiency in ducts and aircraft platforms. Experimental observations have demonstrated that shrouding an inner diffuser enhances isokinetic sampling by reducing particle flow velocity from the true air speed of the aircraft to a velocity more reasonable for sampling prior to entry of the inner sampling tip [[Torgeson, 1996](#)]. Collection of air within the shrouded volume is also thought to help compensate for imperfect isoaxial alignment making particle collection less sensitive to changes in aircraft speed, altitude, and fuel load [[Mcfarland et al., 1989; Torgeson, 1996](#)]. The open shroud surrounding the inner inlet implemented by Antony Clark, has the added effect of making the air flow more laminar as it enters the inlet tip [[Huebert et al., 2004](#)].

Sampling efficiency, as described by [[Huebert et al., 1990](#)] refers to the ratio of particles effectively sampled with respect to the ambient concentration and is a product of the inlets aspiration efficiency (isokinesis), passing efficiency at the inlet tip, and transmission efficiency of the particles to the measuring or collection device. Evaluations of Clark's shrouded NASA diffuser during field experiments DICE and PELTI [[Huebert et al., 2004; McNaughton et al., 2007](#)] indicate a 50% passing efficiency for 3-4  $\mu\text{m}$  particles over the dry desert with decreasing passing efficiency in a marine environment. This inlet was observed to outperform the low turbulence inlet (Figure 2.3) and inlets with solid conical diffusers (Figure 2.4) (i.e., the community aerosol inlet) on planes flying at speeds and altitudes similar to the UMD Cessna 402 research platform. Some sampling platforms positioned the inlet forward of the aircraft

nose such as the CIRPAS Twin Otter conical double diffuser (Figure 2.5) [Hegg et al., 2005] and the NCAR C-130 community aerosol inlet (Figure 2.3) with a triple diffuser [Blomquist et al., 2001]. An advantage to this configuration is the long straight distance provided for deceleration of particles before reaching the optical instruments. Bends in the tubing should be kept to a minimum to reduce opportunity for losses due to inertial impact.

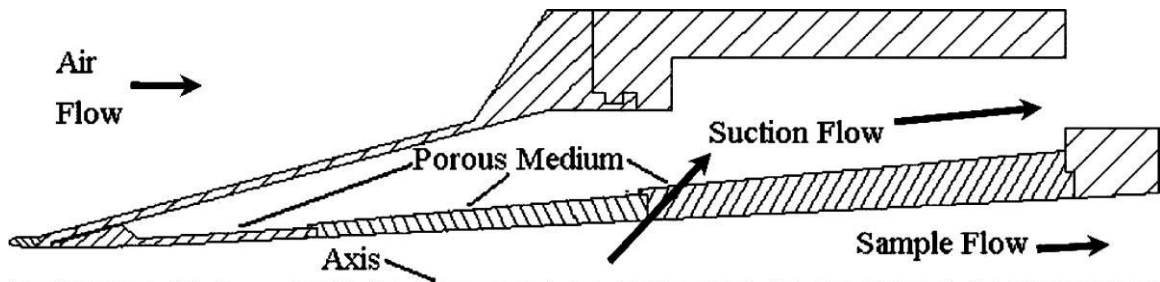


Figure 2.3 Low turbulence inlet [Wilson et al., 2004]. This inlet was used in PELTI.

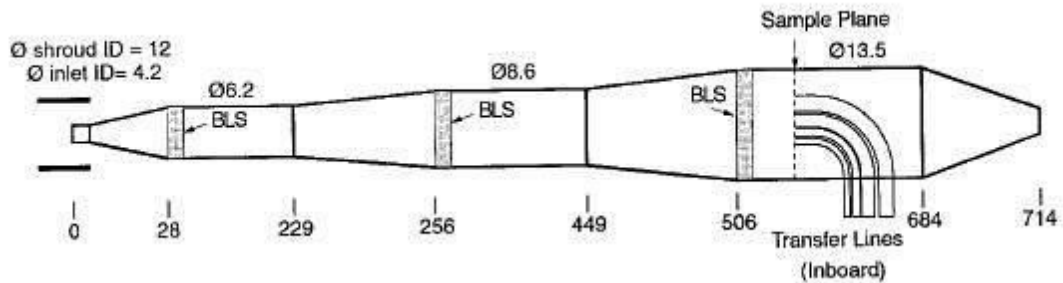


Figure 2.4 Community aerosol inlet, a conical triple diffuser [Blomquist et al., 2001]. Used in INDOEX.

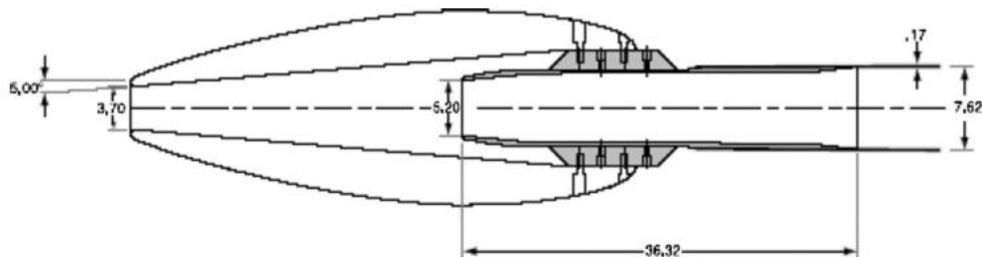


Figure 2.5 Forward mounted, shrouded, conical double diffuser inlet [Hegg et al., 2005]. Used in BRACE

Rigorous evaluation of the CIRPA and NCAR conical diffusers mounted forward of the aircraft nose have demonstrated passing efficiencies up to at least 50% for particles up to 2-3  $\mu\text{m}$  diameter. Passing efficiencies typically increase rapidly when the aerodynamic diameter is less than 1 micrometer and rapidly decreases for aerodynamic diameters greater than 2-3 microns [[Blomquist et al., 2001](#); [Hegg et al., 2005](#)]. The information presented in this review was used to select and install a new aerosol inlet on the Cessna 402 aircraft.

### 2.2.2 Description of the Cessna 402 aerosol inlet

In 2010, RAMMPP moved its air sampling platform from a Piper Aztec to the Cessna 402. In addition to a greater payload, the program upgraded its aerosol collection capability to collect PM with diameters greater than 1 micrometer by installing an inlet based on Antony Clarke's NASA-sponsored shrouded diffuser and purchased from Droplet Measurement Technologies, Boulder, CO. The selected inlet style was chosen based on the results of DICE and PELTI while the mounting location, forward of the nose, was chosen based on the BRACE and NCARs CAI experimental results. The configuration of the NASA SD mounted onto the UMD Cessna 402 (Figure 2.6) has meticulously followed published aerosol sampling guidelines. The passing efficiency is expected to match those observed by the NASA shrouded diffuser in PELTI and DICE, near 100% for particle diameters up to 2.5  $\mu\text{m}$  and near 50% for particles between 3-4  $\mu\text{m}$ . According to DISCOVER-AQ, P3-B measurements, submicron particles dominate the Maryland nonattainment region (personal communication, Jim Crawford, NASA).

### 2.2.3 Dissertation aerosol inlet objectives

In this work I present results of aircraft aerosol inlet comparisons between the new RAMMPP sampling platform on the Cessna 402 with the NASA P3-B and the Cessna 402 with the old RAMMPP platform, the Piper Aztec. A second objective in the side-by-side comparison flights is to verify the integrity of the archived scattering data collected aboard the Piper Aztec. These comparisons demonstrate that the UMD Cessna 402 aerosol inlet sampling system aerosol scattering values are within 30% of the NASA P3-B scattering values. These results demonstrate the suitability of this sampling system for the evaluation of particulate matter and its effects on human health and climate.

## 2.3 Background part C, Introduction to ambient NO<sub>2</sub> and NO<sub>2</sub> measurements

This information is found in Chapter seven.

## CHAPTER 3: METHODS

The materials and methods used to analyze WSOC content during the peak day and dissipation day of an air quality episode are described in this chapter. To accomplish this analysis, I evaluate the tools for aircraft collection and post collection compositional analysis. This chapter is broken down by the combination of procedural steps used to complete the entirety of this research.

First described in the WSOC Materials and Methods, section 3.1, is the procedure by which molecular constituents of water soluble organic carbon, extracted from atmospheric aerosol, are resolved by ESI-MS/MS after acidic class separation. Using NIST SRM 1649b Urban Dust as a surrogate material we demonstrate the additional resolving power of tandem IC/ESI-MS/MS over IC with conductivity detection and the potential application of this method to other atmospheric aerosol samples. This method is then applied to the aircraft filter sample extract.

The WSOC aircraft collection and analysis in section 3.2 describes the quartz fiber filter pre and post sampling preparation, storage, and extraction. Also included is a description of the meteorological, optical particle sizing and trace gas instruments run simultaneously with filter collection in the aircraft.

Section 3.3 describes the inlet installation and the materials and procedures specific to aircraft aerosol collection. This section also includes a description of the meteorological and light scattering instruments used in the side by side inlet evaluation experiment.

For the cavity ringdown instrument, design, theory and calibration procedures are presented separately in the instrument description and calibration methods of Chapter Seven.

### 3.1 Materials and methods part A, WSOC IC/MS/MS method development

#### 3.1.1 Chemicals

Nitrate Anion Standard solution SRM 3185 ( $\text{NO}_3^-$ ), Phosphate Anion Standard solution SRM 3186 ( $\text{PO}_4^{3-}$ ), and Chloride Anion Standard solution SRM 3182 ( $\text{Cl}^-$ ) were used in the determination of inorganic ions (Table 4.1) (Office Reference Materials, NIST, Gaithersburg, MD). Organic Acids Calibration Standard, SRM 3286, was used to quantify citric, malic, quinic, shikimic and tartaric acids (Office Reference Materials, NIST, Gaithersburg, MD). Additional standards used for quantitation of galacturonic, glycolic, isocitric, oxalic, and sodium sulfate were purchased from Sigma Aldrich (St. Louis, MO). The purity of these commercially obtained compounds was verified by LC-UV (210 nm) to exceed 99 % (mass fraction) except for isocitric acid whose purity was 93.5 %. All other reagents used for qualitative analysis were purchased from Sigma Aldrich, (Table 4.2). Deionized water,  $18 \text{ M}\Omega \text{ cm}^{-1}$ , delivered by a Milli-Q Advantage A10 ultrapure water purification system (MA, USA) was used for IC mobile phase and dilutions.

#### 3.1.2 Sample collection and extraction

Details on the collection and handling of the first issue of SRM 1649 have been reported (NBSIR-82-2595, 1982). Briefly, the material was collected at the Navy Yard in



Washington, D.C. in specially designed bag houses from 1977 to 1978. SRM 1649b is a fraction of the SRM 1649 material sieved to a smaller particle size (63 $\mu$ m sieve), repackaged and reissued in 1999 [[Wise, 2000](#)].

Portions of approximately 100 mg of SRM 1649b were placed into 50 mL centrifuge tubes and their masses recorded. Triplicate samples of SRM 1649b were analyzed. Tubes were diluted with deionized water and shaken for several hours. Prior to concentrating the extract to approximately seven mL under nitrogen, the SRM 1649b samples were filtered using a 0.2  $\mu$ m Luerlock syringe (National Scientific, Rockwood, TN) and filter (Chrom Tech Inc., Apple Valley, MN). Gravimetric quantities of nitrite and fumaric acid were added as internal standards after extraction and concentration. Two mL aliquots of the water soluble extract were transferred to HPLC vials for analysis.

### 3.1.3 Standard solutions

Stock solutions for qualitative analysis were prepared gravimetrically by adding known quantities of five inorganic salts (Table 4.1) and 34 organic acids (Table 4.2). The mass fractions of the 34 acids were approximately 3  $\mu$ g/g and quantities of the inorganic salts were 22  $\mu$ g/g  $\text{PO}_4^{3-}$ , 30  $\mu$ g/g  $\text{Cl}^-$ , 30  $\mu$ g/g  $\text{NO}_3^-$ , and 113  $\mu$ g/g  $\text{SO}_4^{2-}$ .

Calibrants for quantitative analysis were made by gravimetric dilution of the stock solutions containing the SRM acids citric, malic, quinic, shikimic, and tartartic plus, galacturonic, isocitric, glycolic and oxalic acids. Five salts were added to the calibration solution:  $\text{PO}_4^{3-}$ ,  $\text{Cl}^-$ ,  $\text{NO}_2^-$ ,  $\text{NO}_3^-$ , and  $\text{SO}_4^{2-}$ . The calibration solutions were targeted to bracket the SRM concentrations.

### 3.1.4 Analysis

Separations were performed on a dual system, Reagent-Free™ ICS 3000 (Dionex at Thermo Fisher, Sunnyvale, CA). The Dionex dual ICS 3000 contains two complete chromatographic systems enclosed in one instrument convenient for simultaneous anionic and cationic analysis. The system is equipped with two, built-in, degasser pumps and two eluent generators for running ionic gradients. Continuously regenerating ion trap columns are installed between the pumps and their respective columns removing all ionic contaminants in the eluent. After injection, compounds are separated on an ion-exchange column. Before CD the total eluent conductivity is suppressed by electrolytically removing the excess hydroxide ions across a membrane in the self-regenerating suppressor (SRS). Typically, these systems are plumbed in recycle mode directing the CD waste effluent back to the SRS as the source of hydration and counter flow for electrolytic exchange across the membrane.

Injections were made using a 10 µL injection loop onto an IonPac AS 17-C hydroxide-selective anion-exchange column, 250 x 2mm (Dionex, Sunnyvale, CA). The analytical column was preceded by an IonPac AG17-C guard column, 50 x 2mm. In contrast to the standard recycle mode plumbing described above, this system was plumbed in external water mode to accommodate tandem MS analysis. After SRS suppression the CD effluent was directed to the ESI chamber for tandem MS/MS analysis. Plumbed in external water mode, the SRS electrolytic counter flow was provided by the second, integral pump, at a flow of 2 mL/min. The eluent flow rate is 0.25 mL/min with the gradient program is described below. In increments of min/mmol/L KOH:

| Time, min | mmol/L KOH |
|-----------|------------|
| 0         | 0.6        |
| 6         | 0.6        |
| 11        | 5.0        |
| 18        | 10         |
| 28        | 20         |
| 32        | 32         |
| 38        | 60         |
| 43        | 80         |

After each sample, 80 mmol/L KOH was run for 10 min as a post column wash and regeneration. A 7 min re-equilibration period at 0.6 mmol/L KOH preceded each new analysis.

Mass spectrometric detection was performed by interfacing the Dionex IC with an Agilent 6410 mass spectrometer (Santa Clara, CA) equipped with an ESI source and a triple quadrupole mass analyzer. Source settings were: capillary voltage 3500 V, desolvation gas temperature 350 °C and flow 11 L/min, and nebulizer gas pressure  $2.5 \times 10^5$  Pa. Compound identification was determined through multiple reaction monitoring (MRM) in the negative ionization mode. The MS/MS of each standard was individually optimized by scanning for the precursor ion then using collision induced dissociation to determine the most abundant product ions. The two most intense precursor-to-product ion transitions were selected for peak assignment. The MRM method was set so that all precursor-to-product ion transitions were scanned continuously

throughout the entire run (See Table 4.2 in the results and discussion for the list of transitions monitored).

## 3.2 WSOC aircraft collection and analysis

### 3.2.1 In Situ optical and trace gas aircraft measurements

Description of the instruments and calibration procedures has been previously provided by Taubman (2004) and Hao (2013) [[H. He et al., 2013a; Taubman B.F., 2004](#)]. In fall 2010, RAMMPP upgraded its air monitoring platform from the Piper Aztec with roof mounted inlets and sensors described by Taubman (2004) to a larger Cessna 402. The new aircraft is configured with the inlets and sensors mounted to the aircraft nose as shown in Figure 6.2. For the measurements included in this analysis, atmospheric gases sulfur dioxide (SO<sub>2</sub>) and ozone (O<sub>3</sub>) were measured with modified commercially available Thermo Environmental ambient monitors (Franklin, MA). Condensation nuclei with particle diameters ranging from 0.01 to >1.0 μm, were counted per unit volume with a TSI Condensation Particle Counter, model 3007 (Shoreview, MN). A Met One Instruments 6 channel particle counter Model 9012 (Grant Pass, OR) also measured particles per unit volume but with respect to six size bins. Gas monitors receive pre-and post-flight season calibrations using NIST traceable gas standards, while the aerosol instruments receive periodic factory calibrations.

### 3.2.2 Filters

Prior to use, quartz fiber filters were baked at 900<sup>0</sup>C for at least eight hours to remove any organic impurities. The baked filters were placed in a nitrogen purged,

humidity controlled desiccator. Other than being removed for tarring, filters remained in the low humidity, temperature controlled box under a nitrogen blanket until transport for sampling. Filters were transported from NIST to the airport in sterile petri dishes sealed with Parafilm and placed in Ziploc bags. Aerosol was collected onto the filters using a TFIA Staplex®, high volume air sampler (Brooklyn, NY). Connection to the aerosol inlet tubing was achieved by use of a 100 to 25 mm (4" to 1") adapter machined from a 100 mm aluminum face plate welded to a 25 mm tube. This adapter concentrated the sample volume onto a 25 mm diameter area on the filter. Volumetric flow (ball flow meter) was calibrated using a Bios DryCal ML-800® flow sampler (Mesa Labs, Butler, NJ). The air sampler flow rate was 52.324 LPM. The volumetric flow rate, as observed by an additional ball flow meter connected to the Nephelometer outlet, was observed to fluctuate only with extreme changes in angle of attack (i.e., take off), but not with respect to altitude. Post sampling, filters were returned to their petri dishes for transport back to their desiccator. After 24 hours of exposure to the nitrogen purged humidity controlled environment, post sampling masses were obtained. The filters remained in the dry box until extraction for analysis.

Filter extraction was conducted prior to analysis. A clean razor blade (washed and baked at 500<sup>0</sup> C for 72 hours) was used to separate the sampled area from the rest of the filter. The 1" diameter cutout material was placed into a vial and immersed in approximately 30 g of deionized water. The vial was sealed and put on a rotating mixer overnight. After extraction, the sample volume was filtered via a 0.2 µm Luerlock syringe (National Scientific, Rockwood, TN) and nylon filter (Chrom Tech Inc., Apple Valley, MN) and concentrated to approximately 5 g under N<sub>2</sub>. Gravimetric

measurements of each volume were collected at each step. Extracted volumes were refrigerated until analysis.

### 3.2.3 Calibration standards

In addition to the chemical standards listed in section 2.1, cation Standard Reference Materials were added to the series of reference standards used for the aircraft sample analysis. The cation materials are as follows: Sodium SRM 3152a ( $\text{Na}^+$ ), Calcium SRM3109a ( $\text{Ca}^{2+}$ ), Magnesium SRM 3131a ( $\text{Mg}^{2+}$ ), and Potassium SRM 3141a ( $\text{K}^+$ ) were used in the determination of inorganic ions (Office of Reference Materials, NIST, Gaithersburg, MD). Ammonium iodide ( $\text{NH}_4\text{I}$ ) was purchased from Inorganic Ventures (Christiansburg, VA). Deionized water,  $18 \text{ M}\Omega \text{ cm}^{-1}$ , delivered by a Milli-Q Advantage A10 ultrapure water purification system (MA, USA) was as the IC mobile phase and for the dilutions.

Quantitative and qualitative evaluation of aerosols collected onto the QF filters was conducted by reference to standard solutions prepared via gravimetric dilution. Standard stock solutions were composed of 25 organic acids at  $\sim 1 \mu\text{g/g}$ , 9 organic acids at  $\sim 7 \mu\text{g/g}$  and 5 inorganic ions at  $\sim 10 \mu\text{g/g}$ . The organic and inorganic ion ratios were targeted to reflect the expected natural matrix.

### 3.2.4 Filter sample analysis

The stock solutions were prepared via gravimetric dilutions as done above during analysis of SRM 1649b.

### 3.3 Materials and Methods part B, Inlet materials, design and comparison

#### 3.3.1 Materials

##### 3.3.1.1 Hardware

Hardware used for aircraft structures requires additional corrosion resistance and tensile strength beyond that of materials purchased in hardware and automotive stores. All hardware used for this inlet installation is identifiable by an Air Force–Navy (AN) or Military Standard (MilSpec) part number and purchased from designated aircraft hardware suppliers. Bolts were purchased from Haire Aviation LLC Aircraft Fasteners, Sanger TX or Aircraft Spruce, Peachtree City, GA. Standard nuts, elastic stop nuts, set screws, flat washers, lock washers and Adel clamps were purchased from Aircraft Spruce. Helicoils were purchased from Emhart Technologies, Shelton, CT. Mil Spec Buna-N/Nitrile rubber grommets were purchased from Grainger, Chicago, IL. Safety wire was provided as a gift from Tom Gorman, Tipton Airport Service, Fort Meade, MD.

##### 3.3.1.2 Inlet and Tubing

The shrouded diffuser inlet is commercially available through Droplet Measurements Technologies, MP-1806-A and MP-1807-A (Boulder, CO). The inlet is crafted from 6061-T6 aluminum using a stainless steel Swagelok (nylon ferule and frit) for connection to 1” OD aluminum tubing. The aluminum tube is composed of 6061 T-6 seamless tube, 1” O.D. x 0.65 wall x 29”, part No. 200364, Access Metals (Essex, MD). Conductive tubing, 1” O.D. from American Hose & Coupling Corporation (Glen Burnie, MD) delivers aerosols to the fuselage.

### 3.3.1.3 Support

Two Aluminum cross blocks secured to a previously mounted and Federal Aviation Administration (FAA) approved aluminum scaffolding in the Cessna nose are used to secure the aerosol inlet and aluminum tubing. The aluminum mounting blocks, labeled forward and aft, were cut from aircraft grade aluminum 6061-T6 and 2024 T-351, respectively, Access Metals (Essex, MD). See Appendix A for pictures and drawings.

### 3.3.2 Installation configuration

The tip of the shrouded diffuser protrudes 18 inches forward from the nose of the aircraft. The inlet nozzle is Swagelocked to 1" OD, 29" L tubing that runs through the aluminum cross supports and into the airplane. A worm drive clamp secures the aluminum tubing to conductive tubing that travels the length of the plane, through the cockpit and into the cabin. A brass manifold was used to split the inlet flow between the filter sampler and the optical instruments. A stainless steel manifold was used to distribute the aspirated flow to the aerosol instruments. Set screws are used to secure the aluminum tubing to the support blocks. The aluminum cross supports are fastened to the aluminum scaffolding by steel bolts. For strengthening the bolt grip between threading of two different metals Helicoils are inserted into the aluminum blocks. For added security, safety wire was run between the platform and the bolts securing the aft aluminum block to the platform. The inlet angle of attack can be adjusted manually at the scaffold by adjusting both the position of the aft aluminum block in the slide and the vertical placement of the forward aluminum block along the bolts that secure it to the platform. The tubing is tilted downward  $4^{\circ}$  from horizontal to facilitate isoaxial sampling.



Also mounted to the inlet face plate of the Cessna are a stainless steel aft-facing gas inlet, and temperature and humidity probes. The candy cane shaped air intake is fabricated from 0.50 inch 316 stainless steel tubing attached to the aluminum face plate via a bulkhead Swagelok union and stabilized by Adel clamps to the aerosol inlet probe.

### 3.3.3 Note on aircraft modification FAA regulations

By FAA guidelines, aircraft modifications that include fixing equipment and materials to an aircraft require FAA approval delivered by signature of an FAA representative on a FAA form 337. This process requires external review of inlet installation plans by a Designated Engineering Representative (DER). The DER engineer performs his own calculations validating the structural integrity of an aircraft modification, which are reviewed by the FAA. Any changes made to the inlet installation configuration must undergo a similar review. A copy of FAA Form 337 is shown in Appendix A and the package submitted to the FAA is included in Appendix B. Appendix C lists the instructions for installation and removal. This inlet installation configuration was conducted under the guidance of Bray Besse, from the University Research Foundation and Tom Gorman, aircraft mechanic and owner of Tipton Airport Service for helicopter and fixed-wing repair.

### 3.3.4 Instruments

#### 3.3.4.1 Light Scattering

A light scattering inter-comparison with NASA was performed using TSI 3563 integrating Nephelometers. The total light scattering and backscattering coefficients at

450, 550 and 700 nm are continuously monitored over an angular range of  $\sim 7^\circ$  to  $170^\circ$  and  $90^\circ$  to  $170^\circ$ . A 75 watt quartz-halogen lamp shining through an opal glass diffuser creates a Lambertian light source. During the measurement process, passive dry heating of the sample aerosol occurs due to the combined effects of particles warming as they travel from outside through the cabin tubing to the instrument plus increased temperatures in the optical cavity because heat is radiated by the instrument electronics and light source. Scattering coefficients are determined by ratioing the number of photons counted by the PMT during the measure phase against photons counted during the dark phase. Rayleigh and wall scattering are also subtracted. Pre and post campaign calibrations were performed using CO<sub>2</sub> and filtered (HEPA filter, (TSI, Shoreview, MN)) ambient air.

#### 3.3.4.2 Meteorological Data

A Vaisala PTU300 combined pressure, humidity, and temperature sensor is used to measure meteorological parameters during flights. The temperature probe is a platinum resistance temperature detection sensor. Relative humidity is measured using a thin film capacitive sensor. The sensor monitors changes in dielectric constant induced by the absorption of water by a thin film of polymer deposited between two conductive electrodes. The unit is sent back for calibration on a biannual basis. Each of these variables are recorded to the data logger every 10 s.

#### 3.3.4.3 Data processing

The UMD Nephelometer is set for ten second averaging and writes data points to the internal log file every ten to 12 seconds. The NASA Nephelometer is set for one

second averaging and writes to the file every second. During our processing, the NASA data are averaged over ten seconds before applying corrections. This is different from the P3-B merges public website for which corrections were applied to the 1 second data (<http://www-air.larc.nasa.gov/cgi-bin/ArcView/discover-aq.dc-2011#2>). The Nephelometer is designed to scatter light in the forward direction over an angular range of  $7^{\circ}$  to  $170^{\circ}$ , but the actual angular range shows size dependent truncation errors requiring correction [[Anderson et al., 1996](#)]. The Angstrom exponent, an intrinsic aerosol property governing the transfer of light through air as a function of changes in scattering with respect to measurement wavelength, was used as the limiting factor for size dependent corrections. Particles with an Angstrom exponent  $> 0.75$  were corrected using the submicron correction factors in Table 4B of Anderson and Ogren (1998). The no cut correction from Table 4A was applied to scattering values whose Angstrom exponent was  $< 0.75$  (Anderson and Ogren 1998). More information about the RAMMPP aircraft data processing procedures is available in the internal report, DISCOVER-AQ Documentation and Raw Data, Cessna 402 Aircraft Measurements [[Arkinson, 2012](#)].

# CHAPTER 4: RESULTS AND DISCUSSION (part A) on a method for characterization of low molecular weight organic acids using IC/MS/MS

## 4.1 Introduction

The structural composition of PM<sub>2.5</sub> monitored in the atmosphere is usually divided by the analysis of OC, BC (also called EC), and inorganic salts. The characterization of the chemical composition of carbonaceous aerosols represents a significant challenge to analysts and studies are frequently limited to determination of aerosol bulk properties. To better understand the potential health effects and combined interactions of components in aerosols, a variety of measurement techniques for individual analytes in PM<sub>2.5</sub> need to be implemented. The method developed here for the measurement of organic acids achieves class separation of aliphatic monoacids, aliphatic diacids, aromatic acids, and polyacids. The selective ion monitoring capability of a triple quadrupole mass analyzer was frequently capable of overcoming instances of incomplete separations. In a molecular characterization of SRM 1649b Urban Dust 34, organic acids were qualitatively identified and 6 inorganic salts plus 6 organic acids were quantified.

## 4.2 Results and discussion

### 4.2.1 Optimization of separation conditions

The use of IC instrumentation to produce system-generated pH gradients permits programmed eluent compositions for adjusting ionic concentrations in an aqueous mobile

phase. Because the competing hydroxide ions are removed from the gradient between the column and the detector by the eluent suppressor, the effluent can be introduced directly into the MS. The use of methanol, acetonitrile, and formic acid as mobile phase modifiers was evaluated by their addition to either the IC reservoir or to the effluent with splitting before introduction into the ionization chamber. Because MS signal enhancement was not observed, modifiers were not used in the final method.

Figures 4.1A and 4.1B compare separations of a 25 compound solution achieved with IonPac<sup>®</sup> AS11-HC and IonPac<sup>®</sup> AS17-C columns. The mixture contained 9 monoacids, 9 diacids, 1 poly acid and 6 inorganic salts. The IonPac<sup>®</sup> AS11-HC is designated a high capacity column intended for applications requiring resolution of inorganic and organic ions (IonPac<sup>®</sup> AS 11-HC manual). Separations with this column have been used for aerosols collected onto filters or particles into liquid samplers (PILS), for both ground and aircraft sampling [[Healy et al., 2013](#); [Mayol-Bracero et al., 2002](#); [Rohrl and Lammel, 2002](#); [Topping D., 2004](#)]. The IonPac<sup>®</sup> AS 17-C column is designated a low capacity column with applications for inorganic ion separations (ref. IonPac<sup>®</sup> AS17-C manual). Gradient conditions are indicated on the figures. Figure 4.1C shows a separation of the same 25 compound solution on the IonPac<sup>®</sup> AS 17-C column but differs from Figure 4.1B by using a mobile phase program similar to that reported by [[Domingos et al., 2012](#)].

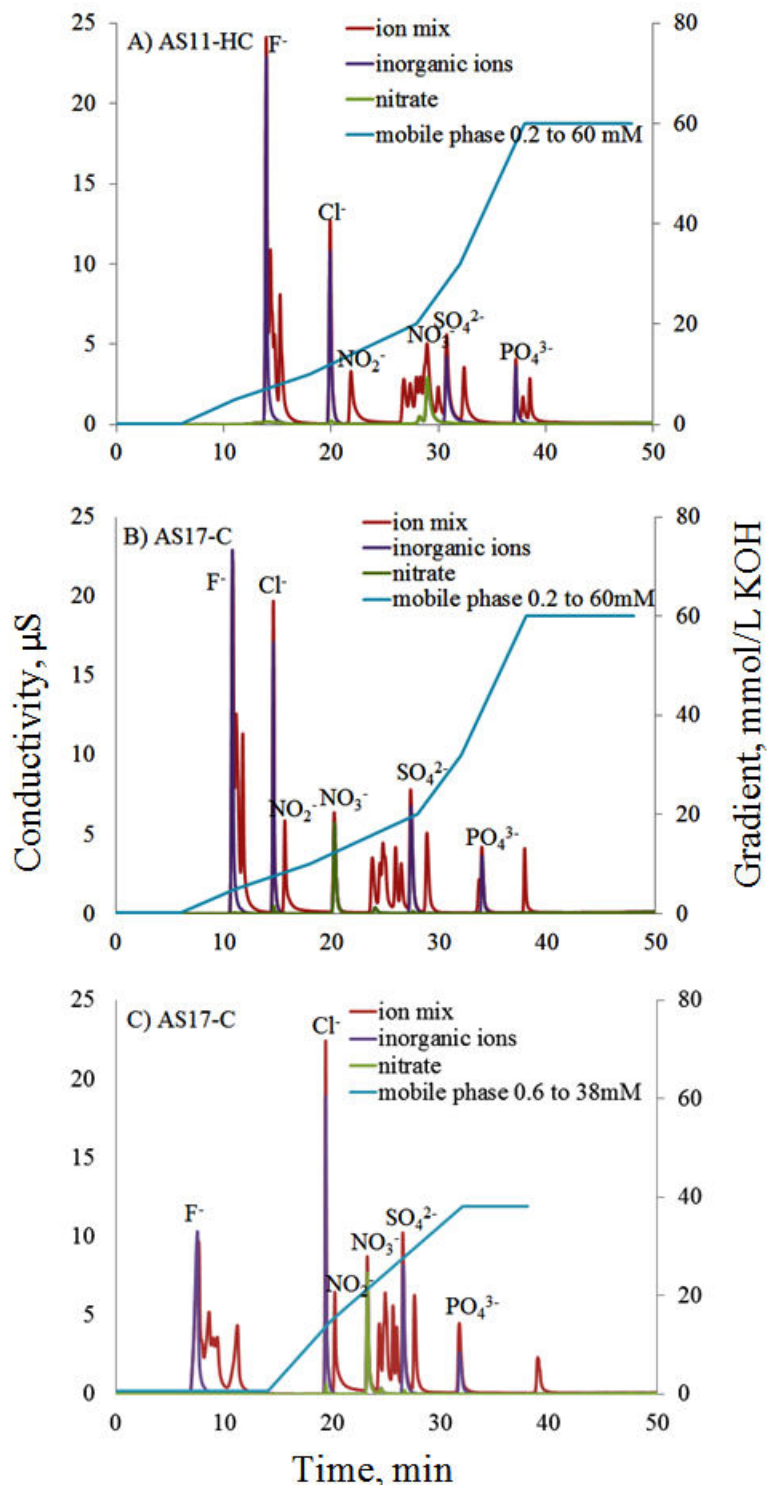


**Figure 4.1** Chromatographic separations of 25 compounds, 9 monoacids, 9 diacids, 1 polyacids and 5 inorganic salts on two columns and two different mobile phases. A) Separation with IonPac AS11-HC column and [0.2 to 60] mmol/L KOH gradient. B) Separation with IonPac AS17-C column and [0.2 to 60] mmol/L KOH gradient. C) Separation with IonPac AS17-C column and [0.6 to 38] mmol/L KOH gradient.

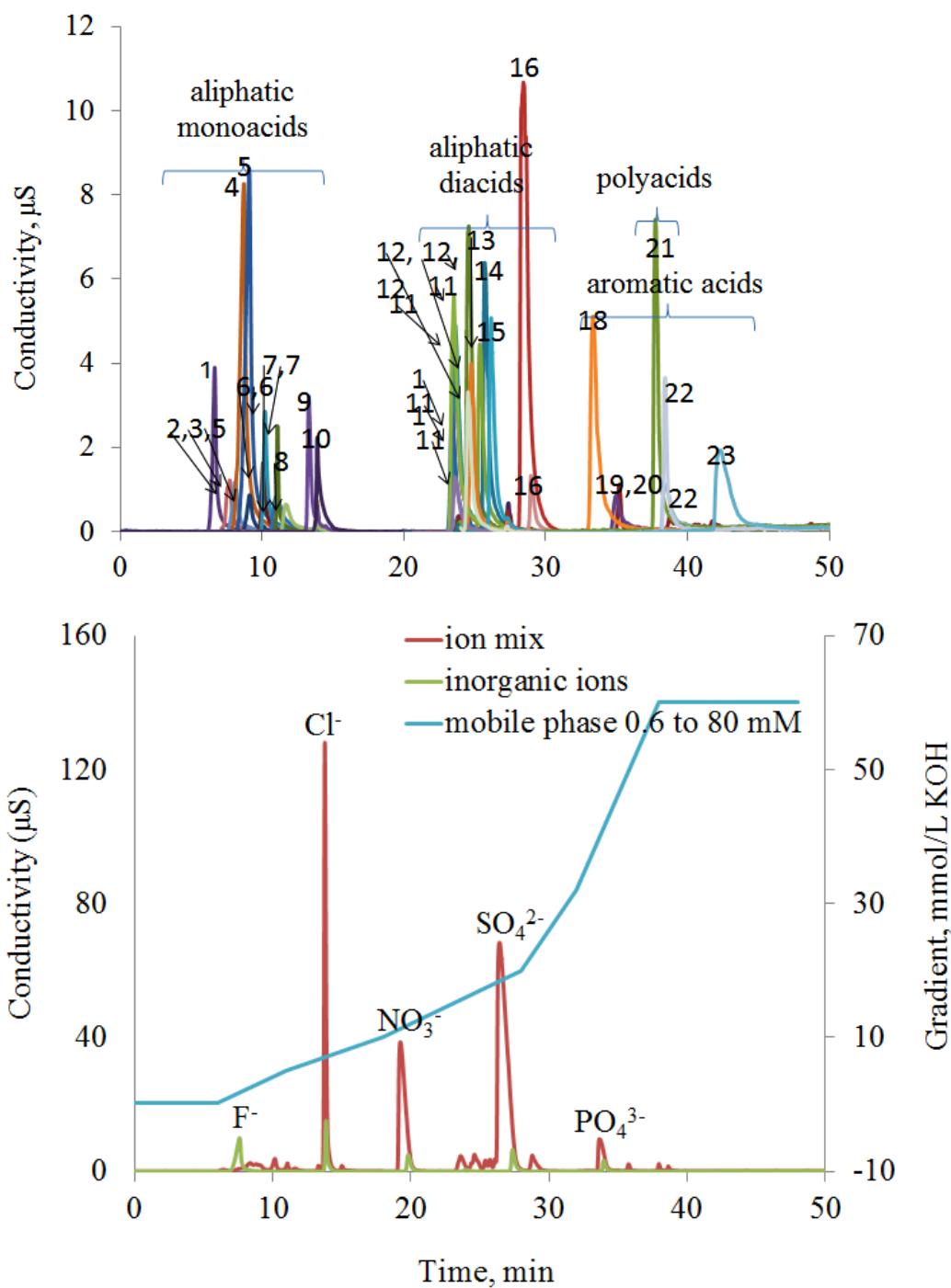


**Figure 4.2** Retention of organic and inorganic species. 4.2A) separation of organic acid classes. Organic acids are identified as follows; Monoacids: 1) quinic, 2) lactic, 3) levulinic, 4) glycolic, 5) 2-hydroxybutyric, 5) propanoic, 6) butanoic, 6) dipicolinic, 6) 2-hydroxy-3-methylbutyric, 7) cis-pinonic, 7) pyruvic, 8) valeric, 9) galacturonic, 10) hexanoic. Diacids: 11) 3-methylglutaric, 11) methylsuccinic, 11) adipic, 11) 2-methylglutaric, 11) glutaric, 12) malic, 12) methylmalonic, 12) ethylmalonic, 13) malonic, 14) tartaric, 15) maleic, 16) oxalic, 16) fumaric. Aromatic acids: 18) phthalic, 19) 4-hydroxybenzoic, 20) 3,4-dihydroxybenzoic, 22) 3-hydroxybenzoic, 23) 2-hydroxybenzoic. Polyacids: 21) citric, 22) isocitric. 4.2B) Separation of inorganic ions

The use of a gradient program with a higher initial KOH concentration results in better baseline separation between the aliphatic mono- and diacids, and a gradual increase in KOH concentration across the dicarboxylate region, as shown in Figures 4.1A and 4.1B, results in better separation of the individual diacid ions. Stronger mobile phase conditions are used after the elution of dicarboxylates to elute aromatic and trivalent ions.

The trends noted above were considered in the development of the elution conditions described in the methods section. Figure 4.2A shows the organic acid class separation achieved by this gradient. Organic acid standards range from 8 to 15  $\mu\text{g/g}$ . Aromatic acids with poor CD response, cinnamic, syringic, and ferulic, are not shown in Figure 4.2A, but are observed to have retention similar to phthalic acid by MS. In this series, the only instance of incomplete ion class separation is the coelution of polyacids citrate and isocitrate with aromatic acids 3-hydroxybenzoic acid and ferulic acid. Figure 4.2B shows the separation of a standard solution, containing 34 organic acids and 6 inorganic anions. The proportion of small organic acid concentrations to large inorganic anion concentrations in the standard solution captures the expectation that organic acids in ambient aerosol exist at significantly smaller concentrations than the inorganic anions. As analyte concentrations approach naturally expected abundances the peak shape becomes more Gaussian during application of this method on a 2 mm column. The disparate conductimetric response observed complicates the simultaneous analysis of organic acids and inorganic salts by CD because signal response to organic ions is frequently overwhelmed by the presence of inorganic ions. This problem is particularly significant in sampling environments heavily loaded with sulfate as observed by Tsai et al. (2008) in Taiwan [[Tsai, 2008](#)].



#### 4.2.2 Mass spectral identification of compounds

With ESI the most common precursor ion prior to collision induced dissociation (CID) is either  $[M+H]^+$  or  $[M-H]^-$  resulting from addition or loss of a proton. Of the 51 reference standards initially studied, most exhibited  $[M-H]^-$  precursor ions. Sulfate ( $SO_4^{2-}$ ) and phosphate ( $PO_4^{3-}$ ) formed dimerized precursors  $[2M-H]^-$  in the ionization chamber and underwent transition to their molecular ions (195→97) during CID.  $PO_4^{3-}$  underwent an additional 195→177 transition corresponding to a loss of water, while  $SO_4^{2-}$  did not. The ability to distinguish phosphate by this additional transition is important for samples that contained very high levels of sulfate, since loss of chromatographic baseline resolution may result. Inorganic ions monitored in this work are listed in Table 4.1. Nitrite ( $NO_2^-$ ) (MW 46) and nitrate ( $NO_3^-$ ) (MW 62) are chromatographically resolved but both compounds are identified by  $m/z$  62 suggesting possible oxidation of  $NO_2^-$  to  $NO_3^-$ . The mass spectral detection of  $NO_2^-$  at the same  $m/z$  as the  $NO_3^-$  precursor ion indicates that  $NO_2^-$  to  $NO_3^-$  oxidation occurs after elution from the column and is not a product of mobile phase interaction. Under these conditions, fluoride and chloride did not produce a MS signal and are not reported here.

**Table 4.1** Precursor and product ions monitored for the inorganic ions

| Compound  | Structure   | Transition        | Precursor ion | Suggested Fragment                           |
|-----------|-------------|-------------------|---------------|--|
| Fluoride  | $F^-$       | NA                | NA            | NA   |
| Chloride  | $Cl^-$      | NA                | NA            | NA   |
| Nitrite   | $NO_2^-$    | 62→62             | $[M-H]^-$     | SIM of precursor ion which has been oxidized |
| Nitrate   | $NO_3^-$    | 62→62             | $[M-H]^-$     | SIM of precursor ion                         |
| Sulfate   | $SO_4^{2-}$ | 195→97            | $[2M-H]^-$    | Molecular ion                                |
| Phosphate | $PO_4^{3-}$ | 195→97<br>195→177 | $[2M-H]^-$    | Molecular ion<br>H <sub>2</sub> O            |

During the method development for organic acid identification, a few instances were observed in which ESI simultaneously produced deprotonated dimers and monomers. Adjustment of the MS cavity accelerator and fragmentation voltages influenced the abundance of the  $[M-H]^-$  versus  $[2M-H]^-$  ions in standard solutions with concentrations of a few  $\mu\text{g/mL}$ . Dimerized product ions periodically observed in higher concentration standard solutions were not observed in solutions with concentrations relevant to ambient samples nor in the analysis of SRM 1649b. This indicates that, unlike  $\text{SO}_4^{2-}$  and  $\text{PO}_4^{3-}$ , the organic compounds are susceptible to concentration-dependent noncovalent dimerization [[Ding and Anderegg, 1995](#)]. Pan et al., (2008) observed that noncovalent dimerization can be both instrument and mode dependent [[Pan, 2008](#)]. Spray chamber conditions were always optimized to favor production of the monomer target for MRM. Concentration dependent dimerization in the ESI chamber could become relevant to smog chamber experiments if initial reactant concentrations lead to reaction products whose concentrations significantly exceed ambient atmospheric concentrations.

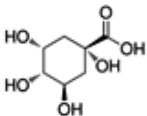
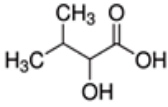
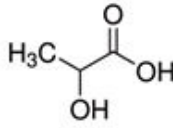
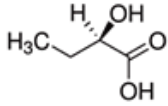
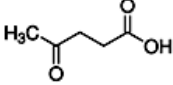
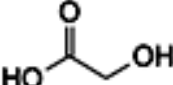
A list of acids selected for qualitative and quantitative evaluation, and relevant information is provided in Table 4.2. The CID trends observed in this study can be summarized.

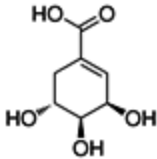
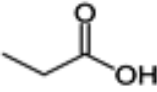
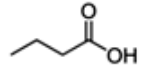
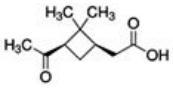
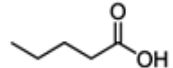
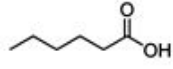
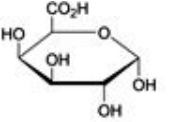
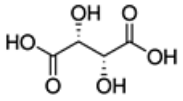
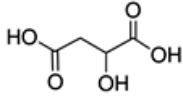
- 1) Nonbranched, straight chain aliphatic monoacids do not fragment under the specified ionization conditions. These species were monitored by targeting the precursor ion and maintaining the collision energy at zero.
- 2) Branched aliphatic monoacids and branched and straight chain aliphatic diacids typically produced product ions corresponding to losses of COO

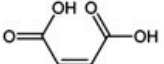
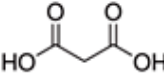
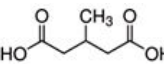
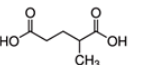
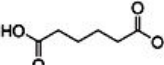
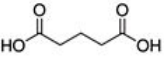
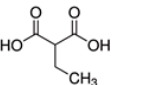
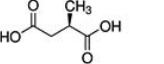
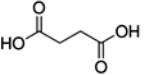
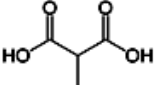
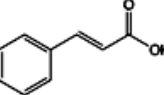
( $m/z$  44),  $H_2O$  ( $m/z$  18), and  $CO$  ( $m/z$  28) or combinations of losses  $CO$  and  $H_2O$  ( $m/z$  46) and  $COO$  and  $H_2O$  ( $m/z$  62).

- 3) Cyclic compounds always produced at least two transitions, resulting from loss of  $COO$  and loss of a second, unspecified fragment. Frequently, aromatic rings remained intact.

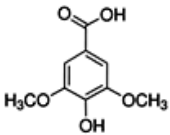
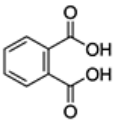
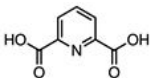
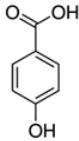
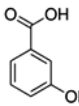
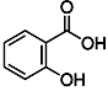
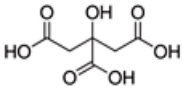
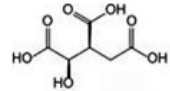
**Table 4.2** Precursor and product ion transitions monitored for the organic ions

| Compound   | Structure   | RT  | Transition | Mass loss | Suggested Fragment loss |
|--|---|-----|------------|-----------|-------------------------|
| *Quinic<br>$H_{12}C_7O_6$  |    | 3.6 | 191→85     | 106       | $H_2O$ , 2x $COO$       |
|  |   |     | 191→59     | 132       | ---                     |
| 2-OH-3- $CH_3$ -butyric<br>$H_9C_5O_3$   |   | 4.2 | 117→71     | 46        | $H_2O$ , $CO$           |
|  |   |     | 117→45     | 72        | $COO$ , $CO$            |
| Lactic<br>$H_6C_3O_3$<br>(Marine, rain forest, urban mix, Domingos et al., 2012) |  | 4.7 | 89→43      | 46        | $H_2O$ , $CO$           |
|  |   |     | 89→89      | NA        | NA                      |
| 2-OH-butyric<br>$H_8C_4O_2$  |  | 4.7 | 103→45     |           | ---                     |
|  |   |     | 103→57     |           | $H_2O$ , $CO$           |
| Levulinic<br>$H_8C_5O_3$   |  | 5.0 | 115→97     | 18        | $H_2O$                  |
|  |   |     | 115→71     | 44        | $COO$                   |
| *Glycolic<br>$H_4C_2O_3$<br>(Greenland, Jaffrezo et al., 1998)                   |  | 5.2 | 75→47      | 28        | $CO$                    |
|  |   |     | 75→45      | 30        | $HCOH$                  |

|   |   |      |         |     |                            |
|---|---|------|---------|-----|----------------------------|
|   |   |      | 173→137 | 36  | 2xH <sub>2</sub> O         |
| Shikimik acid<br>H <sub>10</sub> C <sub>7</sub> O <sub>5</sub>  |    | 5.4  | 173→111 | 62  | H <sub>2</sub> O, COO      |
|   |   |      | 173→93  | 80  | H <sub>2</sub> O, HCOO, OH |
|   |   |      | 173→73  | 100 | ---                        |
| Propanoic<br>H <sub>7</sub> C <sub>3</sub> O <sub>2</sub><br>(motor exhaust,<br>Kawamura,<br>1985)                  |    | 5.5  | 73→73   | NA  | NA                         |
| Butanoic<br>H <sub>8</sub> C <sub>4</sub> O <sub>2</sub>  |    | 7.8  | 87→87   | NA  | NA                         |
| Cis pinonic<br>H <sub>16</sub> C <sub>10</sub> O <sub>3</sub><br>(Eucalyptus<br>globulus forest,<br>Kavouras, 1998) |    | 8.2  | 183→57  | 126 | ---                        |
|   |   |      | 183→139 | 44  | COO                        |
| Pentanoic<br>H <sub>10</sub> C <sub>5</sub> O <sub>2</sub>  |  | 9.8  | 101→101 | NA  | NA                         |
| Hexanoic<br>H <sub>12</sub> C <sub>6</sub> O <sub>2</sub>   |  | 8.8  | 115→115 | NA  | NA                         |
| *Galacturonic<br>H <sub>19</sub> C <sub>6</sub> O <sub>7</sub>  |  | 10.9 | 193→59  | 134 | ---                        |
|   |   |      | 193→73  | 120 | ---                        |
| *Tartaric<br>H <sub>5</sub> C <sub>4</sub> O <sub>6</sub><br>(Amazon,<br>Claeys et al,<br>2004)                     |  | 18.6 | 149→87  | 62  | H <sub>2</sub> O, COO, H   |
|   |   |      | 149→73  | 76  | ---                        |
| *Malic<br>H <sub>6</sub> C <sub>4</sub> O <sub>5</sub><br>(Amazon,<br>Claeys et al,<br>2004)                        |  | 18.7 | 133→115 | 18  | H <sub>2</sub> O           |
|   |   |      | 133→71  | 62  | H <sub>2</sub> O, COO      |

|  |   |      |         |    |  |
|--|---|------|---------|----|--|
| Maleic<br>H <sub>3</sub> C <sub>4</sub> O <sub>4</sub><br>(Urban, Taiwan,<br>Tsai et al., 2008)        |    | 18.7 | 115→115 | NA | NA   |
|  |   |      | 115→71  | 44 | COO  |
| Malonic<br>H <sub>4</sub> C <sub>3</sub> O <sub>3</sub><br>(Urban, Taiwan,<br>Tsai et al., 2008)       |    | 18.7 | 103→103 | NA | NA   |
|  |   |      | 103→59  | 44 | COO  |
| 3-methylglutaric<br>H <sub>10</sub> C <sub>6</sub> O <sub>4</sub>                                      |    | 20.1 | 145→101 | 44 | COO  |
| 2-methylglutaric<br>H <sub>10</sub> C <sub>6</sub> O <sub>4</sub>                                      |    | 20.3 |         |    |  |
| Adipic<br>H <sub>10</sub> C <sub>6</sub> O <sub>4</sub><br>(Smog chamber,<br>Hamilton et al<br>2006)   |    | 20.3 | 145→83  | 62 | H <sub>2</sub> O, COO                        |
| Glutaric<br>H <sub>8</sub> C <sub>5</sub> O <sub>4</sub><br>(Smog chamber,<br>Hamilton et al<br>2006)  |  | 20.3 |         |    |  |
| Ethylmalonic<br>H <sub>8</sub> C <sub>5</sub> O <sub>4</sub>   |  | 20.3 | 131→113 | 18 | H <sub>2</sub> O                             |
|  |   |      | 131→87  | 44 | COO  |
| Methylsuccinic<br>H <sub>8</sub> C <sub>5</sub> O <sub>4</sub>   |  | 20.3 |         |    |  |
| Succinic<br>H <sub>6</sub> C <sub>4</sub> O <sub>4</sub><br>(Urban, Taiwan,<br>Tsai et al., 2008)      |  | 20.8 | 117→73  | 44 | COO  |
|  |   |      |         |    |  |
| Methylmalonic<br>acid<br>H <sub>6</sub> C <sub>4</sub> O <sub>4</sub>                                  |  | 20.8 | 117→55  | 62 | H <sub>2</sub> O, COO                        |
| Cinnamic<br>H <sub>9</sub> C <sub>9</sub> O <sub>2</sub><br>(Controlled<br>burning,<br>Hoffman et al., |  | 26.1 | 147→77  | 70 | H <sub>2</sub> C <sub>3</sub> O <sub>2</sub> |
|  |   |      | 147→103 | 44 | COO  |

2007)

|  |   |      |         |     |                          |
|--|---|------|---------|-----|--------------------------|
| Syringic<br>H <sub>11</sub> C <sub>9</sub> O <sub>5</sub>  |    | 26.9 | 197→121 | 76  | COO, OCH <sub>3</sub> ,H |
|  |   |      | 197→123 | 74  | COO, OCH <sub>2</sub>    |
| Phthalic<br>H <sub>6</sub> C <sub>8</sub> O <sub>4</sub><br>(Urban, Italy,<br>Balducci et al.,<br>2010)  |    | 28.3 | 165→165 | na  | na                       |
|  |   |      | 165→121 | 44  | COO                      |
| Dipicolinic<br>H <sub>5</sub> C <sub>7</sub> O <sub>4</sub> N<br>(Aerosol<br>chamber,<br>Russell et al.,<br>2004)  |    | 28.2 | 166→78  | 88  | COO, COO                 |
|  |   |      | 166→122 | 44  | COO                      |
| 4-<br>hydroxybenzoic<br>H <sub>6</sub> C <sub>7</sub> O <sub>3</sub>   |   | 29.3 | 137→93  | 44  | COO                      |
| 3-<br>hydroxybenzoic<br>H <sub>6</sub> C <sub>7</sub> O <sub>3</sub>   |  | 34.0 | 137→41  | 96  | ---                      |
| 2-<br>hydroxybenzoic<br>H <sub>6</sub> C <sub>7</sub> O <sub>3</sub><br><i>*Citric</i><br>H <sub>8</sub> C <sub>6</sub> O <sub>7</sub><br>(Mountain and<br>urban, Chang et<br>al., 2003, Po<br>Valley, Italy,<br>Decesari et al.,<br>2001) |  | 37.2 |         |     |                          |
|  |   |      | 191→85  | 106 | 2xCOO,H <sub>2</sub> O   |
|  |  | 35.0 | 191→111 | 80  | COO, 2xH <sub>2</sub> O  |
| <i>*Isocitric</i><br>H <sub>8</sub> C <sub>6</sub> O <sub>7</sub>  |  | 35.8 | 191→173 | 18  | H <sub>2</sub> O         |

Acids in this table are listed in their order of elution. The reference under an acid name refers to previously reported observation of that acid. Blue font with an asterisk indicates acid was quantified against SRM or purity checked reference standard. --- indicates that fragment structures are not suggested.

Understanding fragmentation patterns is useful for obtaining structural information on unknown compounds. In this work, the above trends were used in conjunction with acid class retention for structural determination of WSOC in SRM 1649b.

#### 4.2.3 SRM 1649b

The atmospheric PM constituting SRM 1649b was collected over a 12 month time frame at the Navy Yard in Washington, D.C. (shown in Figure 4.3). The baghouses used for collection are shown in Figure 4.4. The composition of this time-integrated sample typifies the analytical challenges associated with the chemical analysis of atmospheric particulate matter [[May and Wise, 1984](#)]. As reported for water soluble extract collected around the globe, a full spectrum scan ( $m/z$  40 to 1000) of SRM 1649b extract indicates that the water soluble contents are composed primarily of low molecular weight ions with the intensity of abundances tapering off around  $m/z$  400 [[Decesari et al., 2001](#); [Mayol-Bracero et al., 2002](#); [Russell et al., 2011](#)].

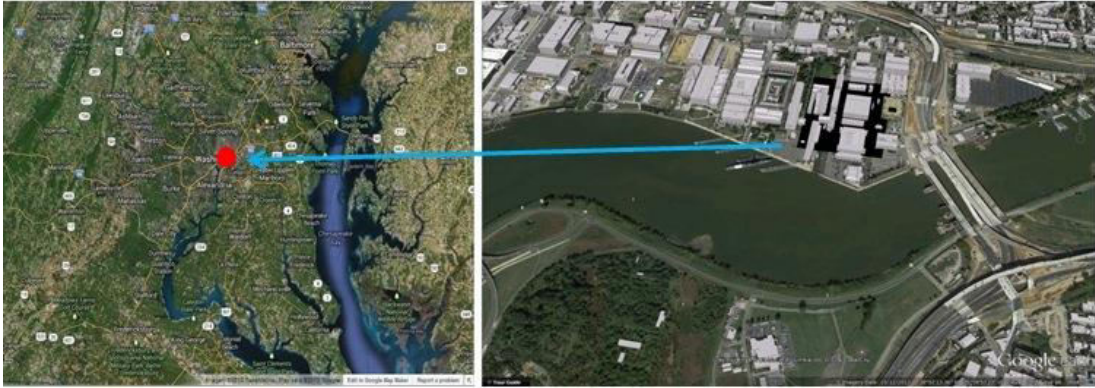


**Figure 4.3** Site of SRM 1649b collection in Washington D.C. The Navy Yard is located in the southeast section of Washington, DC on the Anacostia River, latitude  $38^{\circ}52'28''$ , longitude  $76^{\circ}59'40''$  W, altitude, 3 m AMSL. During the period of collection, 1977 to 1978, the area was surrounded by Interstate 395 to the north and South Capitol Street to the south, nearby industry included production of ship products, weapons, and ammunition.



**Figure 4.4** Baghouses used for SRM 1649b Urban Dust collection. Courtesy of Lane Sander.



#### 4.2.3.1 Qualitative analysis

A multistep approach was applied in the qualitative identification of organic acids in SRM 1649b WSOC extract. SRM 1649b was screened for alkanolic acids previously reported to have been observed in atmospheric particulate matter (see Table 4.2). Ions that did not match the initial list of standards were tentatively identified based on precursor ion  $m/z$  and retention data. Verification was made through comparison to reference standards. For example, in Figure 4.5A,  $m/z$  191 was tentatively identified as citric acid. The presence of such polyacids in aerosol was reported by Decesari et al., (2000) and Chang et al., (2005) [[Chang, 2005](#); [Decesari et al., 2000](#)]. As shown in Table 4.2, MS/MS of citric acid produces product ions corresponding to losses of COO and H<sub>2</sub>O. The doublet peak shape with the same  $m/z$  precursor and product ions suggested that an isomer of citric acid was also present, possibly isocitric acid. An isocitric acid standard was obtained and confirmed to be present in SRM 1649b. Another constituent with precursor ion  $m/z$  191 was observed in the monoacid region of the separation. The molecular weight was inconsistent with water soluble nonbranched alkanolic acids and tentatively attributed to either a linear branched or cycloalkanoic acid. The presence of quinic acid (a cycloalkanoic acid, MW of 192, present in the leaves of many plants) was confirmed based on reference standards.

The same process was used to confirm the presence of levulinic, shikimic, 2-hydroxybutyric, 2-hydroxy-3-methylbutyric, and galacturonic monoacids. The presence of alkanolic monoacids butanoic, pentanoic and hexanoic acids was also evaluated since shorter straight-chained monoacids have been reported [[Kawamura et al., 1985](#)]. Due to incomplete resolution by this method, the presence of monoacids in the SRM is only

tentatively confirmed. In the aromatic region, this process was used to identify syringic plus the three hydroxyacid isomers. Isomeric dicarboxylates were, at best, partially resolved by IC and not resolved by CID. In these cases, only the total area under the respective  $m/z$  can be estimated. These initial screening methods should be followed up with more precise quantification methods. Decomposition or hydrolysis of condensed phase composition and the stability of these complex samples warrant additional study.

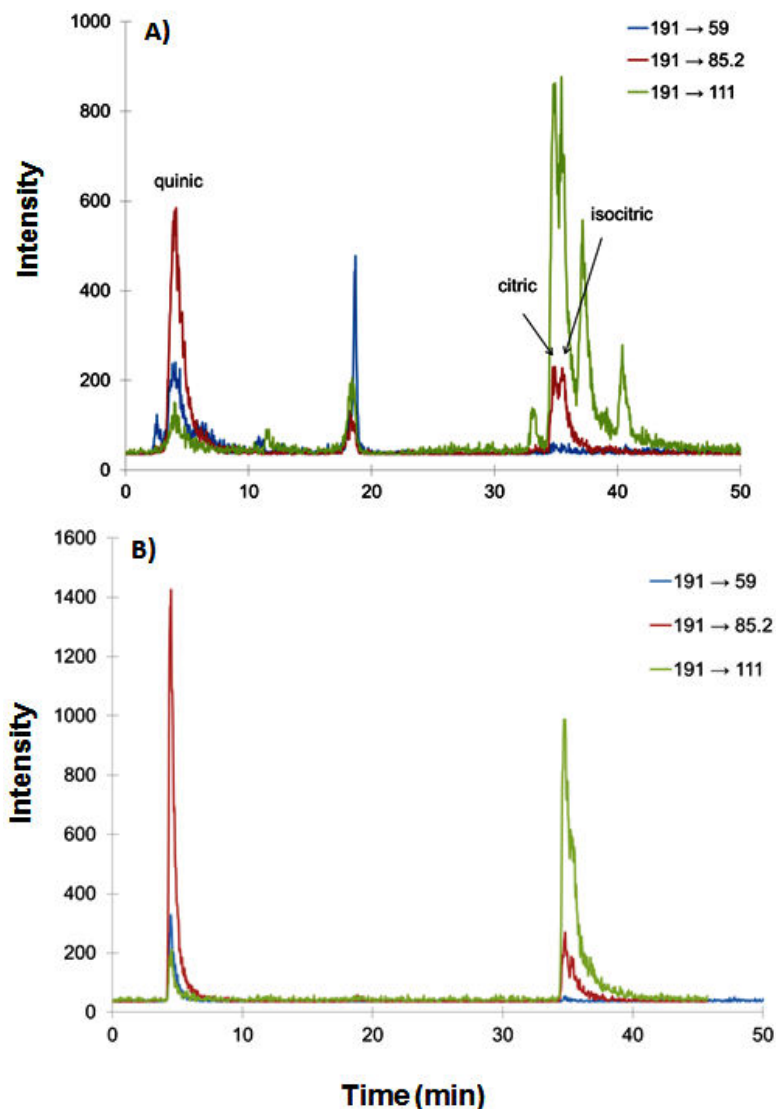


**Figure 4.5** MRM transitions for  $m/z$  191 in stock solution and SRM 1649b. A) MRM transitions for  $m/z$  191 observed in SRM 1649b. B) MRM  $m/z$  191 transitions observed in the calibration standard.

#### 4.2.3.2 Quantitative results

Six water-soluble species were quantified by MS/MS (Figure 4.6 and listed in Table 4.2) using SRM-based calibrants. Requisites for quantification are: 1) baseline resolution and 2) CID transition intensity ratio match with reference standards.

Quantitative evaluation was limited to acids that could be referenced against an SRM or a purity verified standard.

Shifts in solute retention were observed for extracts of SRM 1649b compared with calibration solutions. These retention shifts were caused by high concentrations of sulfate and nitrate in SRM 1649b; shifts of several minutes were observed in the diacid region. The source of the retention shift was verified by comparing organic acid stock solutions, spiked with different levels of organic species and inorganic species, to WSOC SRM 1649b extract. As ratios of the inorganic to organic species in the stock solution approached ratios representative of SRM 1649b, the diacid retention times of the standard and the SRM 1649b samples approached one another. Shifts in retention did not significantly affect quantitation of the organic acids.

Selection of appropriate internal standards with complex matrix samples is challenging. Several internal standards representative of the constituents in each molecular class are needed. In this work, two species which achieved baseline resolution in standard solutions (nitrite and fumaric acid) and whose presence was not observed in 1649b did not result in baseline resolution when added to SRM 1649b. Quantitation was based on an external calibration approach using SRM-based calibrants.

The acid mass fraction in SRM 1649b ranges from 0.143 to 20.28  $\mu\text{g} / \text{g}$  (see Table 2).  $R^2$  values for all calibration curves were greater than 0.99. Single factor analysis of variance was run to evaluate the intraday precision and the interday precision. The intraday precision represents variation of the mean as a result of the measurement method and interday precision represents variation of the mean resulting from the extraction procedure. A dash for the interday precision indicates that the variation measured between extractions was greater than day to day method variation. Limits of detection and limits of quantitation, calculated as 3X and 10X the standard deviation of the blank and divided by the slope of the calibration curve, were in the high pg/g to low ng/g range by this method. Individual compound signal to noise ratios would be improved with single reaction monitoring instead of simultaneously scanning all MRMs throughout the entire run.

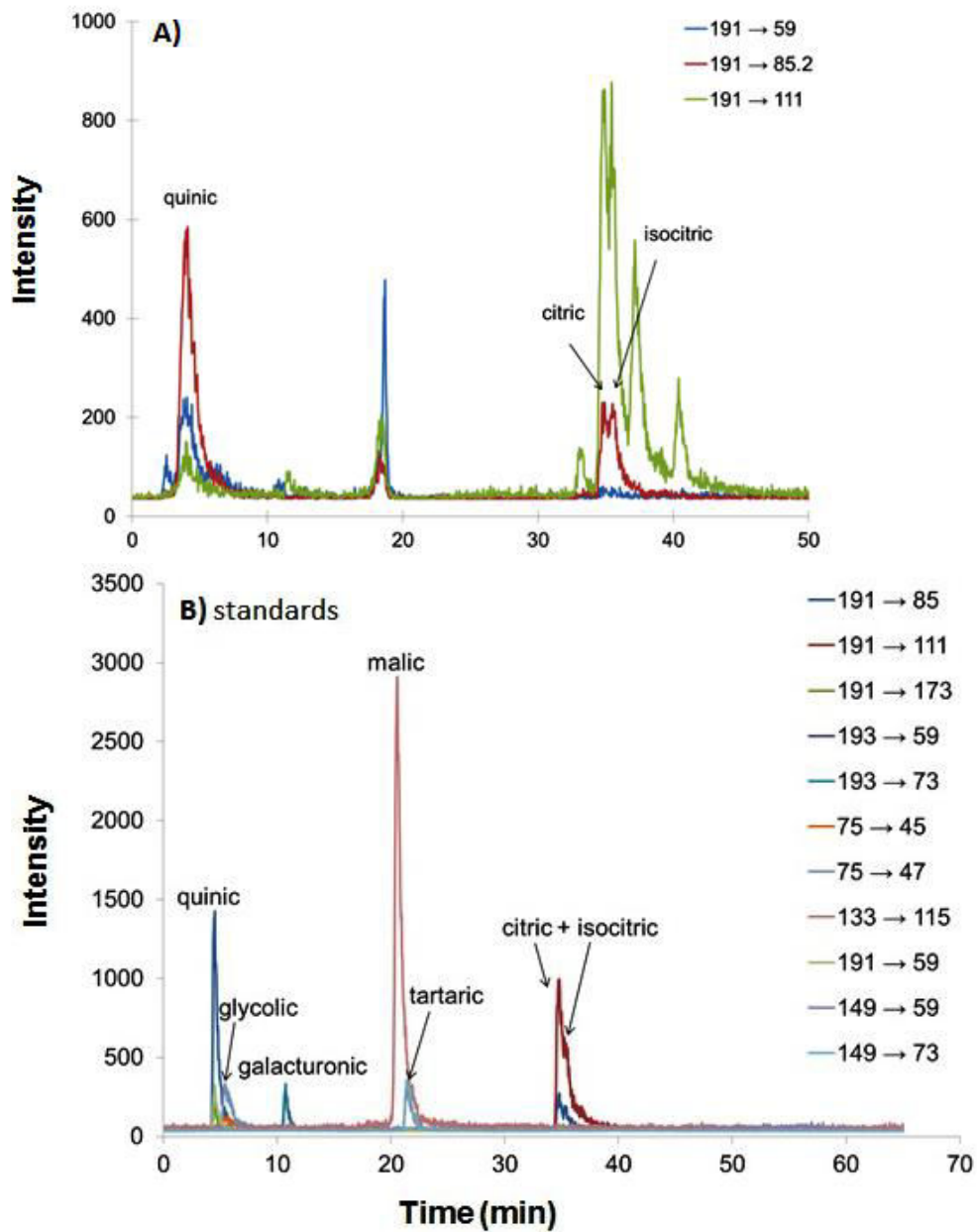


*Figure 4.6 IC/QQQ analysis of acids selected for quantitation. A) SRM 1649b and B) organic acid reference standards by IC/MS/MS*

**Table 4.3** Measurements of 6 *m/z*s in SRM 1649b. The average is calculated as the averaged acid value of each extract measured over 5 days. The uncertainty of the mean is the standard deviation of the averaged values. LOD is 3 times the blank signal divided by the slope of the calibration curve ( $LOD=3*S_{bl}/m$ ).  $LOQ = 10*S_{bl}/m$ .

| Acid                             | Acid Avg. ( $\mu\text{g/g}$ ) | Sigma | 95% confidence interval | LOD        | LOQ        | intraday precision | interday precision | calibration range ( $\mu\text{g/g}$ ) |
|----------------------------------|-------------------------------|-------|-------------------------|------------|------------|--------------------|--------------------|---------------------------------------|
| Quinic<br>191→85                 | 4.163                         | 0.012 | 0.032                   | 0.000<br>2 | 0.000<br>5 | 0.213              | -                  | 12 to 485                             |
| Glycolic<br>75→47                | 20.28                         | 0.26  | 0.709                   | 0.023      | 0.078      | 1.365              | 0.839              | 19 to 795                             |
| Galacturonic<br>193→73           | 3.823                         | 0.007 | 0.019                   | 0.000<br>6 | 0.002<br>1 | 0.239              | -                  | 2 to 97                               |
| Tartaric<br>149→73               | 0.143                         | 0.063 | 0.175                   | 0.003      | 0.009      | 0.035              | 0.228              | 12 to 507                             |
| Malic<br>133→115                 | 3.641                         | 0.086 | 0.238                   | 0.003      | 0.009      | 0.155              | 0.306              | 12 to 496                             |
| citric +<br>Isocitric<br>191→111 | 7.219                         | 0.031 | 0.085                   | 0.002      | 0.007      | 0.544              | -                  | 17 to 695                             |

### 4.3 Conclusions

This study reports the application of directly coupled IC/MS/MS to the molecular characterization of organic acids in atmospheric PM. The combination of ion chromatography and mass spectrometry significantly increases the number of ions for which a single IC procedure can be optimized due to the increased selectivity of the approach.

The application of tandem IC/MS/MS resulted in the identification of 9 additional compounds present in SRM 1649b that were not initially selected for screening against known standards. Both the IonPac<sup>®</sup> AS 17-C low capacity column and the IonPac<sup>®</sup> AS11 HC columns achieve organic acid class separation. Baseline resolution between nitrate and organic diacids was achieved with an IonPac<sup>®</sup> AS 17 column. Baseline

resolution of individual acids with their acid class was achieved through selective detection provided by MRM.

The molecular speciation of aerosol composition is important for understanding mechanistic pathways and ultimately for apportioning aerosol sources. Atmospheric aerosols are complex matrices with many sources that lead to multiple products. Only through a combination of methods can the link between sources and products be fully discovered and properly integrated into models. Further development of IC/MS/MS based methods is planned for application to the quantification of WSOC components in particulate matter.

## CHAPTER 5: RESULTS AND DISCUSSION (part A continued) on the correlation of particulate matter size and density to aerosol composition

### 5.1 Introduction

Prior to the mid-1990s understanding inorganic particles of anthropogenic origin, such as sulfate and nitrate in addition to measurements of natural sources such as sea salts and other minerals was the primary focus of aerosol studies [[Andreae et al., 1988](#); [Hegg et al., 1993](#); [J Z Sheridan, W.H., 1989](#)]. As observations (both surface-based [[Novakov and Penner, 1993](#)] and airborne [[Novakov et al., 1997](#)]) revealed that carbonaceous aerosol also constitute significant PM fractions, focus shifted to understanding both the organic and the inorganic composition. Airborne observations are particularly useful for understanding aerosol sources and transport. In the GoMACCS flight experiment, August – September 2006, Houston, TX, Sorooshian et al. (2007), reported a 5% increase in oxalic acid due to cloud processing. Data from 22 flights up to 5 km altitude also showed changes in mono- and dicarboxylate concentrations with respect to BL versus FT sampling, a power plant plume, a shipping channel, a port area and over the Gulf of Mexico. Carlton et al (2008) compared ICARTT flight data to models and found that inclusion of SOA formed through cloud processing improved OC model and measurement agreement. The ability to estimate the additional impact of regional emissions on local air quality is necessary for the development of policy which effectively limits adverse human health, maintains visibility for productive commerce, and limits contributions to global radiative forcing. As the primary industrial and



transportation fuel sources change both nationally and globally, so will the resulting emissions products. The conceptual framework of models used to manage air quality must be capable of capturing the impacts these changes. This can be achieved only with a thorough understanding of the source, fate and transport of atmospheric pollutants.

As reviewed in chapter 2, aircraft measurements for the vertical resolution of carbonaceous aerosol typically rely on bulk property observations obtained by AMS [[Heald, 2011](#)], inorganic ion concentrations sampled by PILS-IC, total PM, TC and/or TOC . While these measurements have the benefit of better temporal resolution they lack the molecular resolution of end state aerosol products. The previous chapter provides a thorough description of the IC/MS/MS method developed for the analysis of water soluble organic aerosols collected onto quartz fiber filters during flights with the UMD Cessna 402. The results discussed in this chapter are of the molecular species resolved by IC/MS/MS from aircraft filter collection and the correlation of these observations to simultaneous *in situ* observations of particle size, ozone and sulfur dioxide abundances and local meteorology.

### 5.1.1 Flight description and sampling conditions

The 21<sup>st</sup> and 23<sup>rd</sup> of July 2011 are the third and last day of a six-day air quality episode. A description of the meteorological conditions driving the air quality episode can be found on the Maryland Department of Environment website, [http://www.mde.state.md.us/programs/Air/AirQualityMonitoring/Documents/Summaries/AQSummaryDC\\_2011\\_Jul.pdf](http://www.mde.state.md.us/programs/Air/AirQualityMonitoring/Documents/Summaries/AQSummaryDC_2011_Jul.pdf). Briefly, a combination of record high temperatures, a lingering tropical storm off the Atlantic delivering warm humid air to the region, while a

current of westerly winds across the Appalachians resulting in a Lee-Side trough along the I-95 corridor produced a stagnation event. The resultant air quality index due to exceedances in ozone was a string of code orange, USG, days over eastern Maryland. Maryland, west of the I-95 corridor maintained code yellow or a moderate AQI for all days except 22 July. USG conditions due to O<sub>3</sub>, unhealthy for sensitive groups, extended east of the I-95 corridor on 22 July. A discussion of the air quality episode and impacts of the bay breeze occurring east of the I-95 corridor has been published [\[H. He et al., 2013a\]](#).

Filter samples were collected at ~ 1 km above mean sea level during a boundary layer transect beginning southwest of Baltimore, MD and extending into the Appalachian mountains of rural western Maryland. The land beneath the collection track is covered primarily with deciduous trees and dotted sporadically with open fields and small cities. The landscape of the flight tracks are shown in the Google earth view of Figure 5.1A. Table 5.1 lists the collection parameters and meteorological conditions across the sample transect. Following the filter collection during the horizontal transect, three vertical profiles were flown over the rural area upwind of the Baltimore / Washington, D.C. metropolitan area. The relationship between our measurement altitude and our position within the troposphere was determined by the first spiral at the completion of filter sample collection. This spiral, over Cumberland, MD, verified that collection was conducted within the BL. See Figure 5.2. NOAA HYSPLIT trajectories are used to correlate the flight observations to the air mass. Figure 5.3 shows 24 hr. backward and forward trajectories across the sampling region at altitudes of 0.5, 1.0, and 1.5 km (red, blue and green, respectively). Each 24 hr. backward trajectory is paired with a 24 hr.

forward trajectory to illustrate the recirculating air pattern influencing the 21 July aerosol composition. Trajectories for 20 and 21 July show a re-circulating pattern including winds from the Ohio River Valley, east by southeasterly winds influenced by marine air from the tropical storm and recycled air from the northeast. By the morning of 22 July, the re-circulating pattern ceased and the 23 July sampling region was fed by an influx of air from the west by northwest only.

**Table 5.1** Collection parameters and average meteorological conditions across the sampling region. Numbers in parenthesis are RSD %.

| Sample date                  | Sample Time (EDT) | Sample Time (min) | Altitude (km) | Aerosol concentration ( $\mu\text{g}/\text{m}^3$ ) | $T_{\text{avg}}$ ( $^{\circ}\text{C}$ ) | $\text{RH}_{\text{avg}}$ (%) |
|------------------------------|-------------------|-------------------|---------------|--|---|------------------------------|
| 21 July<br>2011 Filter<br>19 | 0927– 1005        | 38                | 0.91 (0.5)    | 35 (6)   | 24.2 (2)                                | 62.1 (8)                     |
| 23 July<br>2011<br>Filter 11 | 0741 – 0823       | 42                | 0.76 (0.6)    | 32 (6)   | 25.1 (6)                                | 63.1 (3)                     |

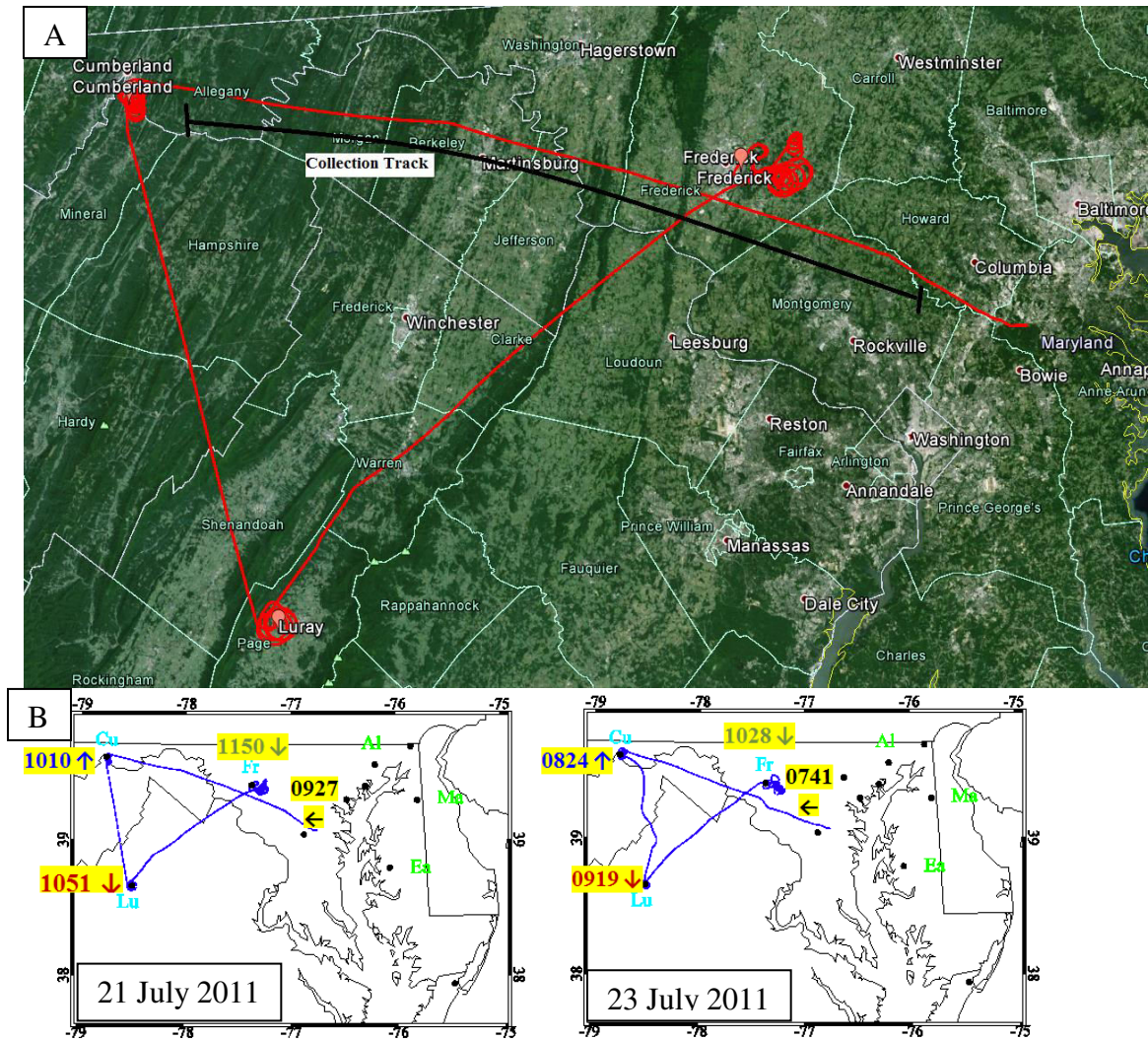


**Figure 5.1** Flight tracks. Figure 5.1A. Flight tracks laid over Google Earth show the topography over which filter sample collection occurred. Figure 5.1B. Flight tracks shown with respect to sampling phase during the UMD research flights. Each time stamp is the beginning of that sampling phase. The initial horizontal transect was 35 to 40 minutes. Column measurements (spirals) took approximately 20 minutes.

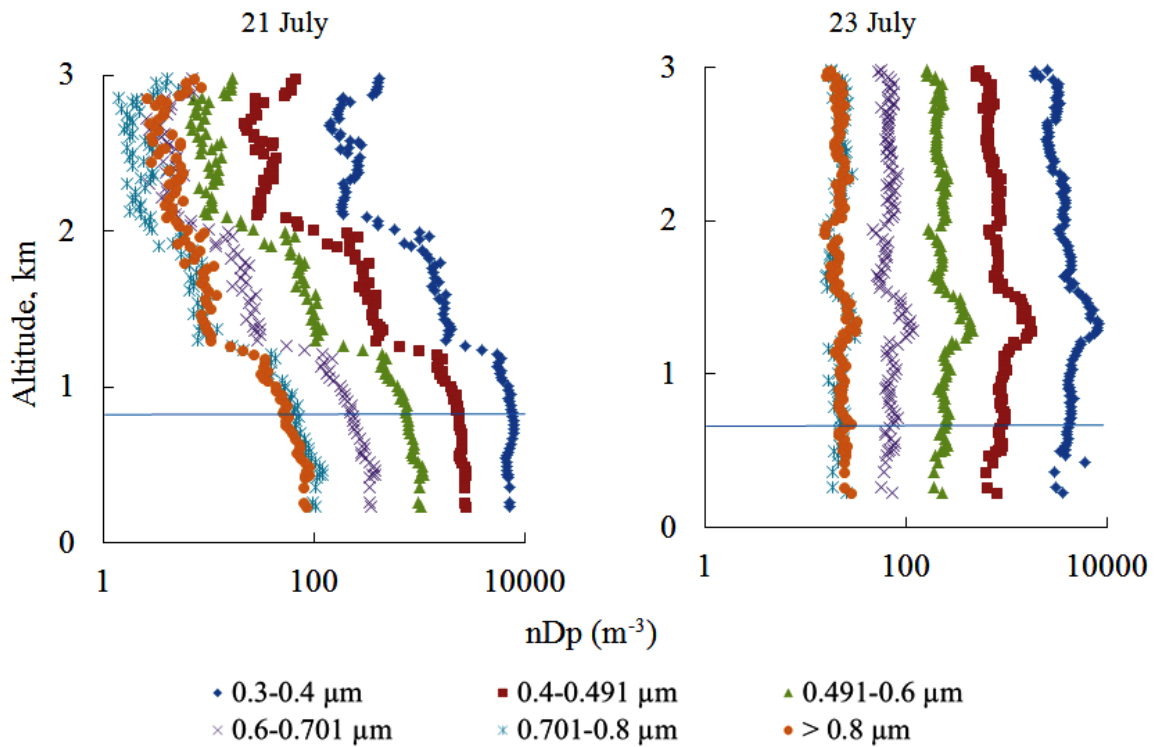


**Figure 5.2** Vertical profiles of particle number density over Cumberland, MD, 2011. Spirals flown at approximately 90 m/s show the vertical distribution of particle density upwind of the Baltimore / Washington D.C. metropolitan area. The altitude range is 0.23 to 3.0 km. The blue line shows the preceding filter collection altitude.

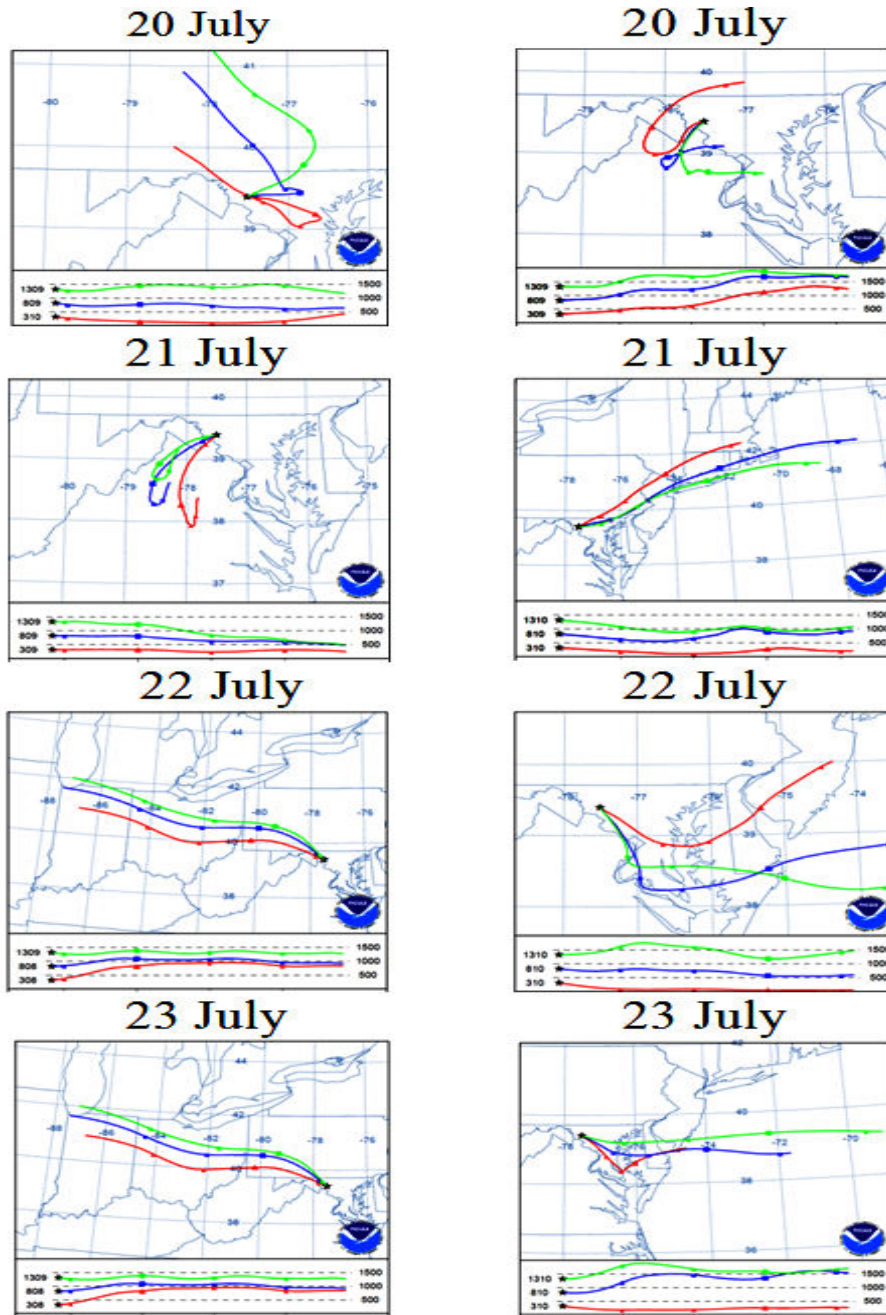


**Figure 5.3** NOAA HYSPLIT model, 24 hr. trajectories over the region of filter sample collection. GDAS meteorological data. Backward trajectories end at 0700 UTC, Forward trajectories start at 0700 UTC. Colors red, blue, and green are for altitudes 0.5, 1.0, and 1.5 km, respectively. The weak, recirculating winds of the 20<sup>th</sup> and 21<sup>st</sup> gave way to strong westerlies on the 22<sup>nd</sup>. The location is 39.39 N 77.51 W.

## 5.2. Results

### 5.2.1 *In Situ* optical measurements

The particle density and size measurements from 21 and 23 July, the 3<sup>rd</sup> and 6<sup>th</sup> day of the air quality episode, Figure 5.4 and Table 5.2, show average *in situ* trace gas and particle size information observed during the collection period. The relative standard deviation (RSD in percent) for the averages is shown in parenthesis. While all gas and aerosol measurements were higher on 21 July 2011 than on 23 July 2011 the differences are within or nearly within statistical uncertainty of each other. The low RSD for ozone reflects a more constant or homogeneous mixing ratio across the measurement transect while the higher RSD for SO<sub>2</sub> and particle counts indicates greater variability with respect to time and location. SO<sub>2</sub> and particles are not evenly distributed across the sampling transect. The last row of Table 5.2 reports 21 July to 23 July ratios for each transect average.

**Table 5.2** *In situ* aircraft trace gas and aerosol size data. Reported in this table are the average measured values across the measurement time period for the two days in this study. In parenthesis next to the average is variability of the average (%) across the measurement. Ratios are the ratio of the ratio of the measurement averages on 21 July / 23 July. Lastly, the instrument DL's in nmole/mole or measurement uncertainty (%) are reported. The standard deviation of the average particle counts across the measurement period is significant only if it is greater than the instrument uncertainty.

| Sample date             | O <sub>3</sub><br>ppb | SO <sub>2</sub><br>ppb | 0.3-0.4<br>µm<br>nDp m <sup>-3</sup> | 0.4-0.5<br>µm<br>nDp m <sup>-3</sup> | 0.5-0.6<br>µm<br>nDp m <sup>-3</sup> | 0.6-0.7<br>µm<br>nDp m <sup>-3</sup> | >0.8<br>µm<br>nDp m <sup>-3</sup> | 0.01-1<br>µm<br>nDp m <sup>-3</sup> |
|-------------------------|-----------------------|------------------------|--------------------------------------|--------------------------------------|--------------------------------------|--------------------------------------|-----------------------------------|-------------------------------------|
| 1                       | 2                     | 3                      | 4                                    | 5                                    | 6                                    | 7                                    | 8                                 | 9                                   |
| 21 July 2011            | 74<br>(7)             | 5 (62)                 | 45 (36)                              | 12 (26)                              | 4 (25)                               | 1 (32)                               | 0.3<br>(33)                       | 0.00135<br>(36)                     |
| 23 July 2011            | 67<br>(3)             | 4 (53)                 | 36 (31)                              | 8 (38)                               | 2 (43)                               | 0.7<br>(47)                          | 0.2<br>(41)                       | 0.00131<br>(23)                     |
| Ratio                   | 1.1                   | 1.25                   | 1.23                                 | 1.49                                 | 1.57                                 | 1.61                                 | 1.53                              | 1.03                                |
| Instrument accuracy (%) | 1.5                   | 3.4                    | 10                                   | 10                                   | 10                                   | 10                                   | 10                                | 20                                  |

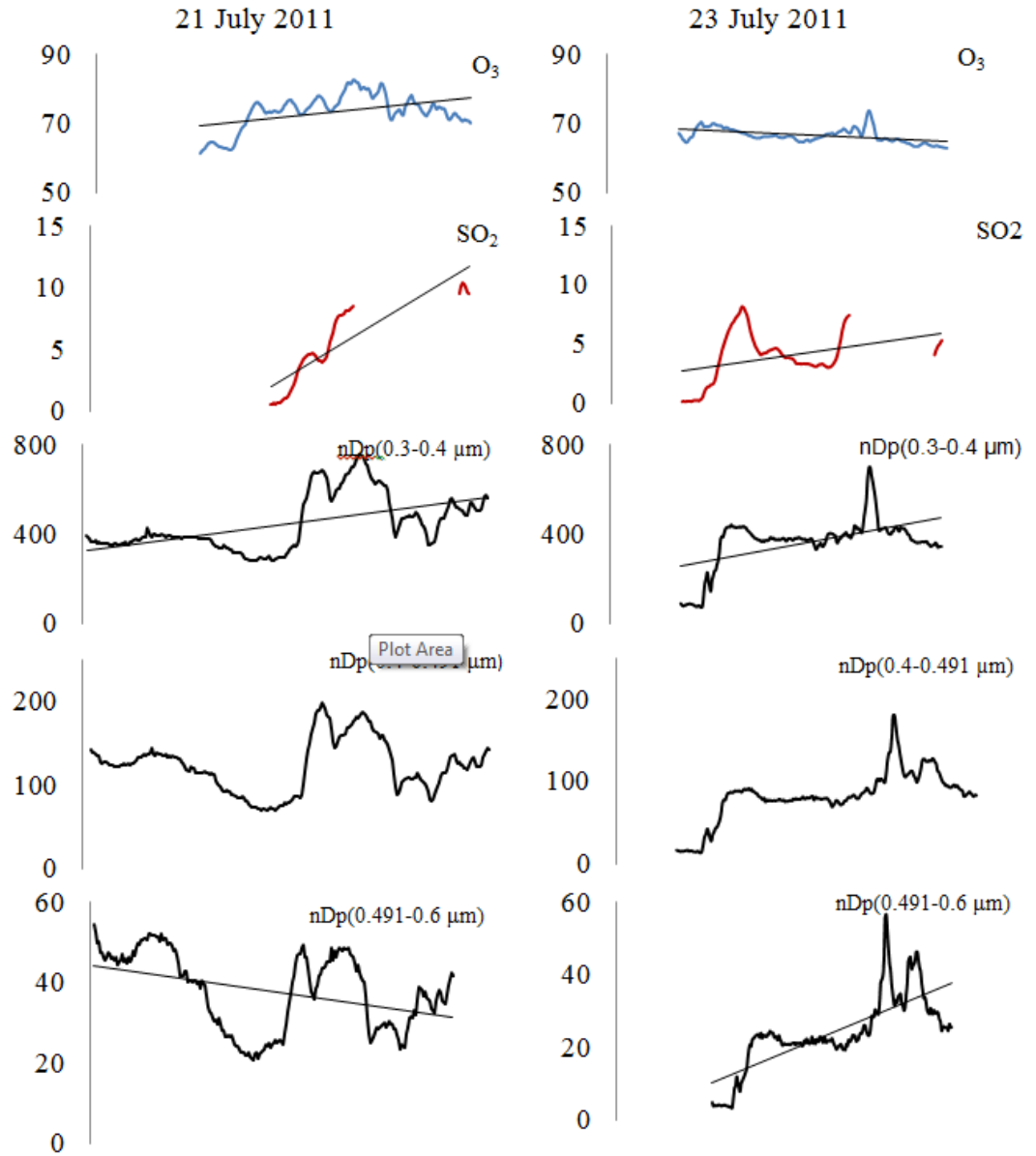
Collection of information on particle size, number density, scattering and absorption through optical methods may provide clues about aerosol sources and fate. Aerosols have been observed to show a trimodal size distribution. In this distribution the supermicron fraction composes the coarse mode, the 0.1 to 1.0  $\mu\text{m}$  fraction composes the accumulation mode and everything less than 0.1  $\mu\text{m}$  is assigned to the nucleation mode. The accumulation mode has been found to be bi-modal itself. Within the accumulation mode, particles with diameters of 0.2  $\mu\text{m}$  +/- 0.1  $\mu\text{m}$  are classified as condensation mode particles. Particles with diameters of 0.7  $\mu\text{m}$  +/- 0.2  $\mu\text{m}$  are classified as droplet mode particles [John *et al.*, 1990]. Condensation mode particles are proposed to be products of gas phase chemistry and are important to cloud formation. Droplet mode particles are aged condensation mode particles and grow as a result of further atmospheric processing in the presence of sulfate, nitrate and organics [Meng and Seinfeld, 1994; Pandis, 1993]. In this work, Table 5.2 shows that beginning with particle bin 0.4  $\mu\text{m}$  and extending through bin >0.8  $\mu\text{m}$ , the ratio of day 3 to day 6 transect averages is approximately 1.5. While the number of condensation mode particles dominates on both days the droplet mode particles on 21 July exceed 23 July droplet mode particles by ~ 50%. These data suggests a correlation between recirculating aged urban air with a greater abundance of droplet mode particles. The CPC does not size segregate the particles, it reports 1 bin for 0.01 to 1  $\mu\text{m}$  diameter. The CPC Day 3 to Day 6 ratio approaches 1 indicating that even though the fractionated ratios change, the total number of particles counted remains relatively constant.

Figure 5.4 shows the *in situ*, trace gas and particle counts for each size bin plotted with respect to time. A trend line is also plotted for each transect. The slope of the trend



line shows very generally whether the trend beginning east of Baltimore running out to western Maryland border is positive or negative. From this time series it is observed that:

- 1) SO<sub>2</sub> and condensation mode particles (particle diameter < 0.32 μm) show more fine structure than larger particles across the sampling transect. Droplet mode particles are more evenly distributed.
- 2) On 21 July droplet mode particles do not trend with the condensation mode particles, while on 23 July droplet mode and condensation mode particles do trend with one another.
- 3) Higher density of larger particles at the early stage of collection on 21 July is correlated to the aged, recirculating urban air.



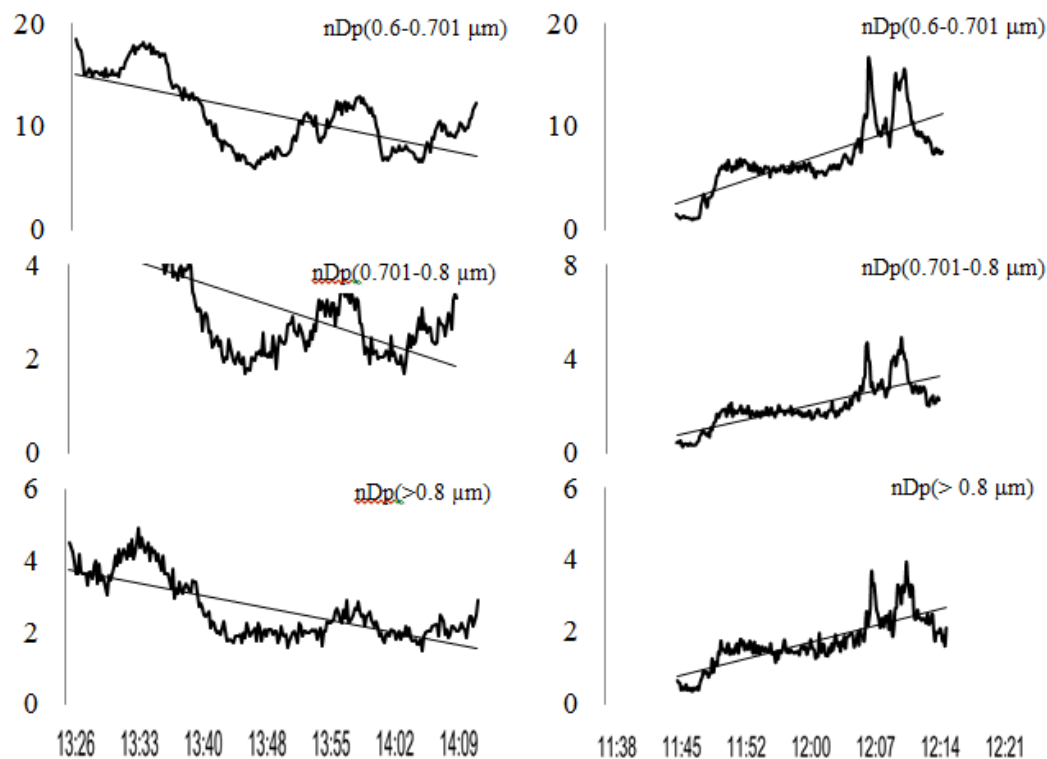


**Figure 5.3** *in situ* trace gas and particles observed across the collection transect on 21 and 23 July 2011. Collection began just south of Baltimore, MD and near the state's western border close to Cumberland, MD.

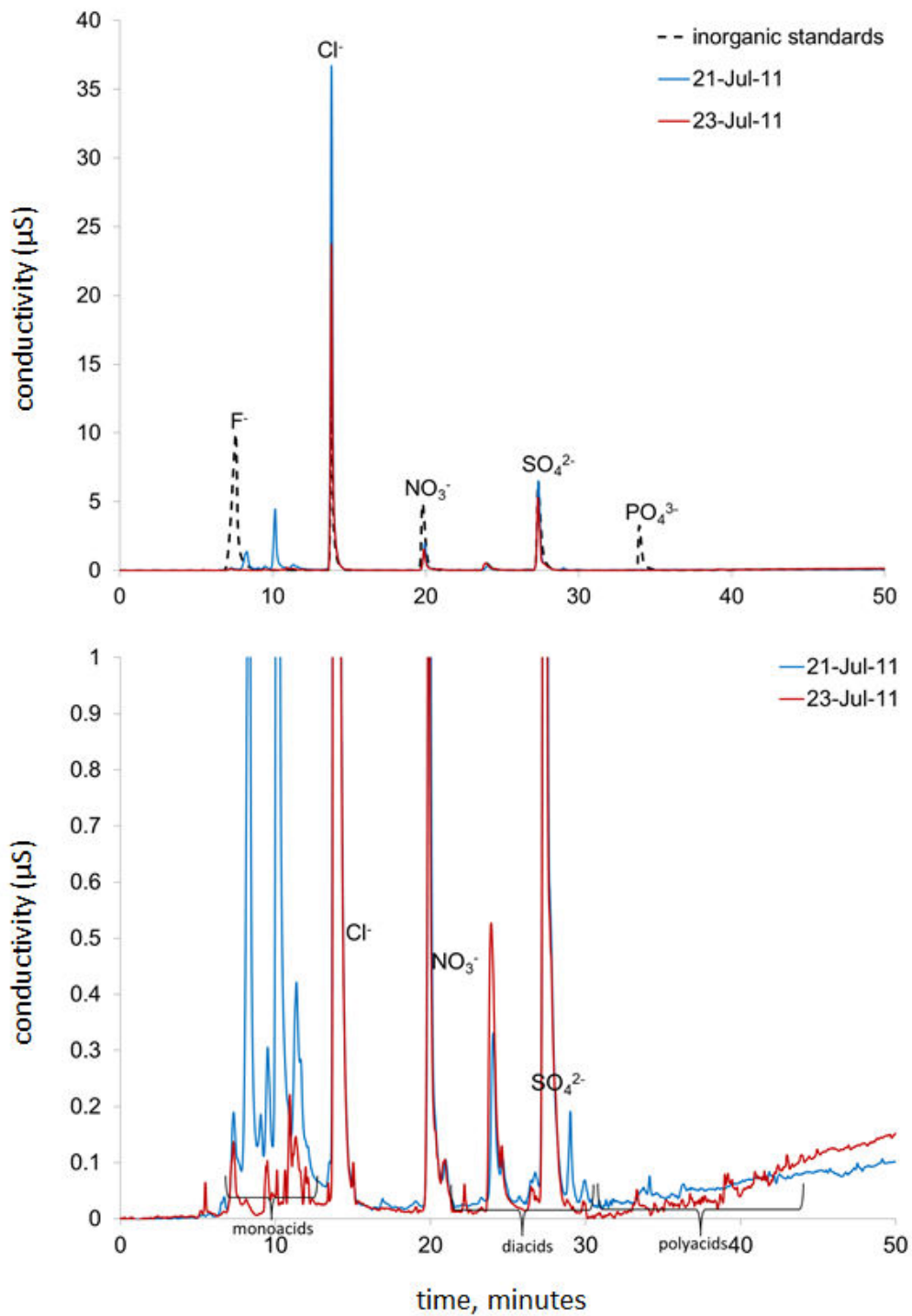
### 5.2.2 Filter sample analysis

Figure 5.5 shows the conductimetric response to the chromatographically separated water extract of the aerosol filter samples. The overlay of inorganic standards shown in Figure 5.5A demonstrates the suitability of this nonselective detector for the sampling of inorganic ions that typically dominate IC aerosol analysis [[Edney et al., 2003](#); [Matta et al., 2003](#); [Surratt et al., 2007](#); [Wang et al., 2002](#)]. The conductimetric response between 0 and 1  $\mu\text{S}$  (Figure 5.5B) indicates a number of partially resolved compounds, with less intense conductimetric responses.

Tandem MS/MS analysis of the aircraft filter samples included monitoring 27 precursor to product ion transitions for 37 species. Of the 31 transitions monitored, 74%

of the organic and inorganic ions could be observed qualitatively. In total, 16 organic acids, three inorganic anions, and five inorganic cations exceeded the LOD (3xSbl/slope). 12 of the 16 organic acids exceeded the limit of quantitation (LOQ) on at least one of two collection days. Table 5.3 lists the acids observed with respect to collection day. An estimation of acid concentration is provided only if the measurement exceeded the LOQ. While all compounds observed on 23 July were also observed on 21 July, filters taken on 21 July included 12 additional organic acids above the LOD and 8 organic acids with concentrations greater than the method LOQ.

Quantifiable organic aerosol mass measured by IC/MS/MS accounted for approximately 10% of the total mass on 21 July. This fraction was dominated by oxalic acid, which constituted approximately 66% of the fraction. On 23 July, quantifiable organic aerosol measured by IC/MS/MS accounted for 2% of the total mass with cis-pinonic acid comprising the dominant fraction.



**Figure 5.5** IC separation of aerosol collected onto filters during flights. Figure 5.5A is the IC separation of filter samples collected on two poor air quality days over Maryland. The dotted black line is an overlay of reference standards used for peak identification. Figure 5.5B is the same as Figure 5.5A but with the y-axis range limited to 1  $\mu\text{S}$ .

**Table 5.3** Molecular constituents of aerosol measured at 1 km altitude over western Maryland on the third and sixth day of an air quality episode in July 2011. Greater than and less than signs are used to indicate if the detection was above or below the limit of detection or quantitation.

| Acid   | 07/21<br>Acid<br>( $\mu\text{g}/\text{m}^3$ ) | % total<br>PM | LOD | LOQ | 07/23<br>Acid<br>( $\mu\text{g}/\text{m}^3$ ) | % total<br>PM | LOD | LOQ |
|--|---|---------------|-----|-----|---|---------------|-----|-----|
| Glycolic   | 0.135   | 0.392         | >   | >   |   |               |     |     |
| Butanoic   | 0.286   | 0.827         | >   | >   |   |               |     |     |
| pyruvic  | 0.079   | 0.223         | >   | >   |   |               |     |     |
| 2-OH-butyric                                     | ---   | ---           | <   | <   |   |               |     |     |
| 2-OH-3-CH3-<br>butyric                           | 0.018   | 0.053         | >   | >   | 0.022   | 0.068         | >   |     |
| Levulinic  | 0.077   | 0.224         | >   | >   |   |               |     |     |
| Cis pinonic                                      | ---   | ---           | --- | --- | 0.615   | 1.907         | >   |     |
| Oxalic acid                                      | 2.290   | 6.627         | >   | >   |   |               |     |     |
| Succinic/<br>methylmalonic                       | 0.410   | 1.188         | >   | >   |   |               |     |     |
| Glutaric/<br>methylsuccinic                      | ---   | ---           | <   | <   |   |               |     |     |
| Tartaric   | ---   | ---           | >   | <   |   |               |     |     |
| Maleic   | 0.008   | 0.022         | >   | >   |   |               |     |     |
| Adipic/3-<br>methylglutaric/<br>2-methylglutaric | 0.116   | 0.337         | >   | >   | ---   | ---           | >   |     |
| Fumaric  | ---   | ---           | >   | <   |   |               |     |     |
| Dipicolinic                                      | 0.030   | 0.087         | >   | >   | 0.033   | 0.102         | >   |     |
| 4-hydroxybenzoic                                 | ---   | ---           | <   | <   | ---   | ---           | <   |     |
| 3-hydroxybenzoic                                 | ---   | ---           | <   | <   | ---   | ---           | <   |     |
| 2-hydroxybenzoic                                 | 0.004   | 0.013         | >   | >   | 0.006   | 0.017         | >   |     |
| citric   | ---   | ---           | >   | <   | ---   | ---           | >   |     |
| Sulfate  | 7.02  | 20.32         | >   | >   | 7.09  | 23            | >   |     |
| Nitrate  | 1.567   | 4.54          | >   | >   | 2.763   | 8.57          | >   |     |
| Nitrite  | 0.218   | 0.63          | >   | >   | 0.013   | 0.04          | >   |     |
| Sodium   | 15.90   | 46            | >   | >   | 7.590   | 23            | >   |     |
| Ammonium   | 0.010   | 0.03          | >   | >   | 0.010   | 0.03          | >   |     |
| Potassium  | 1.737   | 3.69          | >   | >   | 1.058   | 3.28          | >   |     |
| Magnesium  | 0.579   | 1.45          | >   | >   | 0.434   | 1.35          | >   |     |
| Calcium  | 1.153   | 3.34          | >   | >   | 0.905   | 2.81          | >   |     |

### 5.3 Discussion

Comparing the changes of the horizontal profile particle number density and molecular composition to air mass trajectories shows that observations in aerosol size fractions and chemical composition can change significantly with changing air source. Changes to molecular composition can be significant even while other variables such as temperature, relative humidity and trace gas abundances remain relatively constant.

In both extract volumes, a number of peaks are present but not accounted for through comparison to the reference standard solution used in this experiment. An inherent challenge to the application of routine chromatographic methods using nonselective detectors (such as conductivity) for characterization of environmental sampling is the potential for highly variable sample complexity. This challenge is particularly relevant to atmospheric measurements whose composition and species abundance are dependent on several factors, the abundance and availability of precursor molecules, local geology and local meteorology. When assigning peaks using nonselective detectors and standard solutions that are potentially unrepresentative of the sample matrix, the possibility of shifting column retention and/or elution of multiple species under a single, baseline resolved peak must be considered. Figure 5.5B shows an abundance of partially resolved species in the monocarboxylate region. Prior aerosol analysis by GC would suggest that the end state of oxidative processing is often alkylated and hydroxylated carboxylates suggesting the presence of alkylated and alkoxyated carboxylates associated with both air masses [[Chebbi and Carlier, 1996](#); [Edney et al., 2003](#)]. Candidates for tentatively assigning observed extracted ion chromatogram (EIC) peaks  $m/z$  103 and  $m/z$  147 are malonic acid [[Rohrl and Lammel, 2002](#)] and

hydroxyglutaric acid [[Kawamura et al., 2012](#)], respectively. The most commonly reported dicarboxylates, oxalic, malonic, succinic, tartaric, and maleic acids were observed in the air mass influenced with aged, tropical, and recirculating air while only *m/z* 145 adipic acid plus possible isomers were observed in quantity above the LOD in the new, westerly air mass [[Gao et al., 2003](#); [Hsieh, 2009](#); [Kawamura et al., 2012](#); [Rohrl and Lammel, 2002](#)]. Frequently, speciation of organic acids present in aerosol is conducted on ground samples with much higher sample volumes. In the IC/CD organic separations reported from the ground collections, particulate matter analysis of rural, urban and marine air reports higher ratios of dicarboxylate acids to be associated with continental and urban air masses [[Kawamura et al., 2012](#); [Rohrl and Lammel, 2002](#); [Tsai, 2008](#)]. In this work, sample collections were too small for evaluation of ratios from day to day, but the observations of the most commonly reported diacids on 21 July, and only one of the commonly reported diacids on 23 July indicates higher concentrations of the most commonly reported diacids acids with the contribution of aged, urban sources.

Oxalic acid is frequently reported as the most abundant organic acid [[Carlton et al., 2008](#); [Hsieh, 2009](#); [Sorooshian et al., 2007](#)], and indeed on 21 July and in SRM 1649 b, oxalic acid was the most abundant organic acid observed. A greater number of mono- and dicarboxylate aerosols present on 21 July correspond to the greater abundance of droplet mode particles. On 23 July, cis-pinonic acid, a reaction product of pinene after ozonation and photochemical oxidation [[Glausius, 1999](#); [Librando and Tringali, 2005](#)], was most abundant. Measurable levels of cis-pinonic acid in fresh aerosol indicate terpene oxidation as an important local source of PM<sub>2.5</sub>, similar to observations made by



Gao et al (2006) in the southeastern U.S. [[Gao et al., 2006](#); [Kawamura et al., 2012](#); [Rohrl and Lammel, 2002](#); [Tsai, 2008](#)].

On 21 July the air at 0.9 km altitude for the filter sample received pollutants from Washington, DC and surrounding areas. Analysis of just surface data would indicate that this episode was entirely homegrown while altitude profiles show that sources to the west, south, and northeast also contribute to poor air quality.

#### 5.4 Conclusion

Molecular determination of carboxylic acids in aircraft filter extract shows significantly higher concentrations of organic acids associated with recirculating urban and tropical air than with air in strong Westerlies. Higher sulfate to nitrate concentration ratios correspond to higher local SO<sub>2</sub> emissions on 21 July. Prior studies have suggested that higher ratios of certain dicarboxylates correspond to anthropogenic influence. The addition of MS/MS detection to CD detection increases the total number of organic species than can be simultaneously observed making this a useful tool for studying the influence of mon-, di-, and tricarboxylates. Simultaneous optical aerosol observations will help correlate optical properties to molecular characterization.

Routine monitoring and molecular speciation at different stages of air quality episodes can contribute to understanding the chemical and physical properties contributing to particle source, formation and fate. Vertical sampling reveals transport which may not be observed by ground sampling only. As the primary industrial and transportation fuel sources change both nationally and globally, so will the resulting emissions products. The conceptual framework of models used to manage air quality

must be capable of capturing the impacts these changes. This can be achieved only with a thorough understanding of the source, fate and transport of atmospheric pollutants.

## CHAPTER 6: RESULTS AND DISCUSSION (part B) on the evaluation of a newly installed inlet for particulate matter sampling on the Cessna 402.

### 6.1 Introduction

The first aerosol inlet used in the RAMMPP program from 1990-2010 was a Swagelok tube fitting connector. The inlet system aboard the UMD Piper Aztec is not designed for isokinetic sampling and has an unknown sampling efficiency (Figure 6.1). With the change in RAMMPP aircraft platforms, I installed a forward mounted shrouded aerosol inlet (Figure 6.2). To assess the UMD aerosol sampling systems, two side-by-side flights were flown. In the first comparison, the UMD Cessna 402 flew next to the NASA P3-B that carries a well-characterized aerosol system. These planes each flew the same shrouded inlet. To evaluate the archived RAMMPP aerosol scattering data, a side-by-side flight was conducted between the Cessna 402 and the Aztec. Total light scattered was used as the method of inlet comparison because the Nephelometers were common to all three aircraft.



**Figure 6.1** Piper Aztec roof mounted aerosol inlet. “Aztec Antlers” The aerosol inlet faces forward and the gas inlet faces aft. Aztec aerosol inlet was a 3 mm i.d. Swagelok Tube Fitting Connector attached to conductive tubing inserted into the forward facing (right side) antler shown above.



**Figure 6.2** Shrouded inlet diffuser on Cessna 402. This inlet, purchased from Droplet Measurements, Boulder, CO, was mounted onto the Cessna 402 and used for RAMMPP data collection as of the Summer 2011 flying season.

## 6.2 Results and discussion

Aerosol inlet transmission efficiencies were evaluated by side-by-side flights. Nephelometer performance has been thoroughly characterized both in the laboratory and in flight [[Anderson et al., 2003](#); [Anderson and Ogren, 1998](#); [Heintzenberg, 2006](#)]. Flight evaluation of the Nephelometer model 3563 on a C-130 aircraft has demonstrated that

calibration drift with respect to changing pressure (altitude) is negligible for this instrument [[Anderson et al., 2003](#)]. Change in S/N with respect to rapidly changing altitude and RH was observed to be negligible. Instrument noise is dependent upon sampling time and scattering magnitude. The demonstrated repeatability of Nephelometer measurements in conjunction with inter-instrument consistency [[Heintzenberg, 2006](#)] and measurement stability under sampling conditions of rapidly changing pressure and humidity makes this instrument ideal for comparing aerosol inlet system transmission efficiencies on various aircraft.

Table 6.1 describes the sampling configuration and sampling environment respective to each aircraft and aerosol optical cavity.

**Table 6.1** Description of NAS P3-B and UMD sampling configurations

|  | NASA P3-B                          | UMD Cessna 402                                 | UMD Piper Aztec                   |
|--|------------------------------------|--|-----------------------------------|
| Mount location                                   | Fuselage side                      | Forward of nose                                | Roof                              |
| Distance from inlet tip to inlet of Nephelometer | 2.13 m                             | 6.8 m  | 2.3 m                             |
| Cabin conditions                                 | Pressurized and climate controlled | Unpressurized, no climate control              | Unpressurized, no climate control |
| Logging intervals                                | 1 sec                              | 10 sec   | 10 sec                            |
| Comparison avg time                              | 10 sec                             | 10 sec   | 10 sec                            |
| Flow (L/min)                                     | 30                                 | 15   | 15                                |
| Range Neph sampling RH (avg, median)             | 3% to 13% (7.4, 6.2)               | 8% to 28% (17.2, 21.8) and 30% to 40% (33, 32) | 23% to 39% (29, 27)               |

### 6.2.1 Cessna 402 and P3-Binlet comparison

The Cessna SD transmission efficiency was evaluated by a side-by-side flight with the NASA P3-B during DISCOVER-AQ, July 2011. In this side-by-side comparison the inlets were mounted at different locations onto two different aircraft

using different plumbing configurations. A detailed description of the side-by-side flight plan is previously published [[Brent et al., 2013b](#)] (see Chapter 7). Briefly, the 38 minute inter plane comparison includes a 16 minute, 2.6 km transect, a 12 minute spiral from 2.6 km to 0.61 km, and a 10 minute transect at 0.61 km over the DelMarVa peninsula. Aircraft speed ranged from 50 to 110 m/s with a horizontal resolution of 540 to 100 m. The average Mach was 0.28, ranging from 0.23 to 0.32. Figure 6.3 shows the side-by-side flight comparison results where the total scattering coefficient for each wavelength, 450 nm (blue), 550 nm (green), and 700 nm (red), are plotted against time (or experiment transect high, spiral and low). Because the change in particle size with respect to humidity is negligible for RH less than 30% and the RH within the optical cavity of either Nephelometer does not exceed 30%, each of these sampling environments are considered dry even though the Cessna 402 optical cavity was always ~5 % to ~15 % more humid than the NASA Nephelometer [[Anderson and Ogren, 1998](#); [Covert, 1972](#)].

The Cessna 402 /P3-B side-by-side flight comparison has two results. The first result is observable during the spiral as the planes descend from the free troposphere into the boundary layer. During this descent, rapid changes in humidity and aerosol properties were encountered. The comparison of scattering coefficients during the descent (Figure 6.3) indicate that the NASA sampling system responds more rapidly to ambient step changes than does the Cessna 402 sampling system.

The second result was observed during periods of the comparison when ambient humidity is either constant (the high transect) or changes gradually (the low transect). Figure 6.4 is used to illustrate the scattering comparison across the constant humidity

regime. Plotted in Figure 6.4 is the ratio of Cessna 402 scattering to P3-B scattering shown in Figure 6.3 ( $\sigma_{sp}Ces/\sigma_{sp}P3-B$ ) for each point in time.

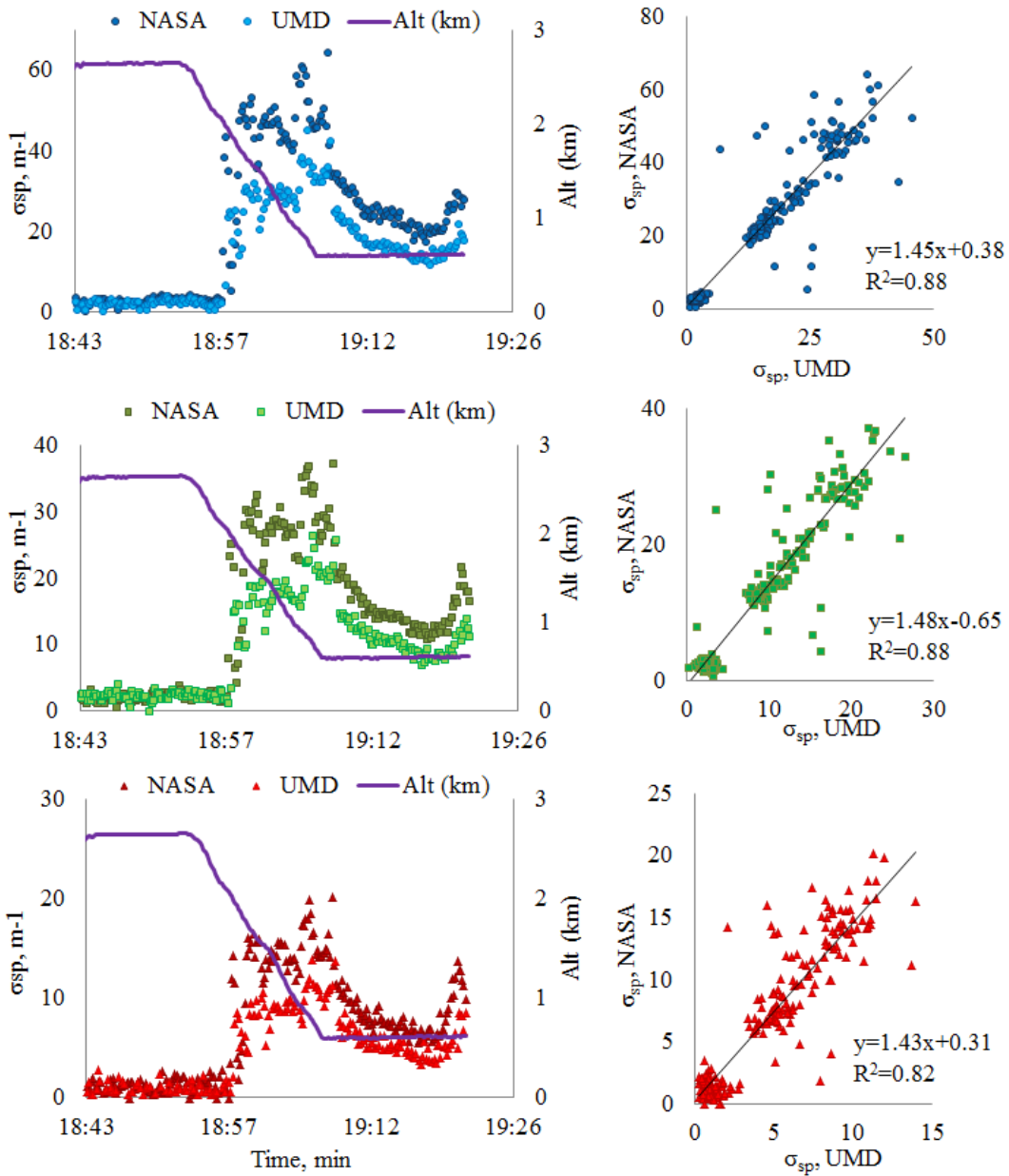


**Figure 6.3** NASA P3-B and UMD Cessna 402 side-by-side aerosol inlet evaluation. A comparison of Nephelometer dry scattering coefficients.

The humidity lines in Figure 6.4A are the humidities inside of the Nephelometers. During the high altitude transect particle abundance is low and both instruments are measuring near their detection limits. While the average ratio of  $\sigma_{sp}Ces/\sigma_{sp}P3-B$  is 1, the variability is large due to the near 100% uncertainty associated with these measurements. Toward the lower end of the spiral and the low altitude transect, changes in humidity become more gradual and the ratio of  $\sigma_{sp}Ces/\sigma_{sp}P3-B$  becomes more constant. Figure 6B shows that during this period Cessna 402 consistently scattered 20 % to 40 % less light than P3-B. Table 6.2A shows the average Cessna 402 to P3-B scattering ratio for each wavelength during the low altitude transect. On average, the Cessna 402 sampling system scattered 31.7 % (+/- 12%) less light than the P3-B.

**Table 6.2.A** Ratio of  $\sigma_{sp}Ces/\sigma_{sp}P3-B$  dry scattering during the low altitude side-by-side transect, 19:10 to 19:22 UTC

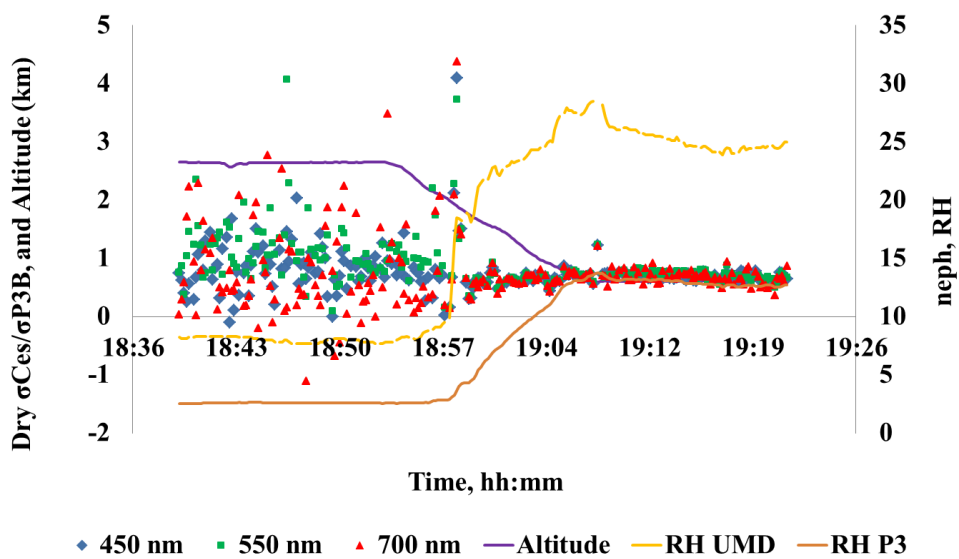
| Statistic | $\lambda$ 450 nm | $\lambda$ 550 nm | $\lambda$ 700 nm |
|-----------|------------------|------------------|------------------|
| Average   | 0.68             | 0.70             | 0.67             |
| Stdev     | 0.06             | 0.08             | 0.11             |
| RSD       | 8.41             | 11.04            | 17.00            |
| Min       | 0.57             | 0.49             | 0.37             |
| max       | 0.78             | 0.88             | 0.94             |

**Table 6.2.B** Ratio of  $\sigma_{sp}Ces/\sigma_{sp}PA$  dry scattering during the low altitude side-by-side transect, 19:10 to 19:22 UTC

| Statistic | $\lambda$ 450 nm | $\lambda$ 550 nm | $\lambda$ 700 nm |
|-----------|------------------|------------------|------------------|
| Average   | 1.03             | 0.99             | 0.96             |
| Stdev     | 0.07             | 0.07             | 0.08             |
| RSD       | 6.7              | 7.3              | 8.1              |
| Min       | 0.89             | 0.85             | 0.73             |
| max       | 1.46             | 1.39             | 1.32             |



6.4 A)



6.4 B)

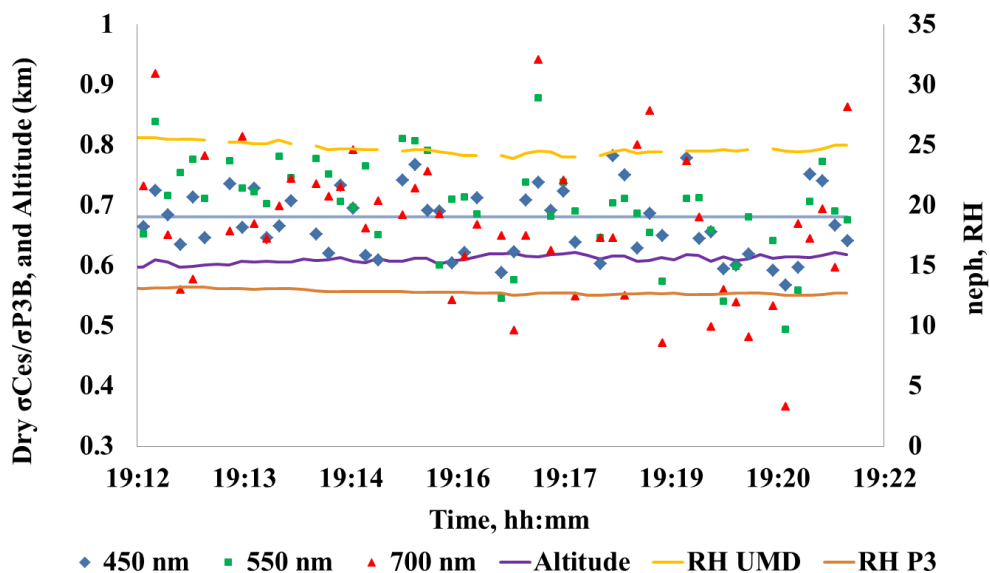


**Figure 6.4** Plots of  $\sigma_{sp}CES/\sigma_{sp}P3-B$  for each point in time. 6.4 A) ratios of dry scattering data. 6.2 B) scattering ratios across the period of the low altitude transect when relative humidity is fairly constant.

Potential sources of aerosol loss are 1) deposition to the tubing during the long 6.8 m travel distance between the nose of the plane and the instrument and/or 2) subkinetic sampling. As mentioned in above in the section 2.3, under the guidelines for aircraft sampling, isokinetic is a requirement of aerosol sampling on an aircraft. Isokinetic sampling is achieved when the velocity of flow at the tip of the inlet ( $U_i$ ) equals the true air speed ( $U_w$ ) or  $U_i = U_w$ .  $U_i > U_w$  results in superkinetic and  $U_i < U_w$  results in subkinetic [[Huebert et al., 1990](#)]. When the particle flow is superkinetic the inertial flow at the inlet tip directs particles into the inlet nozzle causing the number density of sampled air to be greater than ambient and an over estimation of atmospheric aerosols. Under conditions of subkinetic the inertial flow pushes particles around the outside of the inlet causing the observed number density to underrepresent that of ambient atmospheric aerosol. On the P3-B additional adjustable pumping at the end of the sampling system is used to maintain isokinetic throughout the flight. Additional adjustable pumping has not been added to the Cessna. Furthermore, a restricting orifice in the Cessna Nephelometer pumping system exists at the elbow Swagelok fittings used to connect the conductive tubing to the Nephelometer inlet. Reducing the diameter of the inlet and outlet from 1 inch to a fraction of an inch limits the Nephelometer pumping to 15 LPM. Without adequate pumping, particles are pushed around the sides of the inlet tip rather than flowing directly into the inlet as the aircraft moves through the air. The results of the second interplane light scattering comparison, the Cessna and the Aztec side-by-side, will demonstrate why the deposition of particles along the tubing walls is not a major contributor to reduced sampling efficiency.

## 6.2.2 Cessna 402 and Piper Aztec inlet comparison

Similar to the first inter aircraft comparison, the second side-by-side flight compared the aerosol sampling systems through inlets mounted at different locations on two different aircraft with different plumbing configurations (see Figures 6.1 and 6.2). During the second comparison, the two aircraft were within a kilometer horizontal distance of one another, but not nearly wing tip to wing tip like the P3-B and Cessna. In this 80 minute comparison the two aircraft flew a 38 minute high altitude transect at 1.7 m, then spiraled downward for 13 minutes and flew a low altitude horizontal transect for 29 minutes at 0.64 m over the DelMarVa peninsula. Aircraft speed ranged from 30 to 90 m/s. The average Mach was 0.18, ranging from 0.09 to 0.26.

Figure 6.5 shows a comparison between Nephelometer sampling on the Cessna and Nephelometer sampling on the Piper Aztec. The Cessna / Aztec comparison shows that total scattering measured on the respective aircraft was approximately the same. Fig 6.6 shows that the ratios of  $\sigma_{sp}Ces/\sigma_{sp}Azt$  of the blue/green/red scattering coefficients are on average within 1% of each other. Each  $\sigma_{sp}Ces/\sigma_{sp}Azt$  ratio per wavelength is shown in table 6.2B. Because the Aztec tubing is much shorter than the Cessna tubing this comparison indicates that the lesser scattering observed on the Cessna compared to the P3-B is probably not due to line losses.

During post calibration procedures, the Nephelometer flow rates were measured. It was observed that the Swagelok elbow fitting restricted the Nephelometer flow to 15 lpm. Removing the Swagelok fitting resulted in a flow increase to 30 lpm. These results indicate that archived RAMMPP data should be multiplied by a factor of 1.46. A new

method for connecting the inlet tubing to the Nephelometer should be instituted and adjustable pumping should be added.

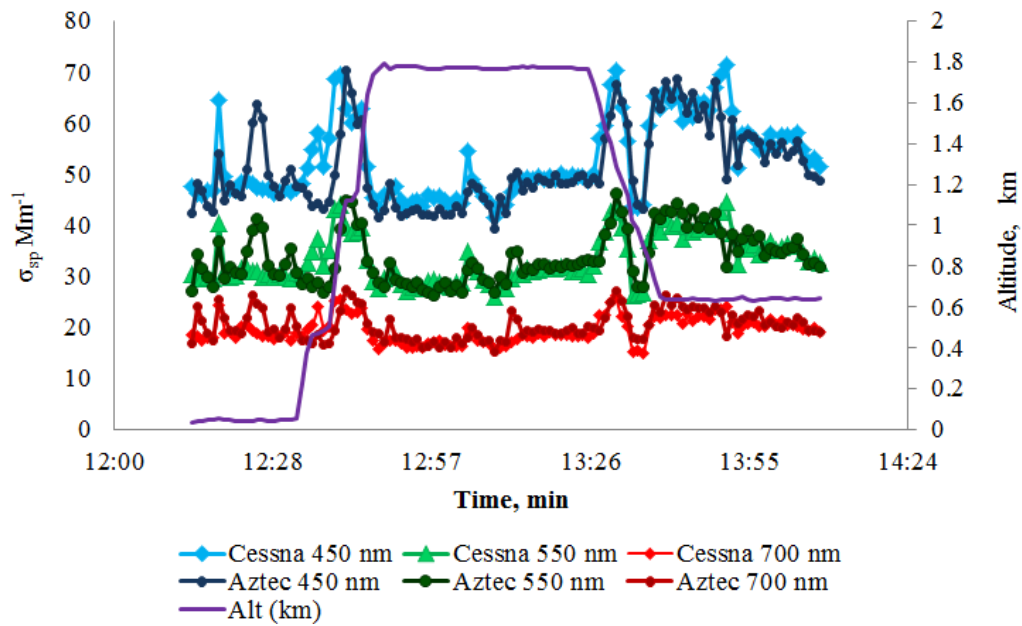


**Figure 6.5** Scattering comparison of aerosols sampled from the Cessna 402 and Aztec. A comparison of Nephelometer dry scattering coefficients

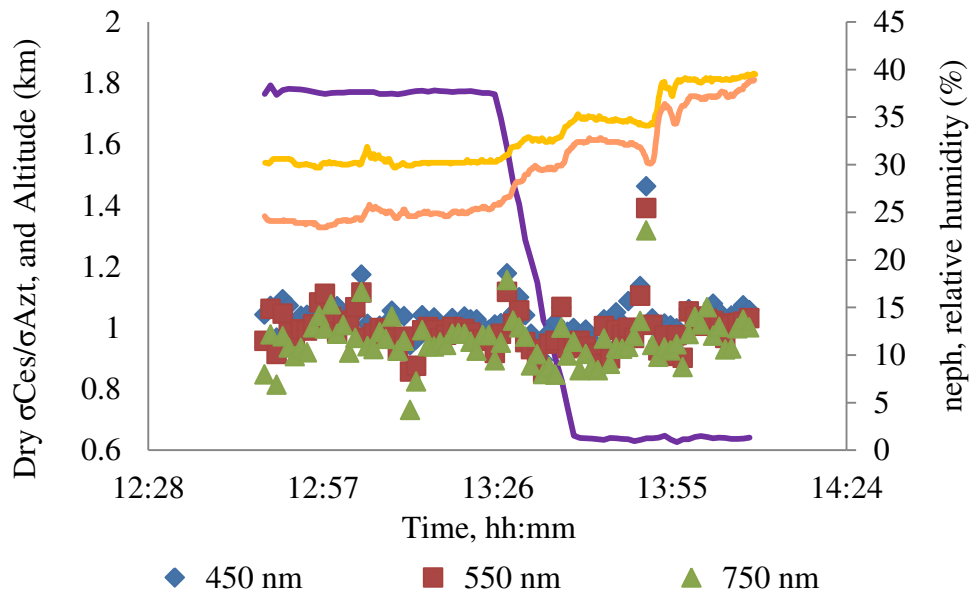


**Figure 6.6** Plots of  $\sigma_{sp}Ces/\sigma_{sp}Azt$  for each point in time. Ratios of Cessna to Aztec Nephelometer dry scattering.

### 6.3 Conclusions

Aerosol collection capability with estimated passing efficiency near 100 % for particles up to 2.5  $\mu\text{m}$  in diameter has been added to the RAMMPP through installation of a shrouded diffuser onto the nose cone of a Cessna 402. The same shrouded inlet is also routinely flown on both NASA and NOAA aircraft.

In a side-by-side flight with the NASA P3-B, the UMD Cessna 402 aerosol scattering measurements were within ~70% of scattering measured by NASA. A second side-by-side comparison between the Piper Aztec and the Cessna 402 showed scattering coefficients within 1% of one another. The tubing used to connect the inlet to the

Nephelometer on the Aztec is 2.3 m shorter than on the Cessna indicating that sampling losses are probably due to inadequate pumping and not significantly affected by line losses. To avoid the flow restriction, a new method for connecting the Cessna 402 Nephelometer to the conductive tubing should be implemented. The best way to achieve isokinetic flow would be to add a flowmeter and adjustable pumping.

The bulk of the aerosols found over the eastern US are in the submicrometer size range. The Swagelok tubing connector used on the Aztec did not inhibit the passage of atmospheric aerosols to the optical instruments. The historical data set of observed aerosol scattering observed over the eastern US (Taubman et al.; Marufu et al., etc.) should be corrected by a factor of 1.47 to account for subkinetic flow. Near 100% sampling efficiency should be achievable once the constricting orifice is removed from the sampling system.

## CHAPTER 7: Evaluation of the use of a commercially available cavity ringdown absorption spectrometer for measuring NO<sub>2</sub> in flight, and observations over the Mid-Atlantic States, during DISCOVER-AQ.

Note, this chapter appeared in the Journal of Atmospheric Chemistry in 2013 [[Brent et al., 2013a](#)].

### 7.1 Abstract

Real time, atmospheric NO<sub>2</sub> column profiles over the Mid-Atlantic States, during the July 2011 National Aeronautics and Space Administration (NASA) Deriving Information on Surface Conditions from Column and Vertically Resolved Observations to Air Quality (DISCOVER AQ) flight campaign, demonstrated that a cavity ring down spectrometer with a light emitting diode light source (LED-CRD) is a suitable technique for detecting NO<sub>2</sub> in the boundary layer (BL) and lower free troposphere (LFT). Results from a side-by-side flight between a NASA P3-B aircraft and a University of Maryland (UMD) Cessna 402 aircraft show that NO<sub>2</sub> concentrations in ambient air from 0.08 nmol/mol (or ppbv) to 1.3 nmol/mol were consistent with NO<sub>2</sub> measurements obtained via laser induced fluorescence (LIF) and photolysis followed by NO chemiluminescence (P-CL). The current LED-CRD, commercially available by Los Gatos Research (LGR), includes the modifications added by [Castellanos et al \(2009\)](#) to compensate for baseline drift and humidity through built in zeroing and drying. Because of laser instability in the initial instrument, the laser light source in the Castellanos et al (2009) instrument has been replaced with a light emitting diode. Six independent calibrations demonstrated the

instrument's linearity up through 150 nmol/mol NO<sub>2</sub> and excellent stability in calibration coefficient of 1.26 ( $\pm$  3.7%). The instrument detection limit is 80 pmol/mol. Aircraft measurements over the Mid-Atlantic States are included showing horizontal and vertical distributions of NO<sub>2</sub> during air quality episodes. During 23 research flights, NO<sub>2</sub> profiles were measured west and generally upwind of the Baltimore/Washington, D.C. area in the morning and east (generally downwind) of the metropolitan region in the afternoon. Column contents (surface to 2500 m altitude) were remarkably similar ( $\approx 3 \times 10^{15}$  molecules/cm<sup>2</sup>) indicating that NO<sub>2</sub> is widely distributed over the eastern US contributing to the regional (spatial scales of approximately 1000 km) nature of smog events.

## 7.2 Introduction

Nitrogen dioxide (NO<sub>2</sub>), an Environmental Protection Agency (EPA) designated National Ambient Air Quality Standard (NAAQS) criteria pollutant, is known to be aggravating to the respiratory system [[Schwartz et al. 1990](#); [Annesi-Maesano et al. 1998](#)]. In addition to its direct health effects, NO<sub>2</sub> also controls the photochemical production of Los Angeles type smog (ozone) [[Jacob et al. 1996](#); [Finlayson-Pitts et al. 2000](#)] and, indirectly, the oxidizing capacity of the atmosphere. NO<sub>x</sub> (NO + NO<sub>2</sub>) released from fossil fuel combustion contributes approximately 13% of the total global fixed nitrogen, both oxidized and reduced. These emissions contribute to the nitrogen cascade, where the same atom can cause multiple biogeochemical effects with consequences for ecosystems and human health [[EPA, 2011](#)].

While the NAAQS for NO<sub>2</sub> is rarely, if ever, exceeded, the photochemical production of ozone in high oxides of nitrogen (NO<sub>x</sub>) conditions leads to frequent



exceedances of the 2008 8 hour ozone standard set in the federal Clean Air Act. A network of ground measurement sites across the United States offers continuous 24 hour monitoring, but this offers limited assessment on how the chemical and physical dynamics of the surrounding atmosphere affect concentrations at the lowest few meters of the planetary BL.

A survey of methods for measuring ambient NO<sub>2</sub> has been thoroughly reviewed and will not be further considered here [Fried et al. 1998](#); [Hargrove et al. 2006](#); [Dunlea, et al. 2007](#); [Fehsenfeld, et al. 1990](#); [Pollack et al. 2011](#); [Dari-Salisburgo et al. 2009](#). The focus of the current work will be on techniques used for measuring NO<sub>2</sub> with respect to altitude. Collections of altitude profiles are used to gain insight into how atmospheric dynamics, both chemical and physical, affect concentrations of gas and aerosol species near the surface. Vertical column distribution provides information on BL depth, photolysis, convection and advection [Halla et al. 2011](#). Several methods exist for measuring NO<sub>2</sub> with respect to altitude. Ground based spectrometers such as NASA's Pandora collect column content with vertical resolution typically on the order of kilometers [Herman et al. 2009](#). Satellite spectrometers take regional snap shots of atmospheric components at regular intervals, i.e.: daily, or weekly, and are often used in global comparisons [Kim, et al. 2009](#); [Leu, et al. 2001](#); [Schaub, et al. 2006](#). Instruments flown on aircraft are useful for measuring large latitudinal and longitudinal cross sections in addition to *in situ* vertical column profiles. Airborne measurements play a useful role in capturing urban versus regional distributions and the regional transport of pollutants.

Several research-grade instruments for monitoring NO<sub>2</sub> offer excellent sensitivity and specificity, but commercially available detectors often suffer from interferences. For

example, ground monitoring stations typically rely on commercially available chemiluminescent NO<sub>x</sub> analyzers with hot molybdenum oxide (C-Mo) converters such as the Thermo 42 series NO/NO<sub>2</sub>/NO<sub>x</sub> analyzers. These analyzers meet EPA standards for monitoring NO<sub>2</sub> compliance, but the hot MoO<sub>x</sub> converters also convert additional oxides of nitrogen NO<sub>z</sub> (NO<sub>3</sub>, N<sub>2</sub>O<sub>5</sub>, HNO<sub>2</sub>, HNO<sub>3</sub>, PAN (peroxyacetylnitrate) and organo nitrates) [Fehsenfeld et al. 1987](#). Flight use of this instrument has been limited to estimating NO and the combination of NO<sub>x</sub> + NO<sub>z</sub> known as NO<sub>y</sub> [Jaeglé et al. 1998](#); [Neuman et al. 2001](#); [Luke et al. 1992](#). Two well characterized research grade instruments, frequently used in flight, are the University of California, Berkeley's (UCB), thermal dissociation laser induced fluorescence (TD-LIF) [Thornton et al. 2000](#); [Day, et al. 2002](#); [DiCarlo et al. 2012](#); [Bucsele et al. 2008](#); [Wagner et al., 2011](#), and the National Center for Atmospheric Research (NCAR) chemiluminescent detector with photolytic NO<sub>2</sub> to NO conversion (P-CL) [Ryerson et al. 2000](#); [Emmons et al. 1997](#); [Pollack et al. 2011](#); [Heland et al. 2002](#). High correlation between these instruments and their specificity for NO<sub>2</sub> was demonstrated by [Fuchs et al. \(2010\)](#) in an atmospheric simulation chamber. Specificity for NO<sub>2</sub> in ambient air was demonstrated by [Suzuki et al. \(2010\)](#) during a ground comparison in Japan. In this comparison, LIF and P-CL measurements were in good agreement; however, measured levels of NO<sub>2</sub> were sometimes several nmol/mol less than levels determined with a simultaneously monitoring C-Mo instrument. The P-CL and LIF instruments have very low detection limits making them useful in low NO<sub>x</sub> environments such as the LFT, but are not available commercially. A research grade laser-CRD for measuring NO<sub>2</sub> has also been used in flight. This instrument achieved a similar in-flight detection limit and compensates for drift by

zeroing with gas instead of a built in chemical scrubber [Wagner et al., 2011](#). An advantage to these instruments, in addition to the low detection limit, is their ability to simultaneously measure multiple trace gas species. The laser-CRD is a part of a larger instrument that measures multiple oxides of nitrogen. The UCB TD-LIF uses thermal dissociation to also measure peroxy nitrates (PNs), alkyl nitrates (ANs), and nitric acid (HNO<sub>3</sub>). The P-CL instrument simultaneously measures O<sub>3</sub> and NO. The LIF and P-CL are the basis of comparison to our LED-CRD, and are described in section 3.

During July 2011, NASA conducted a portion of its DISCOVER AQ air campaign over Maryland, monitoring urban air pollution along the I-95 corridor in the Baltimore/Washington, D.C. metropolitan region. During this period, the University of Maryland complemented NASA's P3-B measurements by measuring many of the same gas and aerosol species while flying a larger regional flight pattern [He, et al. 2013](#). This paper describes the evaluation of a commercially available cavity ring down NO<sub>2</sub> detector for airborne use. While the LED-CRD instrument detection limit and response time make it less suitable than LIF or P-CL for extreme low NO<sub>x</sub> environments, its ease of operation and light weight make it a suitable alternative for routine ground monitoring and air quality studies aloft. The instrument was evaluated in the laboratory for sensitivity, linear dynamic range, interferences and stability. An intercomparison with established research grade instruments (LIF (UC Berkeley) and P-CL (NCAR)) was conducted at altitudes from 0.5 km to 3 km to validate LED-CRD NO<sub>2</sub> measurements in flight. Finally, we present upwind and downwind NO<sub>2</sub> profiles, during smog events in the Baltimore/Washington area, comparing regional and urban mixing ratios of the

dominant ozone precursor molecule. This paper is an extension of the ground evaluation of a similar instrument performed by [Castellanos, et al. \(2009\)](#).

## 7.3 Instrument description and calibration methods

### 7.3.1 Cavity ringdown instrument description

The LED-CRD analyzer, used on the UMD Cessna 402 aircraft during the summer of 2011, was built to replace the prior laser cavity ringdown NO<sub>2</sub> analyzer described by [Castellanos et al. \(2009\)](#). While the previous laser instrument provided accurate measurements, the laser sporadically changed frequency (i.e. “mode-hopping”), limiting the instrument’s long-term sensitivity.

A theoretical and instrument description of the original CRD laser instrument manufactured by Los Gatos Research, Mountain View, CA, has been published by [Castellanos et al. \(2009\)](#). Briefly, as sample air is pulled through the instrument at a rate of  $1.33 \times 10^{-5}$  m<sup>3</sup>/s, it is dried by Nafion® tubing with a counter flow of dry air. The flow stream is separated at a Swagelok T and controlled by a three way solenoid to go either directly to the sample cell or to first go through a chemical scrubber before entering the sample cell. The flow paths are rejoined at a solenoid fitted with Teflon® isolation valves specially designed to have zero dead volume. After the solenoid, the sample flows through a specially designed Parker VSO-EC pressure controller, to a 1.2 μm filter and into the optical cavity. The optical cavity is a 0.408 L stainless steel cylinder separating two fixed, highly reflective (99.995%) dielectric mirrors spaced by 0.285 m. Light enters the optical cavity perpendicular to the gas entrance through one of the mirrors. In reality, only a few micromole per mole photons of incident light is transmitted into the

cavity, while the rest is reflected by the entrance mirror. Once the light is in the cavity, it is reflected back and forth many times increasing the effective path length ( $tc/2L$ ), thereby increasing sensitivity to very small  $\text{NO}_2$  concentrations [Busch et al. 1999](#). Behind the back mirror a photo multiplier tube (PMT) detector measures the light transmitted out of the cavity on each pass as a function of time. The amount of time the light spends resonating in the cavity is inversely proportional to the total loss per reflection [Lehmann et al. 2009](#). After the sample stream exits the cavity, a portion of it is chemically-dried (Drierite®) and used as the sheath flow for the Nafion® tubing. The sheath flow is rejoined with the exhaust gas to exit the instrument. The equations used to relate the  $\text{NO}_2$  absorption coefficient and the rate of attenuation in the optical cavity to  $\text{NO}_2$  concentration through the Beer-Lambert law are shown in Table 7.1.  $\text{NO}_2$  concentrations are determined by the amount of time it takes the light to decay as measured by the photomultiplier tube (PMT). In principle, cavity ringdown should provide an absolute measure of concentration because the technique is dependent upon well-defined physical parameters such as the wavelength dependent molecular cross section, path length, temperature, and pressure of the optical cavity.

**Table 7.1** A table of equations relating cavity length, intensity and the molecular cross section to the Beer-Lambert law so that the  $\text{NO}_2$  concentration can be derived from the difference between the ringdown decay rate and background the background decay rate.

$$tc/2L = \text{path length}$$

$$(1-R) = \text{loss per reflection}$$

$$I(t) = I_0 \exp(-\sigma LN)$$

$$I(t) = i_0 \exp[-(1-R)tc/L]$$

$$\alpha = (1/c\sigma)(1/\tau - 1/\tau_0) = \sigma N$$

---

|       |                       |
|-------|-----------------------|
| t     | Time                  |
| c     | Speed of light        |
| R     | reflectivity          |
| $I_t$ | transmitted intensity |

|          |   |
|----------|---|
| $I_0$    | incident intensity                                      |
| $\sigma$ | wavelength specific cross section of absorbing species  |
| $L$      | Length of cavity  |
| $N$      | number density of absorbing species in $\text{cm}^{-3}$ |
| $\alpha$ | Wavelength dependent absorption coefficient             |

The instrument highlighted in this paper is a modification of the original laser CRD [Castellanos et al. 2009](#) with the most significant difference being that the laser light source was replaced by a light emitting diode (LED) (355 mW, Lumileds, Prolight). The LED emission spectrum is 397 to 412 nm with peak emission at 408 nm. The light is filtered through a 10 nm wide spectral bandpass filter centered at 405 nm. While, in an empty cavity, the ring-down transients are slightly multi-exponential, the mirror reflectivity is flat across this spectral range. In effect the LED is not broad band compared to the mirror band so the signal can be treated as a single exponential. If the ring-down transient were strongly multi-exponential, the calibration curve would deviate from first order with increasing  $\text{NO}_2$ . The LED is temperature stabilized through mounting on a thermoelectrically cooled plate and is current modulated with a fall time of 300 ns and a pulse modulation rate of 5 kHz. Ringdown events are collected using a data acquisition (DAQ) card operating at 1.25 MHz. The convolved LED-PMT-DAQ 1/e response time is 660 ns. Individual ringdowns are boxcar averaged in groups of 1000 and the resulting average trace is fit to a decaying single exponential using a non-linear least squares fit.

The instrument includes a manufacturer installed 1.2  $\mu\text{m}$  filter positioned between the pressure controller and the inlet to the optical cavity, but because submicrometer environmental aerosols can interfere with gas measurements, an additional 0.1  $\mu\text{m}$  filter

has been placed at the instrument inlet. The period over which the filters should be changed is still a subject of study. The internal cavity pressure is maintained at 40,263 Pa, increased from 22,665 Pa in the laser instrument. The stainless steel optical cavity pressure and temperature are monitored to convert the NO<sub>2</sub> number concentration to a mixing ratio. While the optical cavity pressure in this instrument is increased by 30,931 Pa, the sample residence time, defined as volume / flow, is the same because the pumping rate was increased from  $8.3 \times 10^{-6} \text{ m}^3/\text{s}$  (0.56 slpm) to  $1.33 \times 10^{-5} \text{ m}^3/\text{s}$  (0.8 slpm).

### 7.3.2 Calibration procedures

#### 7.3.2.1 Standard addition

Standard dilution at the NIST was a multistep process beginning with the preparation and concentration determination of a nitrogen dioxide working standard, prior to serial dilution and measurements. In our calibration process, a Thermo 42C chemiluminescence detector with a stainless steel thermal converter (C-SS) operating at greater than 600°C was used to verify a NO<sub>2</sub> working standard. While chemiluminescence instruments employing thermal conversion from NO<sub>y</sub> to NO are known to lack NO<sub>2</sub> specificity, [Fried et al. \(1998\)](#), has determined their suitability for this laboratory work through independent comparison to NO<sub>2</sub> specific techniques, tunable diode laser spectroscopy and Fourier transform infrared spectroscopy. In Fried et al. work, the NO<sub>2</sub> values agreed with the chemiluminescence measurements when a Nylon® prefilter for removing the primary impurity, HNO<sub>3</sub>, was placed at the inlet, prior to thermal conversion. In our work, NO<sub>x</sub> to NO thermal conversion efficiency approaching 100% was achieved using a pre converter (Stainless Steel, ~700°C, 101 kPa) in series

with NIST's Thermo Model 42C ambient level instrument which is equipped with a similar thermal converter (stainless steel, 635°C, 10 kPa). The chemiluminescence detector was calibrated indirectly for NO<sub>2</sub> by quantitatively comparing the thermal dissociation of NO<sub>2</sub> to NO to gravimetric standards containing NO in N<sub>2</sub>.

Preparation of the NO<sub>2</sub> standard was as follows. Reagent grade nitrogen dioxide is diluted with nitrogen to achieve the desired concentration of NO<sub>2</sub> in nitrogen. A cylinder containing 2.3 kg of ultra-high purity nitrogen dioxide (99.5 % minimum purity), was obtained from Matheson Trigas in December, 2002. In 2009 the NO<sub>2</sub> standard was analyzed and it was found that the purity had degraded to < 98% of the original concentration. Reaction of the NO<sub>2</sub> with the DOT 3AA specification steel cylinder inner walls evidently produced HNO<sub>3</sub> and H<sub>2</sub>O contamination. The reagent NO<sub>2</sub> was distilled three times and passed through a P<sub>2</sub>O<sub>5</sub> drier to remove water and then passed through a Nylon® membrane filter to remove nitric acid. The final purity was determined to be 99.0% after clean up.

Reagent NO<sub>2</sub> was serially diluted with nitrogen in steps to 4000 μmol/mol > 500 μmol/mol > 100 μmol/mol > 10 μmol/mol. The NO<sub>x</sub> concentration was determined by direct measurement against a NO in N<sub>2</sub> Standard Reference Material (SRM) or NIST gravimetric primary standard at similar NO<sub>2</sub> concentrations of 4000, 500, 100, 10 μmol/mol. NO<sub>2</sub> values were determined by measurement of NO<sub>x</sub> before and after a 1 μm Nylon® membrane filter which trapped HNO<sub>3</sub>. The stability of six working standards containing ≈10 μmol/mol NO<sub>2</sub> in N<sub>2</sub> was evaluated over a period of 5 years. After 2 years, levels of NO<sub>2</sub> in five of the six working standards stabilized after an initial



decrease in NO<sub>2</sub>. The sixth mixture continues to drop for reasons unknown [Thorn, 2010](#).

The working standard was prepared from this batch of NO<sub>2</sub> standards.

The Luxfer DOT 3AL 6L aluminum cylinders used at NIST for all NO and NO<sub>2</sub> standards have an extremely smooth inner wall surface resulting from the high pressure extrusion process used in their manufacture. The surface is aluminum oxide (Al<sub>2</sub>O<sub>3</sub>), an amphoteric oxide, which acts as a weak base in the presence of a strong acid like HNO<sub>3</sub>. To produce stable concentrations of NO in N<sub>2</sub> below 10 μmol/mol it is necessary to titrate the aluminum oxide surface with nitric acid which is done by exposing the walls to 1000 μmol/mol NO<sub>2</sub> in N<sub>2</sub>. NO<sub>2</sub> reacts with the ubiquitously adsorbed water forming adsorbed HNO<sub>3</sub> + HNO<sub>2</sub>. After titrating the cylinder wall, excess HNO<sub>3</sub> + HNO<sub>2</sub> will desorb from the wall into the cylinder gas mixture. Excess NO<sub>2</sub> treatment gas is removed from the cylinder through several purges with 99.999% nitrogen, (purity achieved with Airgas trademarked built in purity technology (BIP<sup>®</sup>)) followed by vacuum elimination. The cylinder is rendered ready for maintaining NO stability at low concentrations. All NIST NO primary standard mixtures are blended gravimetrically using BIP<sup>®</sup> nitrogen to remove trace oxygen (~1 μmol/mol) from nitrogen.

After verification of the C-SS response to NO and verification of complete NO<sub>2</sub> to NO conversion, the UMD NO<sub>2</sub> working standard was evaluated. Calibration of the LED-CRD absorption spectrometer was completed by comparing readings of NO<sub>2</sub> standard serial dilutions to flow dilution calculations and to values obtained on the Thermo 42C. The least squares fit between the Thermo 42C measured NO<sub>2</sub> concentrations and the flow dilution calculations had a slope of 1.01 and correlation coefficient of >0.999.

### 7.3.2.2 Gas phase titration

During gas phase titration (GPT),  $\text{NO}_2$  was produced by reaction of NO with  $\text{O}_3$ . The GPTs conducted at both NIST and UMD used a Thermo 49PS as the ozone source; NO was from either a NIST SRM or a NIST traceable commercial standard. Both Thermo 49PSs were calibrated against the NIST ozone standard reference photometer before use and found to have slopes of 0.9981 and 1.001, respectively. GPT calibrations at NIST and at the Beltsville Agricultural field site were conducted in excess NO. The UMD GPT was conducted in excess ozone.

At UMD the same GPT procedure as published in Castellanos et al 2009 was used. Before calibration, a commercial Scott Marin NO in  $\text{N}_2$  standard was ratioed against the SRM 2627a and determined to be 4.868 nmol/mol (+/- 1 %) NO / 4.818 nmol/mol (+/- 1 %)  $\text{NO}_x$ . During this procedure, NO was diluted with air (9.1 nmol/mol to 96 nmol/mol) and mixed with 300 nmol/mol  $\text{O}_3$  in air in a 3 L round bottom flask. The amount of  $\text{NO}_2$  produced was compared to simultaneous LED-CRD absorption readings on a laser-CRD  $\text{NO}_2$  instrument. The laser-CRD instrument [Castellanos et al. 2009](#) had undergone the same standard dilution calibration at NIST as described above. The slope and correlation coefficient of the laser instrument to the NIST CL-thermal converter was 1.00 and 0.999, respectively.

At NIST the GPT  $\text{NO}_2$  concentrations were verified by measurements of ozone loss, and by measuring the amount of NO loss on a Thermo 42 C NO- $\text{NO}_2$ - $\text{NO}_x$  detector. At the field site,  $\text{NO}_2$  production was verified by  $\text{O}_3$  loss on NOAA's 3-channel chemiluminescence detector with photolytic  $\text{NO}_2$  to NO conversion using a blue light

converter ( $\lambda_{\max}$  395±5) lamp. NO<sub>2</sub> was measured as the difference between NO and NO<sub>x</sub> [Luke et al., 2007](#).

### 7.3.3 Instruments used for flight intercomparison

#### 7.3.3.1 Photolysis followed by chemiluminescence (P-CL)

The NCAR four channel chemiluminescent instrument operated on the P3-B measures NO, NO<sub>2</sub>, NO<sub>y</sub>, and O<sub>3</sub>. A description of this instrument can be found at [http://discover-aq.larc.nasa.gov/pdf/2010STM/Weinheimer20101005\\_DISCOVERAQ\\_AJW.pdf](http://discover-aq.larc.nasa.gov/pdf/2010STM/Weinheimer20101005_DISCOVERAQ_AJW.pdf) (last accessed 24 June 2013). This instrument measures NO<sub>2</sub> with a process similar to that used by the Thermo 42C described above. As the combined oxides of nitrogen enter the instrument, NO is quantified directly after second order reaction with ozone (generated inside the instrument), to produce NO<sub>2</sub>. NO<sub>2</sub> chemiluminescence is proportional to the original NO concentration. NO<sub>2</sub> and NO<sub>y</sub> are converted to NO and measured as an increase in chemiluminescent signal above ambient NO. Like the Thermo 42C, the total NO<sub>y</sub> species are converted to NO (NO<sub>y</sub> + CO → NO + CO<sub>2</sub>) with a heated metal catalyst. This analyzer distinguishes itself from the Thermo 42C by selectively measuring NO<sub>2</sub> on a separate channel. NO<sub>2</sub> is photodissociated to NO by illumination from 400 nm LEDs, with a conversion efficiency near 90% that is measured several times during a flight by calibrating with a known flow of NO<sub>2</sub>. The NO<sub>2</sub> 1 s, 2σ detection limit is 60 pmol/mol with an overall uncertainty of 10 to 15%. The instrument response time for NO<sub>2</sub> measurements is ≈3 sec.

### 7.3.3.2 Laser Induced Fluorescence

The TD-LIF instrument, operated by the University of California Berkeley on the P3-B aircraft, uses LIF to directly detect NO<sub>2</sub>. A custom built, Nd:YAG laser pumps a tunable dye laser ( $\lambda = 585$  nm), which is used to excite a narrow rovibronic feature unique to NO<sub>2</sub>. The laser light is focused into two multipass cells and red shifted fluorescent photons at wavelengths longer than 700 nm are counted. A background signal is referenced by shifting the laser frequency off the NO<sub>2</sub> feature. Instrument zeroing is performed by over pressurizing the inlet with zero air. The NO<sub>2</sub> slope has 5% uncertainty and the 1 second, 2 $\sigma$  detection limit is 30 pmol/mol. The instrument response time is  $\leq 1$  second. For a complete description of LIF see [Thornton et al. \(2000\)](#). Three additional channels sample air through ovens held at temperatures 200°C, 400°C, and 600°C in order to thermally dissociate PNs, ANs, and HNO<sub>3</sub>, respectively, to NO<sub>2</sub> plus a companion radical. PNs, ANs, and HNO<sub>3</sub> are then measured by quantifying the difference between adjacent channels (i.e. ANs are equal to the difference between the 200 and 400°C channels). The accuracy for PNs, ANs, and HNO<sub>3</sub> also includes terms for transmission efficiency through the sampling inlet and the completeness of thermal dissociation and is estimated to be 15%. A complete description of this process is available in [Day et al. \(2002\)](#). See Table 7.2 for a summary of aircrafts, organizations, uncertainties and measurement times respective to each measurement technique.

**Table 7.2** *Intercomparison instrument uncertainties and averaging times*

| Plane      | Technique | Organization | Uncertainty | Avg time |
|------------|-----------|--------------|-------------|----------|
| Cessna 402 | CRD       | UMD          | 5%          | 10 s     |
| P3         | Chemi     | NCAR         | 30%         | 10 s     |
| P3         | LIF       | UC Berkeley  | 5%          | 10 s     |

## 7.4 Aircraft and flight patterns

The UMD aircraft is a Cessna 402, an unpressurized plane whose flight operations are limited to an altitude of 3 km. The NASA P3-B aircraft is a pressurized four engine turboprop that can fly as high as 9 km, but only flew to 5 km for DISCOVER AQ. Both aircraft were outfitted with a series of gas and aerosol instruments, but comparisons in this paper, are limited to NO<sub>2</sub> up to 3 km.

### 7.4.1 Side-by-side flight plan

The Cessna 402 and the NASA P3-B met at 2.6 km due south of the Massey Aerodome Airport, Massey, MD and flew S/SE in a near wing tip to wing tip, side-by-side configuration for 16 minutes. The 2.6 km transect ended over Selbyville, DE, where the two aircraft then spiraled downward to 0.61 km over the Delaware / Maryland border. At 0.61 km, the downward spiraling stopped and the two planes flew a s side by side transect for 12 minutes in a W/NW direction ending near Ridgley, MD. The cavity ringdown NO<sub>2</sub> instrument was zeroed for 3 minutes at 2.6 km before the comparison began and zeroed again at 0.61 km for ten minutes after the P3-B departed. The side by side flight path is shown in yellow on Figure 7.1. The flight speed ranged from 50 to 110 m/s. With a 10 s instrument averaging time, the horizontal measurement resolution was 540 to 1080 m.

### 7.4.2 Westerly transport flight plan

The UMD westerly transport flights are designed to capture transport of pollutants across the Maryland ozone nonattainment region. AM flights include spirals in

rural areas of western Maryland and Virginia, generally upwind of the nonattainment region. Afternoon flights include spirals performed over rural county airports downwind of the Baltimore / Washington region, and in the nonattainment region. Information gathered from these flights is used to gain insight into the local versus regional nature of the Maryland nonattainment problem. In Figure 7.1, the UMD AM/Upwind flight plan is shown in red, the UMD PM/Downwind flight plan is shown in blue, and the NASA P3-B urban corridor flight path is shown in green. The AM flights flew between 1300 to 1630 hours UTC (coordinated universal time) and the PM flights ran from 1730 h to 2030 h UTC. Solar noon ranged from 1607 to 1614 UTC, from the first flight day, June 8<sup>th</sup> to the last day, July 29<sup>th</sup>. A summary of spiral direction with respect spiral location is provided in Table 7.3. The P3-B generally began reporting measurements around 1400 UTC and the flights lasted approximately 7 hours flying 18 profiles per flight.

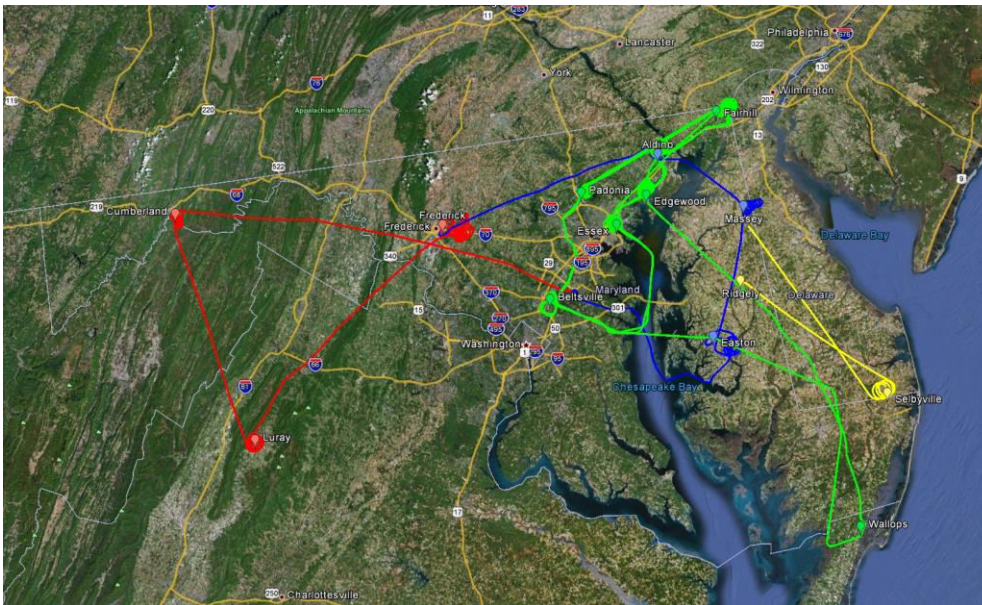


**Figure 7.1** RAMMPP westerly transport flight path and side-by-side flight tracks. The UMD Cessna upwind/rural/AM (1300 – 1630 UTC) flight path is shown in red, the Cessna downwind/rural/PM (1730 – 2030 UTC) flight path is shown in blue, and the NASA P3 flight path is shown in green (usually ~1400 – 2000 UTC). The Cessna / P3-B side by side flight path flown over rural areas of Maryland and Delaware is shown in

yellow. The planes were a few meters apart during the constant altitude phases. Local solar time is approximately 4 h earlier than UTC.

**Table 7.3** The AM and PM Cessna regional flight path consisted of 3 spirals over airports in western Maryland and Virginia and upwind of the metropolitan nonattainment area and 3 spirals over Maryland downwind of the nonattainment area. Note: the only spiral in our flight plan also flown by the P3-B was the Aldino spiral (0W3). The Cessna flew a downward spiral while the P3-B flew an upward spiral. The Cessna was in close proximity to the P3-B during four of the Aldino spirals (July 10, 21, 23, and 29).

| AM / upwind flight plan | Coordinates           | AM spiral direction | PM / downwind flight plan | Coordinates            | PM spiral direction |
|-------------------------|-----------------------|---------------------|---------------------------|------------------------|---------------------|
| Cumberland, MD (CBE)    | 39.61500<br>-78.76222 | ↑                   | Aldino, MD (0W3)          | 39.56683<br>-76.20240  | ↓                   |
| Luray, VA (W45)         | 38.66705<br>-78.50058 | ↑                   | Massey Aerodome, MD (MD1) | 39.30458<br>-75.79468  | ↑                   |
| Frederick, MD (FDK)     | 39.41666<br>-77.41666 | ↓                   | Easton, MD (ESN)          | 38.802776<br>-76.06778 | ↓                   |

**Table 7.4** Calibration curve data. To validate the LED-CRD, the instrument was calibrated at NIST through standard dilution. The calibration coefficient was verified four times, at three locations, by two different techniques.  $R^2$  was always greater than 0.99

| Location   | Month     | Technique         | Reference                | Range (nmol/mol NO <sub>2</sub> ) | Calibration curve  |
|------------|-----------|-------------------|--------------------------|-----------------------------------|--------------------|
| NIST       | May       | Standard dilution | Flow control calculation | 3.5 to 99.1                       | $Y = 1.29X - 1.14$ |
| NIST       | June      | GPT               | $\Delta O_3$             | 10.5 to 96.1                      | $Y = 1.26X - 0.39$ |
| NIST       | June      | GPT               | $\Delta NO$              | 10.5 to 96.1                      | $Y = 1.29X - 1.60$ |
| UMD        | June      | GPT               | Laser CRD                | 9.1 to 96                         | $Y = 1.32X - 0.45$ |
| Beltsville | August    | GPT               | $\Delta O_3$             | 33 to 156                         | $Y = 1.19X - 0.06$ |
| NIST       | September | Standard dilution | Flow control calculation | 0.8 to 35.6                       | $Y = 1.23X - 0.18$ |

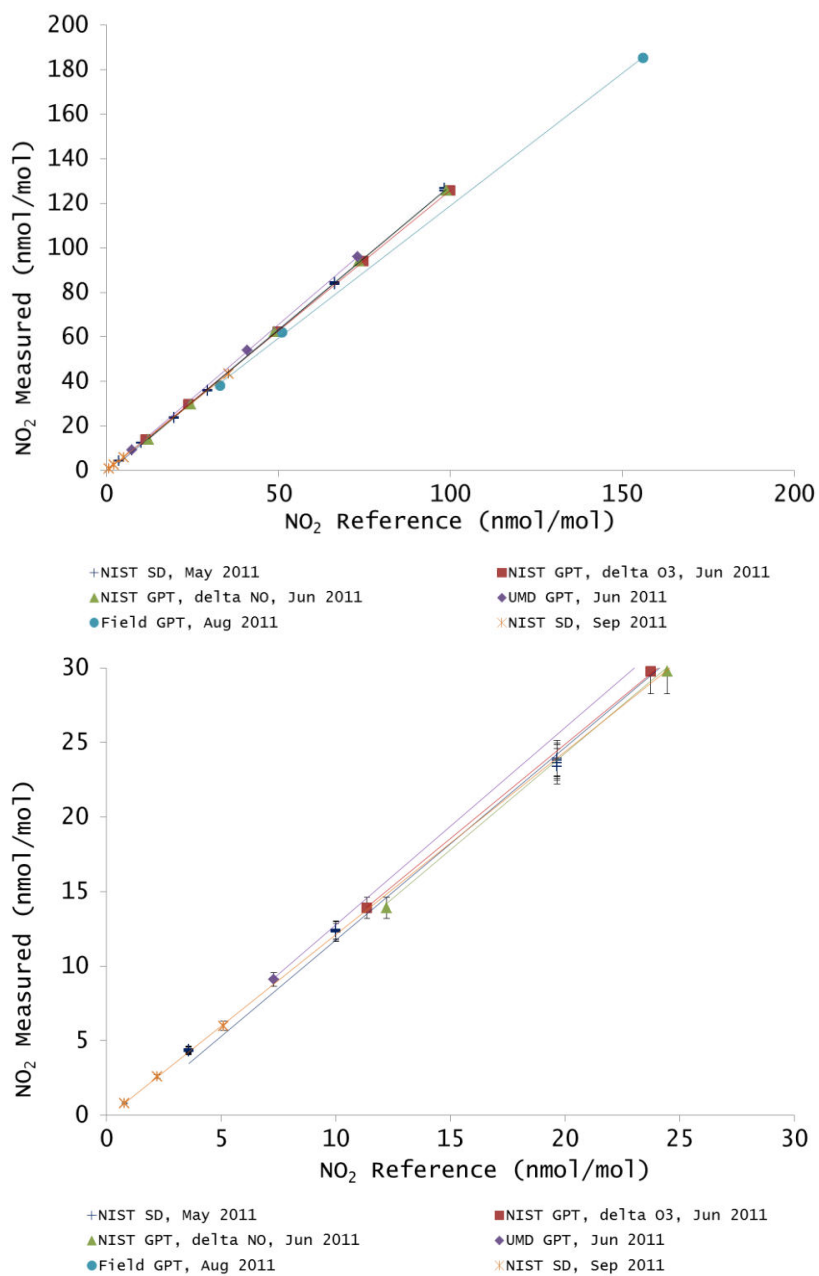


**Figure 7.2** Results from the NIST calibration and periodic calibration verifications. *Figure 7.2A. The curves overlap particularly well in the lower region important for atmospheric measurements, Figure 7.2B. The average calibration factor is 1.26 ( $\pm 3.7\%$ ).*



## 7.5 Results and Discussion

### 7.5.1 Calibration and stability

The NO<sub>2</sub> LED-CRD analyzer was calibrated at NIST by standard dilution resulting in a calibration curve of  $\text{NO}_{2(\text{LED-CRD})(\text{nmol/mol})} = (1.29 \pm 0.004) * \text{NO}_{2\text{ref}(\text{nmol/mol})} - (1.14_{(\text{nmol/mol})} \pm 0.22)$ . Four additional verifications of the calibration coefficient were conducted between May and September 2011. Three gas phase titrations (GPT) were performed, each at a different location (NIST, the Beltsville, MD field site and at the University of Maryland), and another standard dilution was performed at NIST. The average slope of the five calibrations is 1.26 (uncertainty 3.7%). The calibration curves and correlation coefficients for each calibration are shown in Table 7.4. The linearity of the five curves is shown in Figure 7.2. The calibration curves overlap particularly well in the range relevant to atmospheric concentrations (a few pmol/mol to approximately 30 nmol/mol to 50 nmol/mol).

Additionally, a month long comparison to the same NOAA chemiluminescence detector (P-CL, NOAA) using photolytic conversion, as described by Castellanos et al (2010) was conducted. The ground based instrument intercomparison was conducted at the Beltsville, MD, U.S. Department of Agriculture Beltsville, Agricultural Research Center field site, in a climate controlled trailer. The field site continuous monitoring, month long comparison, between the LED-CRD and the P-CL, NOAA measurements yielded a line of  $\text{NO}_{2(\text{LED-CRD})} = (0.98 \pm 0.001) * \text{P-CL}_{\text{NOAA}} - (0.40 \pm 0.006)$ , and correlation coefficient of  $R^2 = 0.97$ . The gas phase titration conducted at the field site, resulted in a

curve of  $\text{NO}_{2(\text{LED-CRD})} = (1.19 \pm 0.019) * \text{NO}_{2(\Delta\text{O}_3)} - (0.06 \pm 1.88)$ ,  $R^2 = 1.00$ . The field site data will be further discussed in a following publication.

The comparison between the laser-CRD and the new LED-CRD for the GPT performed at UMD resulted in a calibration curve of  $\text{NO}_{2(\text{LED-CRD})} = 1.32 * \text{NO}_{2(\text{Laser-CRD})} - 0.45$ . The original  $\text{NO}_2$  cross section used in the LED instrument was approximated from first principles. Because of complicated interplay between the LED spectrum and  $\text{NO}_2$  absorption, the first principle estimate required a 30% adjustment.

### 7.5.2 Detector limit, residence and response time

As is typical for CRDS instruments shot noise dominated the noise of the laser instrument  $3 \sigma$  detection limit [Lehmann et al. 2009](#). From a reading of zero air, the laser instrument  $3 \sigma$  detection limit was estimated as 0.2 nmol/mol integrated over 10 s and 0.06 nmol/mol integrated over 60 s. In the LED instrument, random baseline drift is the dominant source of noise, so even though the detection limit with a 10 s integration time is reduced to 80 pmol/mol, longer integration times do not give the benefit of lower detection limits. Hence, the  $3 \sigma$  detection limit, for a 60 s integration time, remains at 80 pmol/mol. Furthermore, because the drift creates excess baseline variability, the instrument should be zeroed frequently. During the side by side flight, a linear interpolation of zero data, 60 s, before and after the side by side comparison, also resulted in an 80 pmol/mol  $\text{NO}_2$  in ambient air  $3 \sigma$  detection limit.

Quick instrument response time decreases the likelihood of measurement bias during calibration and rapidly changing environments. The EPA Operators Guide to eliminating bias in continuous emissions systems refers to instrument response time as

the seconds required to reach 95% of the asymptotic value after a change in concentration, equivalent to three e-folding time constants for a system with first order response. Similar to the laser-CRD, a first order response to a step change in concentration was observed for the LED-CRD but a faster pump reduced the time to reach 95% of the new signal ( $\ln(0.05)/-k = \tau$ ) to 3.7 seconds (from 18 seconds). The residence time for gas in the optical cavity (time=flow/volume) is 11 seconds.

### 7.5.3 NASA P3-B and Cessna 402 side-by-side flight data comparison

During a side by side flight flown over eastern Maryland and Delaware the University of Maryland, cavity ringdown NO<sub>2</sub> measurements were compared to two separate, NO<sub>2</sub> measurement techniques on the NASA P3-B. Figure 7.3 is a plot of the side by side trace gas data. Figure 7.3A, shows that the LED-CRD compared well to the NCAR P-CL and the UCB LIF research instruments for mixing ratios ranging from the LED-CRD detection limit (80 pmol/mol) to 1.3 nmol/mol NO<sub>2</sub> in ambient air.

The side by side flight experiment consisted of three phases, a 14 min, 2.6 km transect, a 14 minute descending spiral from 2.6 km to 1.6 km, and a 14 minute 0.6 km transect. During the 2.6 km transect, the P-CL and LIF each measured average

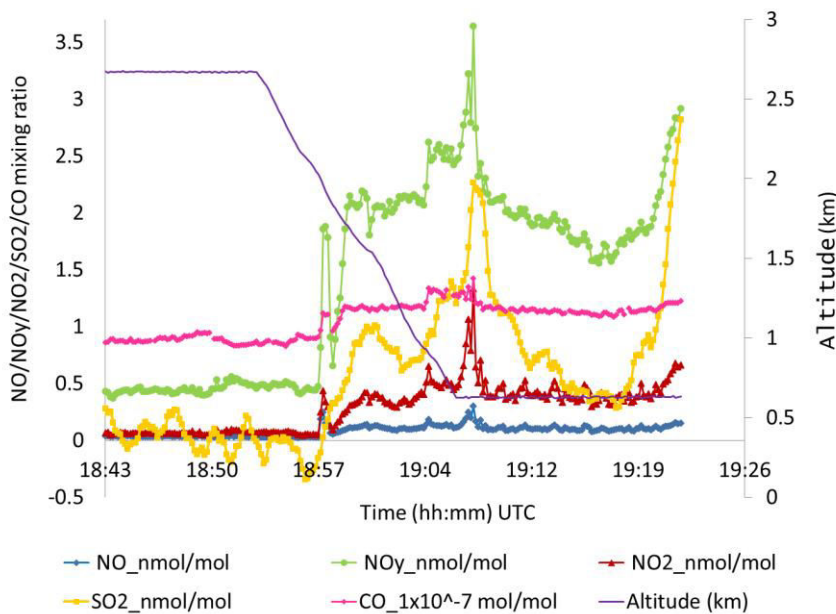
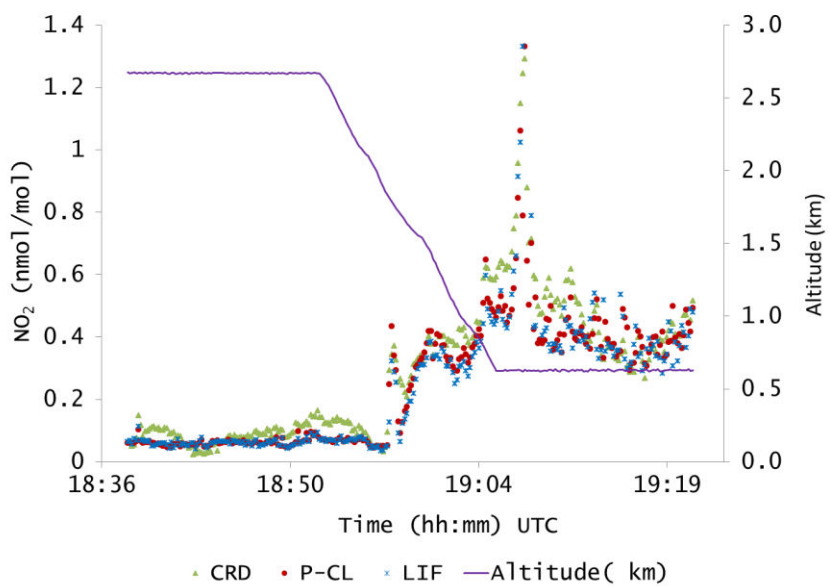


**Figure 7.3** Side-by-side intercomparison trace gas measurements. *Figure 7.3A Comparison of LIF, P-CL, and CRD side-by-side measurements. Figure 7.3B multiple trace gas sensor response to nearby power plant.*

concentrations of 0.06 (+/- 16%) nmol/mol while the LED-CRD average NO<sub>2</sub> was 0.08 (+/- 100%) nmol/mol NO<sub>2</sub> in air (i.e. at the detection limit). The P-CL and LIF LFT NO<sub>2</sub>

concentrations measured here are similar to those reported in [Blonde et al.'s 2007](#) globally

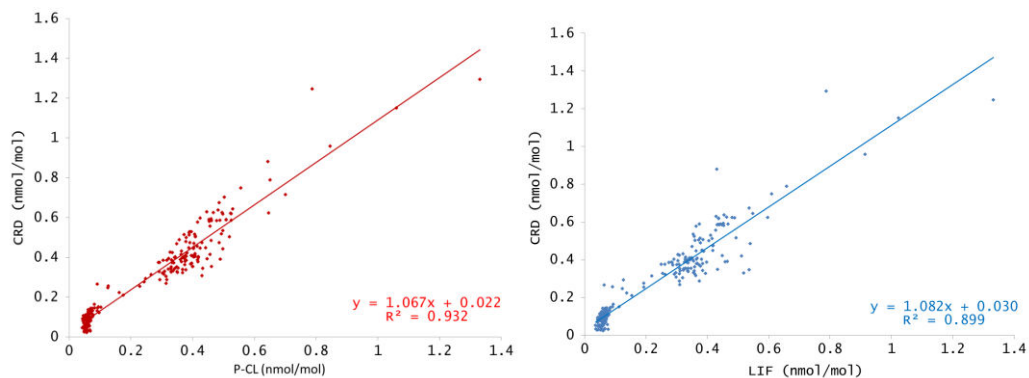


**Figure 7.4** Correlation plots between UMD, and P-CL and LIF from side-by-side flight.

averaged GOME result. A majority of  $\text{NO}_2$  concentrations at this altitude were found to routinely fall near or below the LED-CRD detection limit. During the descending spiral, tropospheric  $\text{NO}_2$  concentrations increase into the  $3\sigma$  detection range, near 1.6 km, thereby increasing the confidence in the reported values [Skoog et al. 2008](#). The peak maximum observed by all three instruments, near the beginning of the low altitude, 0.6 km transect, at 19:09 UTC, corresponds to emissions from the Indian River Generating Station according to a back trajectory of winds performed in HYSPLIT ([http://ready.arl.noaa.gov/HYSPLIT\\_traj.php](http://ready.arl.noaa.gov/HYSPLIT_traj.php)). This is an active, coal-fired electrical generating facility located at the confluence of the Indian River and Island Creek in Sussex County Delaware.  $\text{CO}$ ,  $\text{SO}_2$ ,  $\text{NO}$ , and  $\text{NO}_y$  also showed corresponding peaks and this data is available to the public at <http://www-air.larc.nasa.gov/missions/discover-aq/P3B-extract.html>. See Figure 7.3B. At 1.30 nmol/mol  $\text{NO}_2$  in air, the plume concentration exceeds both the limit of detection and limit of quantitation ( $10\sigma$  baseline noise) and the measurement uncertainty fell to 5.1%. Because the NIST standard

addition calibration uncertainty is estimated to be 1%, baseline drift drives the measurement uncertainty. The peak base is 210 s wide, which corresponds to a horizontal distance of 19 km.

Correlation of the 10 s averaged LED-CRD data to the P-CL and LIF 10 s averaged data is shown in Figure 7.4A and 7.4B. Plots of the LED-CRD data to the P-CL and LED-CRD vs. LIF have slopes 1.07 and 1.08, respectively, with  $R^2$  values of 0.932 and 0.899 respectively. Agreement between LIF versus P-CL has a slope of 0.94 and  $R^2$  of 0.939. The poor correlation between the lowest  $\text{NO}_2$  concentrations is a reflection of the large standard deviation of the LED-CRD instrument in a range very near its detection limit. Table 7.5 extends the comparison to include 1 s and 60 s averaged data. Improved temporal resolution and less of propagated error generated from data binning shows correlation coefficients between CRD and the other  $\text{NO}_2$  measurements closer to unity. This side by side flight data demonstrates that the commercial Los Gatos cavity ring down  $\text{NO}_2$  gas analyzer is suitable for pollution studies in the BL and LFT.

#### 7.5.4 Summary of summer 2011 $\text{NO}_2$ measurements

##### 7.5.4.1 $\text{NO}_2$ column content

In the eastern U.S., the natural abundance of hydrocarbons makes  $\text{NO}_2$  the critical ozone precursor. Once  $\text{NO}_2$  is formed, its complicated lifetime is dictated by a series of pathways such as sequestration into longer lived reservoir species PAN (peroxyacetyl nitrate) and alkyl nitrates, recycling through photolytic dissociation to nitric oxide and odd oxygen allowing for ozone formation, removed by dry deposition or wet and dry

deposition after reaction with OH to produce nitric acid. Knowledge of the vertical distribution and characterizing the abundance in and above the BL is necessary

**Table 7.5** A comparison between the 1 s, 10 s, and 60 s scatter plots for NO<sub>2</sub> measured by three instruments during the 27 July 2011 side by side flight

| Technique    | Slope (m) | $e_m$ | Intercept (b) | $e_b$ | R <sup>2</sup> | Avg time (s) |
|--------------|-----------|-------|---------------|-------|----------------|--------------|
| CRD vs. P-CL | 1.009     | 0.008 | 0.041         | 0.003 | 0.844          | 1            |
| CRD vs. LIF  | 0.950     | 0.011 | 0.062         | 0.003 | 0.812          | 1            |
| CRD vs. P-CL | 1.067     | 0.018 | 0.022         | 0.006 | 0.932          | 10           |
| CRD vs. LIF  | 1.076     | 0.023 | 0.031         | 0.007 | 0.899          | 10           |
| CRD vs. P-CL | 1.136     | 0.036 | 0.007         | 0.014 | 0.959          | 60           |
| CRD vs. LIF  | 1.069     | 0.057 | 0.085         | 0.019 | 0.895          | 60           |

The 10 s data is presented in Figure 7.4. The information below is for the line  $NO_{2(LED-CRD)} = (m \pm e_m) * ref + (b \pm e_b)$ . The reference values are either P-CL or LIF measurements.

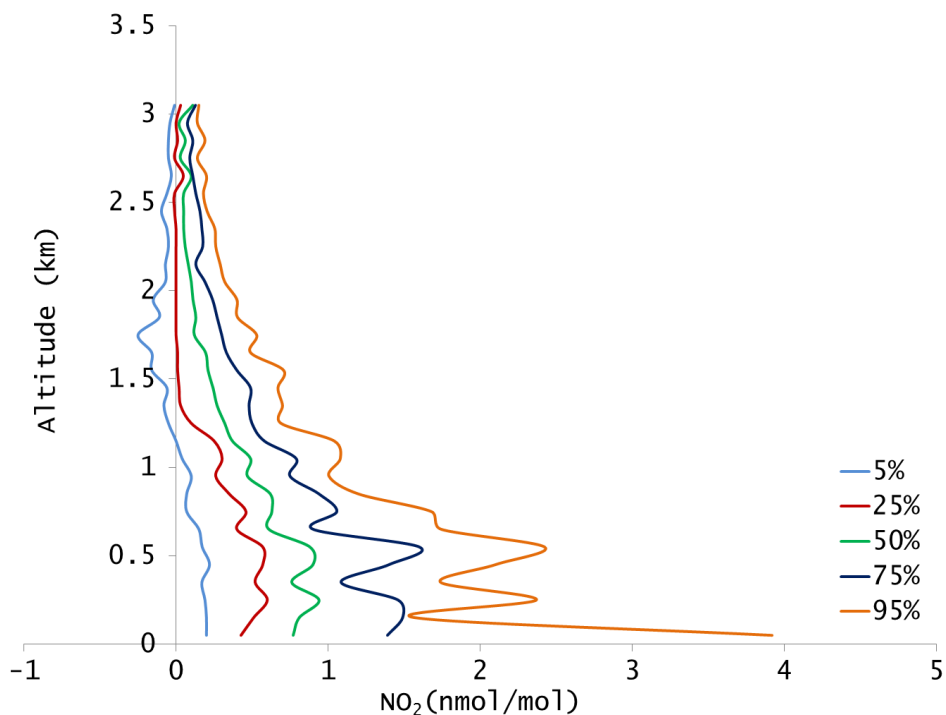


**Figure 7.5** Vertical variability of NO<sub>2</sub> in BL and LFT reservoirs. Percentile analysis of 2011 Flights, 6 June to 31 July. A total of 23 flights and 65 spirals, both AM and PM. BL measurements show more variability, but the variability smooths out with increasing altitude and distance from point sources.

for successful predictive modeling of ground level ozone concentrations [Logan et al. 1989](#); [Napelenok et al. 2008](#).

Percentile binning of the 2011 summertime data, Figure 7.5, show that the BL and LFT can be stratified into three general horizontal cross sections. Looking at the median value, between the ground and 1.3 km, NO<sub>2</sub> has the most variation due to BL fine structure resulting from spatially varying sources. For instance, the highest summer time flight NO<sub>2</sub> measurements were of ship plumes during low-level flights over the Chesapeake Bay. At approximately 17 m above the water surface, spikes up to 14 and 17 nmol/mol ambient NO<sub>2</sub> were observed. Between 1.3 and 2.1 km the degree of spatial homogeneity increases as NO<sub>2</sub> observations gradually slope negatively toward a low NO<sub>x</sub> regime. Between 2.1 km and our maximum altitude, 3 km, NO<sub>2</sub> values are within bounds of a low NO<sub>x</sub> regime. In this 2.1 to 3 km layer, the ozone production rate would be slow [Trainer et al 1993](#); [Kleinman et al 1994](#), but cooler temperatures and greater wind speeds impact the lifetime and transport of NO<sub>2</sub> and NO<sub>2</sub> reaction products (i.e., ozone and particulate matter) contributing to wider ranging regional effects. Negative concentrations, in the lowest percentile bin, are mostly in the LFT and are a reflection of the large standard deviation associated with measurements as atmospheric mixing ratios approach the instrument's detection limit. If the baseline of the cavity ringdown absorption monitor is stabilized, the improved signal to noise ratio at lower concentrations can result in a lower detection limit and the instrument may be suitable for measurements of NO<sub>2</sub> in more pristine environments. Measures to stabilize the optical cavity such as temperature control should be investigated.



#### 7.5.4.2 Regional observations

Summer 2011 Maryland flight observations routinely show the presence of moderate levels of  $\text{NO}_2$  in both upwind and downwind rural spiral locations. Figure 7.6

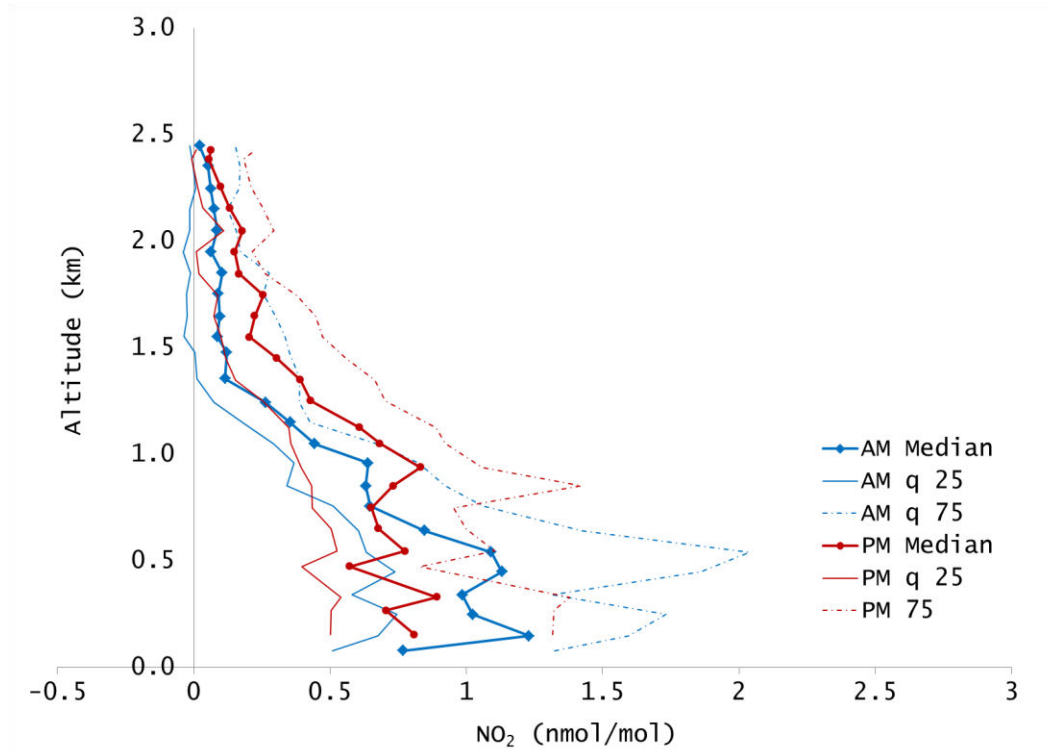


**Figure 7.6** AM/PM  $\text{NO}_2$  quartile analysis. Comparison of  $\text{NO}_2$  observations collected upwind and downwind of the Baltimore Washington metropolitan region. The solid line with dots represents the median values, bracketed by 25% and 75% quartiles. Upwind/AM measurements are before solar noon and downwind/PM measurements are after solar noon.

compares the median and quartile values of upwind and downwind column contents. The AM/Upwind profiles decrease exponentially with a scale height of  $\approx 1.2$  km, while the PM/Downwind column distribution is fairly uniform up to 1.0 km, then gradually reaches the detection limit near 2.5 km. Figure 7.7 compares median  $\text{NO}_2$  values for all DISCOVER-AQ observations in the Washington, D.C. / Baltimore metropolitan

nonattainment area measured on both planes (all three instruments). Measurement sites are posted in Figure 7.1. The P3-B data show slightly higher levels of NO<sub>2</sub> in the BL near 0.4 km, than the downwind LED-CRD Cessna data due to the more urban flight P3-B path. The P3-B sampled five sites in the Baltimore nonattainment region and flew 47 low passes along the I-95 and 295. Between the different aircraft flight paths and spiral locations,

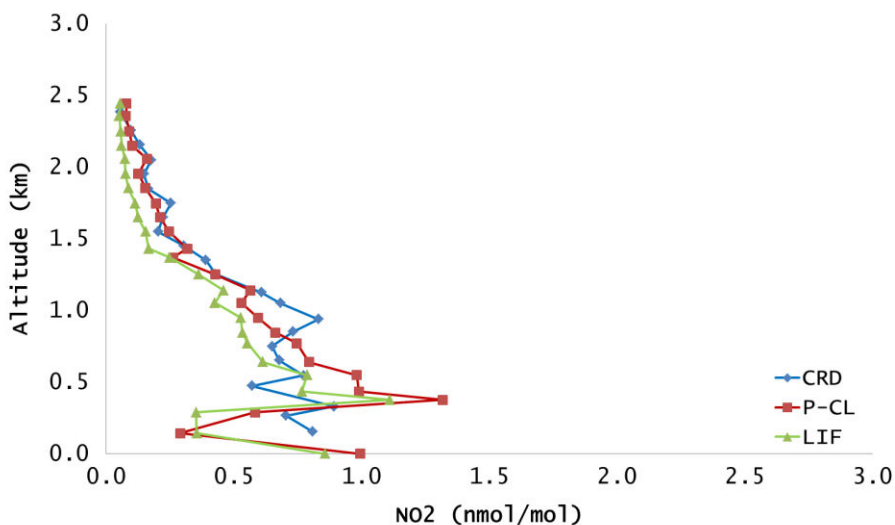


**Figure 7.7** Average vertical NO<sub>2</sub> distribution for the metropolitan region. A comparison of median CRD summertime aircraft measurements downwind of Baltimore to median P-CL and LIF measurements made along the Baltimore/Washington urban corridor during DISCOVER AQ.

the three combined NO<sub>2</sub> profiles show similar vertical columns for July, although BL measurements with more point source influence shows signs of a BL maximum between 0.4 and 0.5 km. The LED-CRD median PM profile over Maryland is similar to P-CL NO<sub>2</sub> observations made over the Donau Valley in Austria, May 2001, between altitudes of 0.9 km and 3 km [Heland et al. 2002](#). 82 % and 75 % of total NO<sub>2</sub> in the AM and PM columns, respectively, is observed to be below 1 km altitude. Similar BL/total column

density ratios were observed in Houston, TX, 2004 and the Po Valley, Italy (2006) [Schaub et al. 2006; Ordóñez et al. 2006](#).

The sum of the binned UMD AM/Upwind column content was  $2.97 \times 10^{15}$  molecules/cm<sup>2</sup> and the sum of the binned UMD PM column content was  $3.05 \times 10^{15}$  molecules/cm<sup>2</sup>. With 5% measurement uncertainty, the averaged Baltimore/Washington, D.C. downwind vertical column content was not significantly different from the upwind column content indicating that changing near-surface measurements are influenced by BL

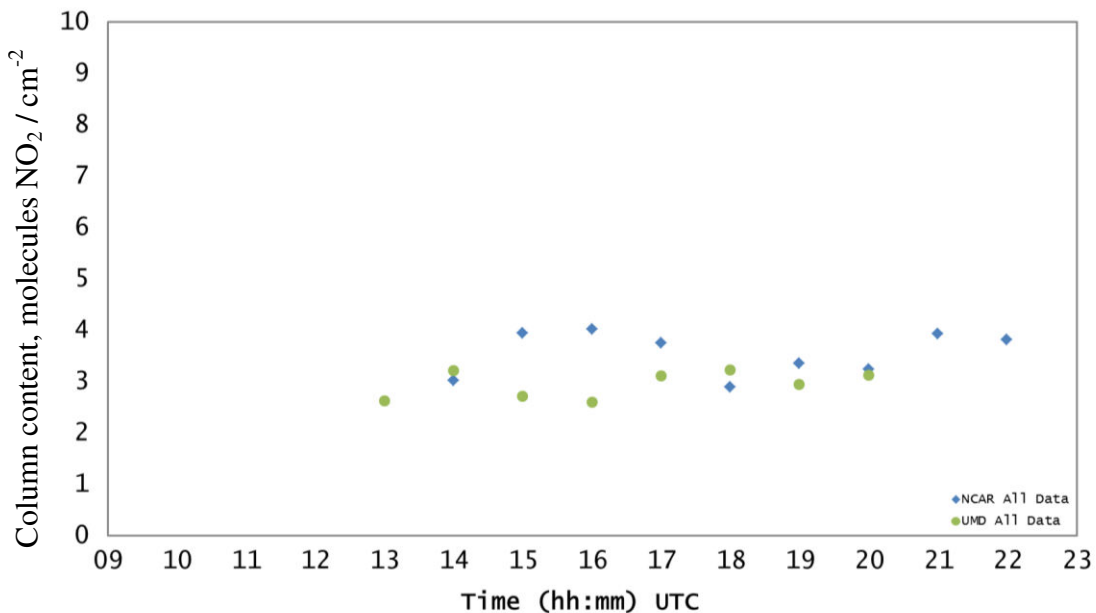


**Figure 7.8** *NO<sub>2</sub> hourly column content. Column content, hourly, from 1430 UTC to 2230 UTC. These are the NCAR P-CL and UMD CRD NO<sub>2</sub> measurements. The variation of the P3-B NCAR hourly column content is 12% while the variation of the UMD CRD column content is 32%.*

dynamics. A Canadian study examining transport of polluted air across Lake St. Claire to rural Canada also observed, via Multi Axis Differential Optical Spectroscopy, that the vertical column density showed less dependence on the time of day than did their BL measurements [Halla et al. 2011](#). Figure 7.8 shows the UMD regional column content

binned by the hour in comparison to the P3-B metropolitan area column content. The column contents shown here are limited to 0.3 km to 3.0 km, the altitude range covered by both planes. The hourly upwind column content is slightly ( $\approx 22\%$ ) smaller than the measured column content for similar times in the metropolitan area. While there is more  $\text{NO}_2$  measured over the urban area, upwind/rural  $\text{NO}_2$  mixing ratios (for the same time of day) are substantial enough for ozone production in the BL, contributing to the regional nature of eastern U.S. air quality episodes [He et al. 2013](#). The regionally averaged  $\text{NO}_2$  vertical distribution with variations in the hourly resolution supports conclusions from [Castellanos et al., \(2011\)](#) indicating model over estimations of urban  $\text{NO}_x$  and under estimations of rural  $\text{NO}_x$  are in part a result of too short  $\text{NO}_x$  lifetimes, and not accurately capturing advection between rural and urban areas.

## 7.6 Conclusions

This chapter describes an updated, stabilized, commercially available cavity ringdown spectrometer that reliably measures ambient  $\text{NO}_2$  at the surface and aloft. In an intercomparison with two well characterized research-grade  $\text{NO}_2$  detectors, this instrument compared favorably for atmospheric  $\text{NO}_2$  mixing ratios ranging from 0.08 nmol/mol and 1.3 nmol/mol in the BL and LFT.

The LED-CRD calibration coefficient was verified five times at three locations over five months via GPT and standard dilution. The sensitivity of the instrument was stable within 4%.

Altitude profiles from 23 research flights (65 profiles) during the summer of 2011 were obtained upwind of the Baltimore/Washington, D.C. metropolitan area in the

morning and downwind of the area in the afternoon. Looking at all observations collected during forecasted ozone events in the Mid-Atlantic States, the median (quartiles) NO<sub>2</sub> mixing ratio was 0.84 nmol/mol (0.5 nmol/mol to 1.4 nmol/mol) in the lowest 0.5 km and 0.21 nmol/mol (0.01 nmol/mol to 0.60 nmol/mol) nmol/mol at 1.5 km. More variability was observed in the BL.

Morning upwind NO<sub>2</sub> mixing ratios showed a rapid decrease between the BL and LFT with an effective scale height of  $\approx 1.2$  km in the morning. Afternoon downwind profiles were more homogeneously distributed with a gradual decrease to the detection limit between 1.6 and 2.5 km. EKMA diagrams e.g., [Chameides et al. 1992](#) show that for the range of BL NO<sub>2</sub> mixing ratios observed here (0.5 nmol/mol to 1.5 nmol/mol) mid-day ozone production rates are relatively insensitive to volatile organic compound levels and range from 1 nmol/mol/h to 10 nmol/mol/h. Total column contents between the AM/upwind and PM/downwind were remarkably similar indicating that NO<sub>2</sub> is widely distributed over the eastern US contributing to the regional (spatial scales of approximately 1000 km) nature of smog events.

*Acknowledgements.* The aircraft flights were funded by Maryland Department of the Environment and the National Oceanic and Atmospheric Administration (NOAA). From NIST we thank Dave Duewer for help with data analysis and Jim Norris for calibrating the ozone monitor and primary standard. We thank Winston Luke, Paul Kelley and Xinrong Ren from the (NOAA) for conducting a month long field comparison to their P-CL NO<sub>2</sub> instrument. We thank Patricia Castellanos for instrument instruction

and support. We thank Ronald Cohen and Andy Weinheimer for sharing data and NASA for supporting the DISCOVER-AQ air campaign and AURA and ACAST funding.

*Disclaimer.* The identification of certain commercial equipment, instruments, or materials does not imply recommendation or endorsement by the National Institute of Standards and Technology. These identifications are made only in order to specify the experimental procedures in adequate detail.

## CHAPTER 8: CONCLUSIONS

A challenge to making effective environmental policy is the need to actively facilitate commerce and stimulate economic growth while simultaneously limiting the harmful side effects of energy sources and industry. The challenge for scientists from academia, industry, and the federal government is to make available scientific conclusions based on accurate and reproducible data. The research results provided in this dissertation enhance the experimental scientist's tool set for data collection and analysis of the NAAQS criteria pollutants most relevant to Maryland, and much of the U.S., nonattainment, ozone, and PM<sub>2.5</sub>. Results appeared as a paper in the *Journal of Atmospheric Chemistry* on NO<sub>2</sub> methods and concentrations as well as in the journal *Analytical Chemistry* where new methods for analysis of organic aerosol appeared. A third paper on organic aerosol observed from aircraft is in preparation.

Water soluble organic carbon frequently dominates ambient PM<sub>2.5</sub>. Aircraft flights during DISCOVER AQ in the NASA P3 demonstrated that this was true for air sampled over the Baltimore / Washington, D.C. metropolitan corridor. The dominance of WSOC elicits the need for analytical methods to elucidate the molecular composition of ambient aerosol concentrations, crucial to understanding and modeling the source, formation and fate of ambient particulate matter.

In this work, I enhanced the RAMMPP aerosol analytical capabilities resulting in a report of 16 organic acids, three inorganic anions, and five inorganic cations exceeding the LOD (3xSbl/slope) present in the boundary layer (1 km above surface) during an epic 6 day pollution episode. Twelve of the sixteen organic acids exceeded the limit of

quantitation (LOQ) on at least one of two collection days. This is the first study of this nature conducted for RAMMPP. In this work I:

1) Developed an IC-MS/MS method demonstrating that mass selective ion monitoring performed with a triple quadrupole mass analyzer overcomes the lack of specificity associated with more commonly used IC methods employing a universal conductivity detector. MS-MS detection enhances IC methods are usually limited to analysis of inorganics and oxalic acid. My method exhibits sensitivity as low as part per trillion concentrations and achieves resolution of molecules not resolved through IC/CD due to incomplete chromatographic separation.

2) Demonstrated the importance of ensuring the similarity between the matrix of the reference standard and the matrix of the sample extracts due to shifting column retention. Incorrect peak assignment would occur, particularly if the nonselective conductivity detector is the only method of species confirmation.

3) Enhanced the RAMMPP aerosol sampling system by installing a shrouded aerosol inlet. With additional pumping, the sampling efficiency of particles up to 2.5  $\mu\text{m}$  in diameter should approach 100%. A comparison of scattering data collected during a side-by-side flight with the NASA P3-B showed that we are within 30% of NASA collection, a value within the combined uncertainty of the two methods.

While *in situ* bulk characterization methods offer better temporal resolution and less sampling complexity they lack molecular resolution. The understanding of bulk particle characterizations can be enhanced through improved molecular resolution. This study demonstrated that significantly higher concentrations of organic acids are associated with recirculating urban and tropical air than with air in strong westerly winds.



An air mass fed by westerly winds off of the Appalachian Mountains showed lower concentrations of the organic acids observed two days prior and was instead dominated by cis pinonic acid. This study indicates that the size fraction and PM composition was correlated to air mass source, but not correlated with temperature, relative humidity or ozone.

NO<sub>2</sub> is also a criteria pollutant, but rarely exceeds NAAQS. More significant to Maryland NAAQS attainment is the role of NO<sub>2</sub> as an ozone precursor. Ozone formation during air quality episodes is a main driver for pushing Maryland out of attainment. After modifying and evaluating a commercially available cavity ringdown NO<sub>2</sub> detector I installed and tested it on a Cessna research aircraft and measured NO<sub>2</sub> profiles west and generally upwind of the Baltimore/Washington, D.C. area in the morning and east (generally downwind) of the metropolitan region in the afternoon. Column contents (surface to 2500 m altitude), collected over 23 research flights, demonstrated that NO<sub>2</sub> is widely distributed over the eastern US. Average distributions  $\approx 3 \times 10^{15}$  molecules/cm<sup>2</sup> contributes to the regional nature of smog events. These NO<sub>2</sub> measurements were referred to in an Amicus Brief to the U.S. Supreme Court case on the Cross State Air Pollution Rule, CSAPR. The Supreme Court later ruled in favor of the EPA's authority to regulate the cross state transport of pollutants.

## CHAPTER 9: FUTURE WORK

### 9.1 Molecular characterization of particulate matter

In this dissertation, the work reported on the molecular resolution of the constituents composing particulate matter, serves as a proof of concept demonstrating that IC-MS/MS methods are suitable for tracer molecule and source apportionment studies from an aircraft platform. The low detection limits afforded by this method are crucial for aircraft sampling success because unlike surface sampling which typically runs on the order of hours or days, aircraft filter sample collections are typically on the order of ~ 30 minutes. The first important future step for this project is to enhance the aircraft sample collection method so that the uncertainty in the sample volume can be evaluated. The uncertainty in the volumetric flow is, at this point, the largest source of uncertainty in the reported data. The Staplex blower should be replaced with a filter manifold and pumping system incorporating a mass flow controller. The mass flow controller should be capable of data logging and provide readout so that the pumping flow rate can be adjusted when necessary. Adjustable flow is already incorporated into the set up. The second future step would be to continue expanding the library of molecules for which this method is applicable. Based on the conductimetric response observed in the monocarboxylate region of the 21 and 23 July 2011 chromatograms, I would begin investigating alkylated and hydroxylated monocarboxylates. A good place to research reasonable molecular candidates for inclusion into the method is in GCMS papers, particularly those published by [Kawamura, 1985 #23;Kawamura, 2012 #47]. Another class of molecules that should be evaluated as candidates to be detected by this

method is amino acids due to their implication in brown carbon formation [Samy, 2011 #35]. At this point, I do not recommend making it a primary goal to drive down the method detection limit. I think the current detection limits are suitable for pollution and source apportionment studies. I would only work to improve method detection limits if a specific and irrefutably useful tracer molecule is observed at very low concentrations.

With minor improvements to the sampling system, the next step is to begin accumulating a data base from as many samples as possible so that correlations between air mass and particulate matter composition can be developed. This work only correlates two trace gases, O<sub>3</sub> and SO<sub>2</sub>, and data from the particle counters. Future research flight planning should also include evaluation of concentrations of NO<sub>2</sub>, CO, and aerosol scattering. Past studies have suggested that certain acids such as malic acid and other C<sub>4</sub> dicarboxylates show enriched concentrations in urban air in comparison to rural air [Kawamura, 2012 #47; Rohrl, 2002 #32; Tsai, 2008 #41]. Some of these studies were conducted using ion chromatography with conductimetric detection while the Kawamura study used GCMS for acid analysis. My IC-MS/MS results indicate that some of the C<sub>4</sub> carboxylates have isomers that were not chromatographically resolvable. This result would not have been observable by IC alone. My preliminary results for 21 and 23 July 2011 agree with prior reported results that urban air shows higher concentrations of the C<sub>4</sub> carboxylates than did the rural air but additional method development could be conducted to determine if dicarboxylate concentrations reported as a function of the area under the C<sub>4</sub> carboxylate peak are attributable to the commonly reported acids only or if these reports should also include additional isomers. More studies of this nature should

be continued upwind and downwind of the Baltimore / Washington, D.C. metropolitan area.

## 9.2 Continued evaluation of the aerosol sampling system

The newly implemented aerosol sampling system was demonstrated, through a comparison of light scattering, to be within 30 % of the NASA P3 measurements. This 30% difference was not likely to have affected the aerosol collection because the volumetric flow of the Staplex blower is approximately 3x greater (~ 50 LPM). Additional pumping and a mass flow controller should be added to the sampling system aft of the aerosol optical instruments. The flow should be adjustable so that isokinetic can be maintained. Furthermore, the tubing and hardware connected to the Nephelometer needs to be replaced so that what should be 30 LPM flow is no longer choked to 15 LPM. After changing the tubing, and adding pumping another side-by-side flight to evaluate isokinetic should be flown when the opportunity presents itself. Preflight planning should include a side-by-side ground test of the Nephelometers to be used in the experiment. The ground test should include sampling of both dry and humidified air. Also refer to the manual and check the slopes of the temperature and relative humidity setting in the Nephelometer program and make sure these are the same for both instruments. With the bias removed, a Lagrangian experiment could be performed to determine the rate of increase in aerosol scattering coefficient on smoggy days.

### 9.3 Measurements of NO<sub>2</sub> by a commercially available CRD instrument

It was demonstrated in this work that the commercially available cavity ringdown NO<sub>2</sub> detector has a detection limit of 80 ppt restricting the use of this instrument to mid NO<sub>x</sub> regimes on the ground and pollution studies by aircraft. Improving the baseline stability will drive down the detection limit making the instrument also useful in low NO<sub>x</sub> regimes. A source for baseline drift could be the sorption of water vapor onto the chemical scrubber. Dr. Xinrong Ren encased the scrubber in a heated box and will evaluate if maintaining the scrubber at a temperature prohibiting water vapor adsorption decreases the magnitude in baseline change and speed with which baseline stability is achieved at different altitudes. Also, a thorough evaluation of ergodic periods on the ground versus during flight will result in better experimental flight planning and lower absolute uncertainty in the aircraft measurements. Continued aircraft data collection by this instrument during pollution episodes will make it possible to evaluate the gap between surface measurements and emission point sources and model output. Measurements of the profiles of NO<sub>2</sub> upwind and downwind (in rural and urban) environments would be useful for evaluating models of NO<sub>2</sub> transport and chemistry as well as for future satellite studies of daily cycles of column content. Winter flights would help elucidate the impact of season on the lifetime and transport of NO<sub>x</sub>.

## Appendix

### Appendix A - Aerosol inlet and sampling specifications

#### Aerosol inlet

##### Aft aluminum block support

**Description:** Aft aluminum block is used as the rear support for the aluminum tubing used to support the aerosol inlet. The aft aluminum block will be secured to a previously mounted camera rack using AN4 bolts, AN960 flat washers and safety wire.

##### Aluminum block:

Material type: 2024 T-351, Cold finished square,

Purchased from Access Metals, Inc., 8866 Kelso Dr., Baltimore, MD 21221

Produced by Kaiser Aluminum Fabricated Products, LLC., Tennialum, PO Box 659, Jackson, TN 38302

Weight: 2.4 lbs\*

Dimensions: 1.5 sq. x 14.125 in

##### Hardware:

**Bolts:** AN4H7, Alloy steel, MS, bolts ¼-28 x .906, Nominal Length: 29/32", Grip: 7/16" Haire Aviation LLC Aircraft Fasteners, hardware, and supply, 9335 Freeman Rd, Sanger, TX, 76266-5914

**Washer :** AN960-416, Flat, P/N AN960-416, PO: 154735, LOT: 30-15445 Aircraft Spruce & Specialty Company, PO Box 3367, 452 Dividend Dr., Peachtree City, GA 30269

<http://www.aircraftspruce.com/catalog/hapages/flatwashers.php>

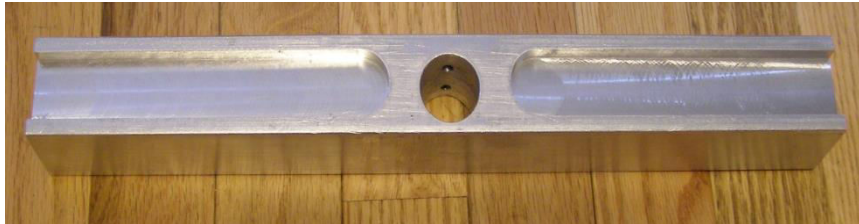
**Heli-Coils:** Heli-Coil, ¼-28, stainless steel, P/N 5528-4, Emhart Teknologies, Shelton, CT 06484

**Set screw:** 10-32 x ¼, Product description: 1032X1/4 set screw, P/N 04-00184, LOC: 05PC, PO: 142815, LOT: 30-15348, Aircraft Spruce & Specialty Company, PO Box 3367, 452 Dividend Dr., Peachtree City, GA 30269

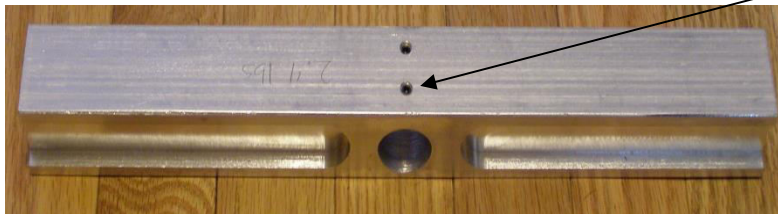
<http://www.aircraftspruce.com/catalog/hapages/setscrews.php>

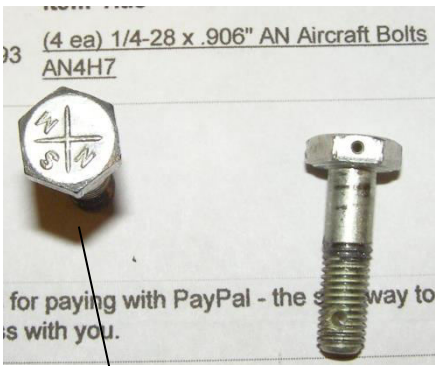
**Heli-Coils:** Heli-Coil, 10-32, stainless steel, P/N 5528-3, Emhart Teknologies, Shelton, CT 06484

\* FAA requirements dictate traditional units for engineering drawings.



2 x 10-32 set screws and 10-32 helicoil inserts to hold Aluminum pipe in place





1/4-20 heli-Coil insert and AN4 bolt is used to secure the Aft Aluminum rod to the camera mount

Holes for safety



## Forward aluminum block support

**Description:** A forward aluminum block will be used to help support the aerosol inlet tubing. The block will be secured to a previously mounted camera rack using threaded AN4-41 bolts.

### Aluminum block

Material type: 6061-T6

Purchased from Access Metals, Inc., 8866 Kelso Dr., Baltimore, MD 21221

Produced by Kaiser Aluminum Fabricated Products, LLC., Tennialum, PO Box 659, Jackson, TN 38302

Weight: 0.5 lbs

Dimensions: 1.5H x .75W x 5.625”L

### Hardware for the Front Aluminum Block

**Threaded Bolts:** AN4-41 Bolt drilled, Nominal length: 4-5/32, Grip length: 3-11/16”

<http://www.aircraftspruce.com/catalog/hapages/an4.php>

The bolts were purchased with threading on the bottom only. The threading was continued to the head of the bolt by hand.

**Washers:** Lock washers, cadmium plated, P/N MS35338-44 (AN935-416), Lot # 30-15482

<http://www.aircraftspruce.com/catalog/hapages/lockwashers.php>

**Nuts:** Elastic stop nuts, AN365-428A, MS21083N4 Stop Nut, Cad plated stop nuts

[http://www.aircraftspruce.com/catalog/hapages/an363\\_1.php](http://www.aircraftspruce.com/catalog/hapages/an363_1.php)

**Steel Tubing:** ½ OD x .125 wall x 1.25 in stainless steel. (id of this tube is 3/8in)

<http://www.accessmetalsinc.com>

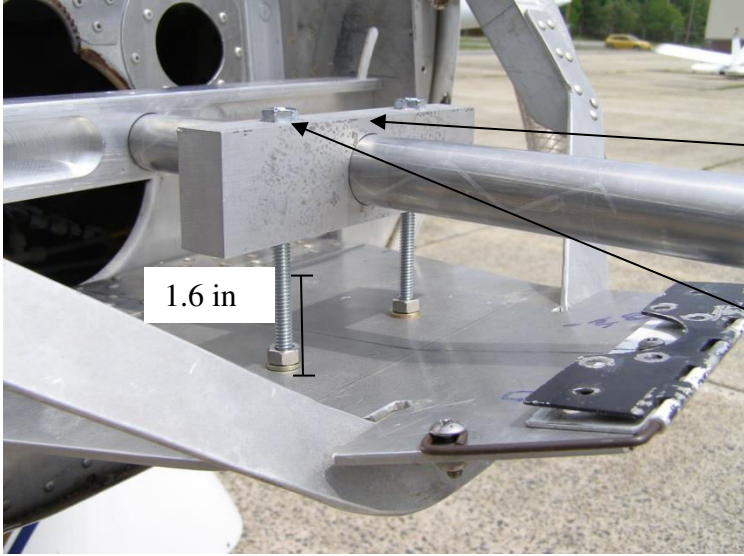
**Set screw:** 10-32 x ¼, Product description: 1032X1/4 set screw, P/N 04-00184, LOC: 05PC, PO: 142815, LOT: 30-15348,

Aircraft Spruce & Specialty Company, PO Box 3367, 452 Dividend Dr., Peachtree City, GA 30269

<http://www.aircraftspruce.com/catalog/hapages/setscrews.php>

**Heli-Coils:** Heli-Coil, 10-32, stainless steel, P/N 5528-3, Emhart Teknologies, Shelton, CT 06484

[http://www.aircraftspruce.com/catalog/hapages/an363\\_1.php](http://www.aircraftspruce.com/catalog/hapages/an363_1.php)



1.6 in



Helicoil inserts

Threaded AN4-41 bolt,  
lock washers and elastic  
stop nuts.

steel tube (1.24 in) will  
case the threaded nuts  
and extra adjustment  
will be achieved by adding  
and removing a couple of  
washers as necessary.



## Aluminum Tube

Material type: 6061 T-5 Alum, seamless tube, Lot #: F00000919

Purchased from Access Metals, Inc., 8866 Kelso Dr., Baltimore, MD 21221

Produced by Kaiser Aluminum Fabricated Products, LLC., 6573 W. Willis RD.,  
Chandler, AZ 85226

Weight: 0.7 lbs

Dimensions: 1 in O.D. x 0.65 wall x 29 in

**Grommet:** Buna-N/Nitrile Rubber, MS 35489-52, Mfr. Model # 3MRP3, Grainger Item  
# 3MRP3, AP# A16-22-400S, LOT# 90413

OD: 1-3/4"

ID: 1"

OT: 1/2"

Groove: 1/8"

Panel ID: 1-3/8"

Accurate Products Inc., 4646 Ravenswood Ave, Chicago, IL 60640

<http://www.grainger.com>



**Inlet nozzle**

Material type: Al 6061-T6

Weight: 1.2 lbs

Dimensions: See attached manufactures sheet

Droplet Measurements Technologies, 2545 Central Ave., Boulder, CO 80301

**Hardware:** Swagelok 316 RAC



## Gas Inlet

**Description:** A welded stainless steel tube will protrude 9” off of the aluminum nose cone plate. The tube will be fixed to the plate using a Swagelok tube fitting. A second point of security for the ss gas intake will be Adel clamps around both the gas intake and the aerosol intake. The two tubes are close enough to one another that the Adel clamps will be attached to each other. Threadlocking compound will be used on the Swagelok fitting and nail polish will be used to assess slippage. A zinc chromate primer will be used to coat the aluminum plate where the plate comes into contact with the steel Swagelok fitting.

### **Aluminum nose cone plate note:**

The aluminum nose cone plate has already been approved for flight as a part of the Camera rack mount. In our design, the plate material will be upgraded to 6061 T6 aluminum, purchased from Access Metals, MD, to provide increased strength and bearing capability. The older, approved, plate used 3003 Aluminum.

### **Stainless Steel Tubing:**

Material type: welded 316 stainless steel  
Weight: 0.283 lbs.  
Dimensions: ½ in OD, x 0.49 wall x 9.25 in  
TW metals, NJ

### **Adel clamps:**

½”, P/N 21919-WDG8, lot # 30-15496  
1”, P/N MS21919-WG16, Lot# 30-15494  
Aircraft Spruce & Specialty Company, PO Box 3367, 452 Dividend Dr.,  
Peachtree City, GA 30269  
<http://www.aircraftspruce.com>

### **Fastener for the Adel clamps and Aluminum strip**

**bolts:** AN3-5 drilled, cad plated, Nominal length: 5/8, Grip length: 1/4, P/N AN3-5  
Aircraft Spruce & Specialty Company, PO Box 3367, 452 Dividend Dr.,  
Peachtree City, GA 30269  
<http://www.aircraftspruce.com>

**Washer :** Lock washers, size 10. P/N MS35333-39 (AN936-A10), cad plated  
Aircraft Spruce & Specialty Company, PO Box 3367, 452 Dividend Dr.,  
Peachtree City, GA 30269  
<http://www.aircraftspruce.com>

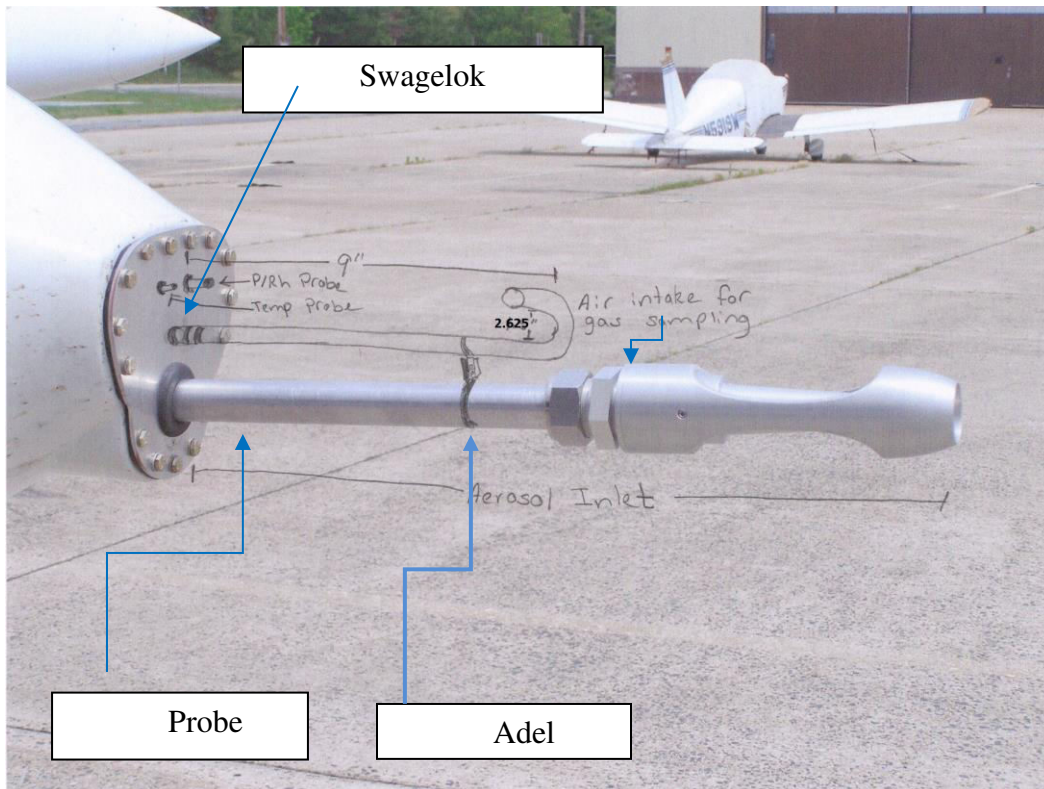
**Nuts:** Elastic stop nut, 10-32, [MS21083N3](#) (AN364-1032A), cad plated

Aircraft Spruce & Specialty Company, PO Box 3367, 452 Dividend Dr.,  
Peachtree City, GA 30269  
<http://www.aircraftspruce.com>

### Zinc Chromate Primer

PTI Zinc Chromate Primer, Yellow, QT. P/N 09-00919  
Aircraft Spruce & Specialty Company, PO Box 3367, 452 Dividend Dr, Peachtree  
City, GA 30269  
<http://www.aircraftspruce.com>

**Bulkhead union:** SS Swagelok tube fitting, ½ in tube O.D., P/N SS-810-61  
Weight: 0.309 lbs.  
[http://www.swagelok.com/search/product\\_detail.aspx?part=SS-810-61#](http://www.swagelok.com/search/product_detail.aspx?part=SS-810-61#)





bolts, lock nuts,



## Temperature, pressure, humidity probe

Weight: 4lbs (includes readout box, cables and 2 probes)

Dimensions: 4.5(W) x 7.25(L) x 3.25(H)

Total length of temp and P/RH probes: 3.25"

### Hardware:

**Machine screws:** 1/4-20 x 0.75 machine screws, P/N: 04-01343, MS35206-281 Screw, Aircraft Spruce

Aircraft Spruce & Specialty Company, PO Box 3367, 452 Dividend Dr, Peachtree City, GA 30269

<http://www.aircraftspruce.com>

**Washer :** Lock washers, 1/4 in. P/N MS35333-40 (AN936-A416),

Aircraft Spruce & Specialty Company, PO Box 3367, 452 Dividend Dr, Peachtree City, GA 30269

<http://www.aircraftspruce.com>

**Nuts:** Hex jam nylock nuts, 18-8 S/S, 1/4-20, P/N 7721

Bolt Depot, 286 Bridge St., North Weymouth, MA, 02191

[www.boltdepot.com](http://www.boltdepot.com)

**Grommet:** Buna-N/Nitrile Rubber, MS 35489-44, Mfr. Model # 3MPN3, Grainger Item # 3MPN3

OD: 1-1/2"

ID: 1/2"

OT: 5/16"

Groove: 1/8"

Panel ID: 1-1/4"

Accurate Products Inc., 4646 Ravenswood Ave, Chicago, IL 60640

<http://www.grainger.com>

**Grommet:** Buna-N/Nitrile Rubber, MS 35489-35, Mfr. Model # 3MRH2, Grainger Item # 3MRH2

OD: 5/8"

ID: 1/4"

OT: 1/4"

Groove: 1/8"

Panel ID: 7/16"

Accurate Products Inc., 4646 Ravenswood Ave, Chicago, IL 60640

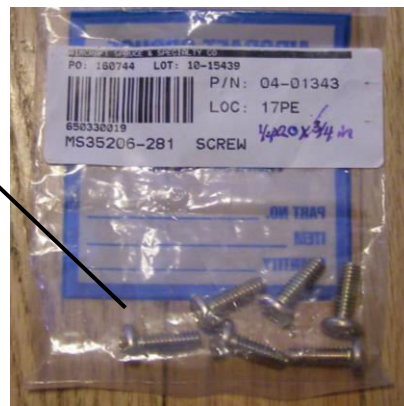
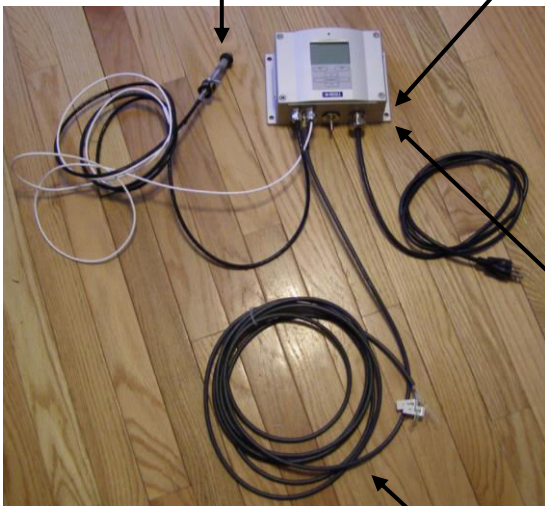
<http://www.grainger.com>

4 lbs. Probe box mounted on nose cone panel used to mount camera rack. Panel consists of two sheets of aluminum. Front sheet is .125 in thick, aft sheet is .0625 in thick.



The actual probe length that will extend past the aluminum plate is 3.25 in for the P/RH probe and 2.75 in for the Temp probe. MS spec grommets will hold the probes in place. See Fig above. The probe cables are 2M long.

The probe readout box casing has 4 pre-positioned points for



Data cable that will be run through the front end of the plane back to the cabin.



These nylock nuts, lock washers (AN960) will be used with the screws above to secure the probe box.

### **337 Attachments**

FAA Form 337\_CameraMount\_Nov94 – Contains 337 referencing the camera mount to which the forward and aft aluminum blocks are attached. Contains 337 referencing the reshaped nose cone through which the aluminum pipe runs.

FAA Form 337\_CameraMount\_Oct98 - Contains 337 referencing the camera mount to which the forward and aft aluminum blocks are attached. Contains 337 referencing the reshaped nose cone through which the aluminum pipe runs.

FAA Form 337\_Probe\_Cessna T206H – Contains 337 referencing a R/H wing mounted air sampling intake

### **Inlet Spec Attachments**

Manufactures sheet describing inlet used on our aircraft. This is the same inlet described by Antony Clark in McNaughton et al and used on the NOAA Cessna T206H.

### **References**

Ogren, J., Sheridan, P., Andrews, B., Long-term, in-situ aerosol profiling for climate and air quality studies. NOAA Earth Systems Research Laboratory, Global Monitoring Division, Boulder, CO. Power Point document: AAON-061020.ppt

McNaughton, C. S., et al. "Results from the DC-8 inlet characterization experiment (DICE): Airborne versus surface sampling of mineral dust and sea salt aerosols." Aerosol Sci. and Technol. 41 (2007): 136-59.

Huebert, B. J., et al. "PELTI: Measuring the passing efficiency of an airborne low turbulence aerosol inlet." Aerosol Sci. Technol. 38.8 (2004): 803-26.

Hegg, D., et al. "Determination of the transmission efficiency of an aircraft aerosol inlet." Aerosol Sci. and Technol. 39 (2005): 966-71.

### **Aircraft Info**

Make: Cessna

Model: 402B

Tail Number/Nationality and Registration Mark:N7875E

Owner: University Research Foundation, 6411 Ivy Lane, Suite 100, Greenbelt, MD., 20770

## Appendix B - Aerosol inlet installation – Extended instructions and pictures

### Materials

1. Aft aluminum block (1.5 sq. x 14.125 in)
  - a. 2 x AN4H7 ( $\frac{1}{4}$ -28 x .906), with hole for safety wire
  - b. Two flat washers
  - c. 2 set screws, 10-32 x  $\frac{1}{4}$
  - d. Safety wire
2. Forward aluminum block (1.5H x .75W x 5.625L)
  - a. 2x bolts (AN 4-41, 4-5/32), threaded
  - b. 6 x elastic stop nuts
  - c. two stacks of lock washers (add number for each side)
  - d. 1 x set screw, 10-32 x  $\frac{1}{4}$
  - e. 2 x stainless steel tube jackets ( 1.25 in)
  - f. 16 x Flat washers
  - g. 4 x lock washers
3. An assistant
4. 7/8" wrench
5. 7/8" ratchet
6. 3/8" wrench
7. 3/8" ratchet
8. Size of Allen wrench for set screws
9. Straight edge screw driver

### Instructions

1. Gather required materials
2. Check the integrity of the nose cone mount. Are the grommets in good condition? Is the bulkhead union secure?
  - a. If the bulkhead union is not secure, then the interface between the ss steal union and the aluminum plate should be coated with zinc chromate primer before securing. Tighten the fitting while the primer is wet.
3. Run the 1in diameter aluminum tubing through both the forward and aft aluminum support blocks. The smaller block should be closest to the inlet nozzle.
4. Connect the aluminum tube to the flexible conductive tubing and secure the connection with a worm drive using a flat head screw driver.
5. Position tubing in aft aluminum block using the black tape as an indicator for placement.

- a. This placement allows for 18" protrusion of inlet from nose plate in front of plane. Protrusion between 18 to 20 inches is acceptable. The inlet needs to protrude out far enough that the sample aerosol is not disturbed by the forward motion of the plane
  - b. The tape is positioned 4 inches from back end of tubing. Proper placement results in proper alignment of front Al block bolts with rack mount screw holes.
6. Screw in the bolts to the aft aluminum block but don't tighten
7. Position forward aluminum block so that the two, threaded 4 inch AN 40 bolts run through the two holes on the camera rack mount base.
  - a. Vertical support comes from ss sleeves and a number of washers
  - b. Refer to figure to see configuration of washers and nuts and ss jackets
    - i. 5 washers on left, 6 on right (because steel jackets are different lengths)
  - c. Below the camera mount plate, add a lock washer and an elastic stop nut.
  - d. Secure block by holding bolt in place with 7/8" wrench up top and using a ratchet wrench on the fiber-locking nut below.
  - e. Vertical adjustment of this block is changed by changing the number of washers.
  - f. Tighten set screws
8. Secure the aft aluminum block
  - a. Tighten AN 40 bolts.
  - b. Helicoils inside of the screw holes help the bolts to stay in place
  - c. Tighten set screws
9. Once the two blocks are bolted into place do the safety wire
10. Safety wire: Is threaded through the holes in the screw, twisted with a tool, then threaded through a hole in the camera mount platform, and twisted again. The pig tail is pushed against the camera mount so that it is up and out of the way
11. Remove all tools from camera mount platform
12. Lift the nose cone up to the plane and run all protruding pieces through nose cone. This is a two people job.
  - a. 1" aluminum tubing goes through big center grommet
  - b. Temp and Rh probes go through grommets
  - c. Teflon tubing goes through candy cane (not all of the way, just until resistance is met)

13. Once all four pieces are running through the plate of the nose cone, the nose cone can be screwed into the plane.
  - a. One person should hold the nose cone into place while the second person secures the top middle screw.
  
14. Check placement and security of each of the temperature and humidity probes. These are not tight fits, but the probes shouldn't be hanging either. Use black electrical tape to fill extra space between grommet hole and probe.
  
15. Use two Adel clamps screwed together to act as a brace between the aerosol and gas inlets. Hold clamps together with an AN3-5 bolt, a size 10 lock washer and a 10-32 elastic stop nut.
  - a. Tighten with 3/8" wrench and 3/8" socket wrench
16. Used 12 inch crescent wrench to tighten aerosol inlet onto 1" OD Aluminum tube
  - a. **DO NOT OVER TORQUE THE INLET SWAGELOK**
  - b. Turn approximately 1/2 rotations past finger tight.
  
17. When finished, call URF and let them know that the pilot needs to inspect the work.

## Aerosol inlet installation – Quick guide

1. Collect tools, get an assistant
2. Thread AI tubing through two aluminum blocks
3. Connect AI tubing to flexible tubing in plane and secure clamp
4. Put Aft block in place, but don't tighten
5. Put forward block in place. Tighten
6. Tighten aft block
7. Safety wire as required
8. Put nose cone on
9. Secure nose cone while assistant holds it up
10. Check placement of temp and humidity probes, add tape if necessary
11. Brace two inlets with two Adel clamps held together by bolt
12. Attach aerosol inlet to AI tube. **DO NOT OVER TORQUE THE INLET FITTING. TURN 1/2 ROTATIONS PAST FINGER TIGHT.**
13. Call URF to let the pilot know the installation is ready for inspection

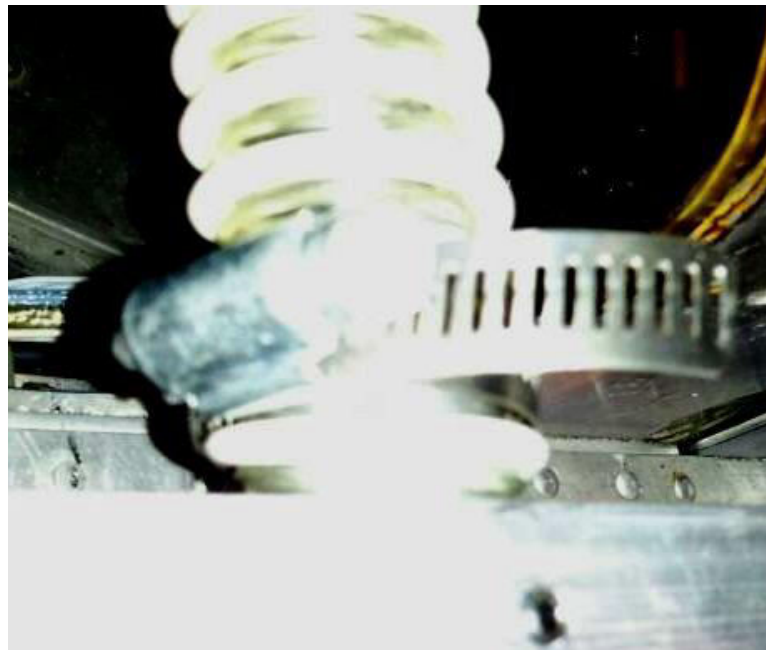
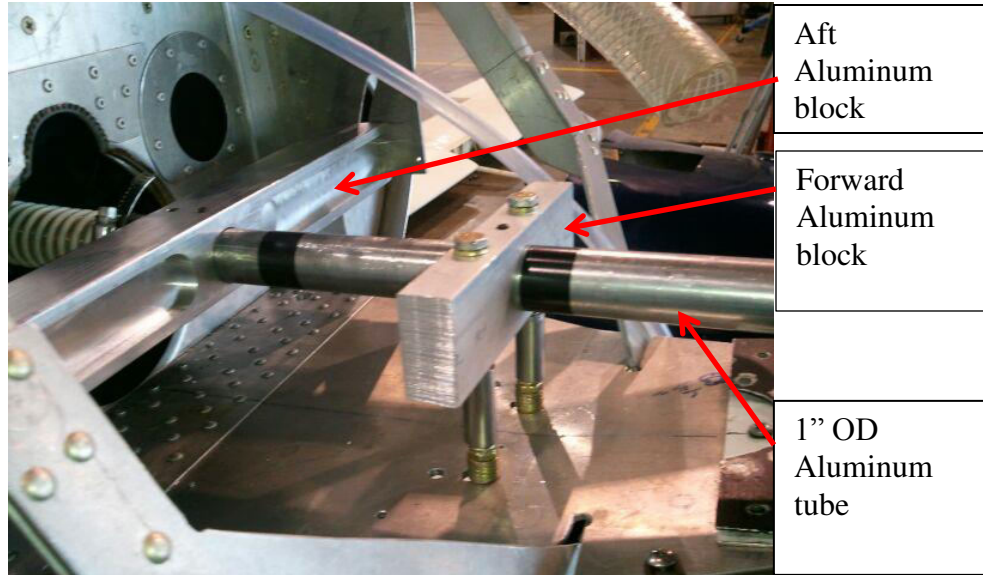
## Deconfiguration

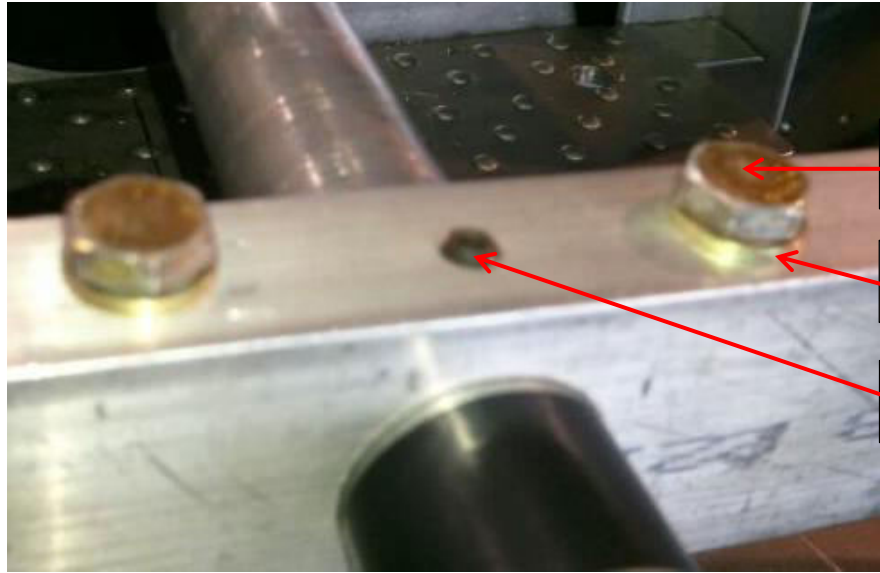
1. Collect tools (wrenches, socket wrenches, Allen wrench, straight edge screw driver, clips for safety wire, huge wrench for aerosol nozzle, an assistant)
2. Remove Adel clamps bracing the gas and aerosol inlets
3. Remove aerosol inlet nozzle
4. Remove nose cone screws from plane (one person holds nose cone while last screws are being removed)
5. Carefully pull nose cone away from plane
  - a. Allow temp and humidity probes to come out (have your assistant catch them)
  - b. Allow Teflon tubing to come out
  - c. Slide cone away from plane over aluminum aerosol inlet tube
6. Cut safety wire
7. Loosen set screw on aft aluminum block
8. Loosen bolts to aft aluminum block but don't remove bolts all together
9. Remove stop nuts and washers on the bottom side of camera mount underneath of forward aluminum block. Gently wiggle the AI tube up so that the bolts disengage from the holes in the rack mount. Once bolts are free of camera rack mount, replace the lock washer and stop nuts to bottom of bolts.
10. With forward block attached, pull aluminum tube forward a half inch or so.
11. Loosen clamp around flexible tubing going into plane
12. Slide aluminum tube forward, so that it is no longer connected to the flexible tubing and bring it forward through the aft aluminum block. The forward block can stay in place.
13. Remove aft aluminum block. Once removed, put bolts back into block



14. Use a zip tie to secure the humidity and temperature probes to the camera rack so they aren't loose.
15. Ask URF pilot if nose cone should be put back on or if they want to put a different nose cone on.
16. Once nose cone is back in place call URF so that the pilot knows to inspect placement of new nose cone.
17. Place all removed components together in a bin so they are available for the next installation.

Pictures

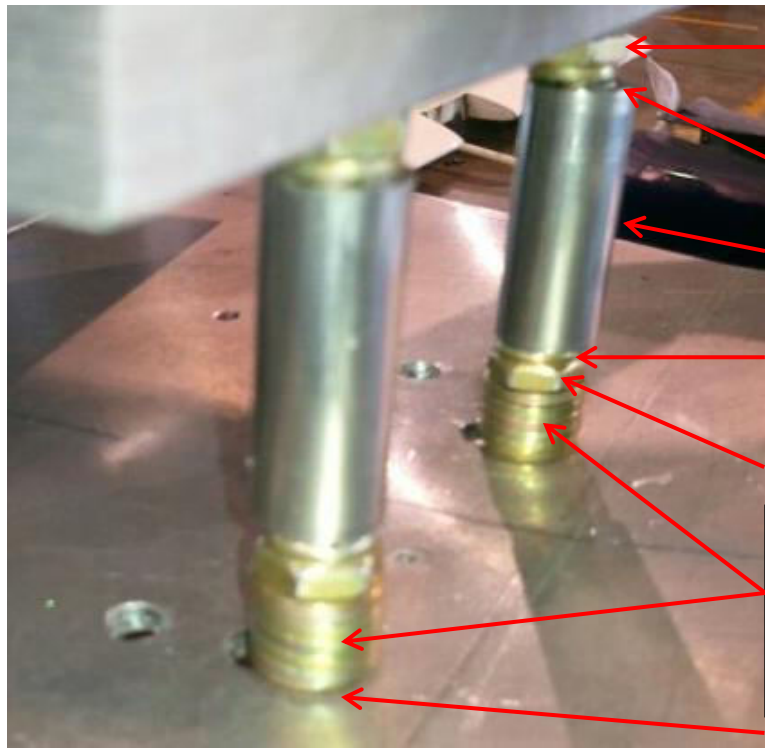




Top of AN40-4 threaded bolt

Flat washer

Set screw 10-32



Elastic stop nut

Flat washer

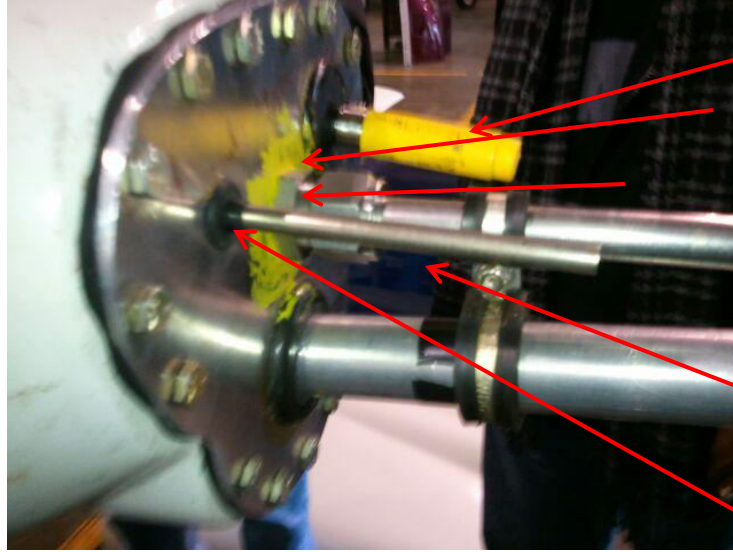
ss jacket

Flat washer

Elastic stop nut

Flat washer stack (5 washers on right, 6 washers on left)

Lock nut



- Humidity probe
- Primer
- Bulkhead fitting
- Temp probe
- Black electrical tape around probe so it doesn't wiggle inside of grommet



Adel Clamps

## Bibliography

- Annesi-Maesano, Epidemiology of chronic obstructive pulmonary disease. In Management of chronic obstructive pulmonary disease; N.M. Siafakas, Ed. European Respiratory Society Journals Ltd: Wakefield, UK, Vol 11, pp41-70.
- Blonde, N., Boersma, K.F., Eskes, H.J., Van der A, R.J. van der, Van Roozendaal, M., De Smedt, I., Bergametti, G., Vautard, R.: Intercomparison of SCIAMACHY nitrogen dioxide observations, *In Situ* measurements and air quality modeling results over Western Europe. *J. Geophys. Research*, 112, D10311, 2007.
- Bucsela, E.J., Perring, A.E., Cohen, R.C., Boersma, K.F., Celarier, E.A., Gleason, J.F., Wenig, M.O., Bertram, T.H., Wooldridge, P.J., Dirksen, R., Veefkind, J.P.: Comparison of tropospheric NO<sub>2</sub> from In Situ aircraft measurements with near-real-time and standard product data from OMI, *J. Geophys. Res.* 113, D16S31, 2008.
- Busch, K.W., Busch, M.A., Introduction to cavity-ringdown spectroscopy. In Cavity-Ringdown Spectroscopy. An ultratrace-absorption measurement technique: Ed. Busch, K.W., Busch, M.A., American Chemical Society, Washington, D.C., 1999; 7-19.
- Castellanos, P., Luke, W.T., Kelley, P., Stehr, J.W., Ehrman, S.H., Dickerson, R.R.: Modification of a commercial cavity ring-down spectroscopy NO<sub>2</sub> detector for enhanced sensitivity. *Rev Sci. Instrum.* 80, 113107, 2009.
- Castellanos, P., Marufu, L., Doddridge, B., Taubman, B., Schwab, J., Hains, J., Ehrman, S., Dickerson, R.: Ozone, oxides of nitrogen, and carbon monoxides during pollution events over the eastern United States: An evaluation of emissions and vertical mixing, *J. Geophys. Res.*, 116, D16307, 2011.
- Chameides, W.L., Fehsenfeld, F., Rodgers, M.O., Cardelino, C., Martinez, J., Parrish, D., Lonneman, W., Lawson, D.R., Rasmussen, R.A., Zimmerman, P., Greenberg, J., Middleton, P., Wang, T.: Ozone precursor relationships in the ambient atmosphere. *J. Geophys. Res.*, 97 (D5) 6037-6055, 1992.
- Dari-Salisburgo, C., Di Carlo, P., Giammaria, G., Yoshizumi, K., D'Altorio, A.: Laser induced fluorescence instrument for NO<sub>2</sub> measurements: Observations at a central Italy background site. *Atmos. Environ.*, 43, 970-977, 2009.
- Day, D.A., Wooldridge, P.J., Dillon, M.B., Thornton, J.A., Cohen, R.C.: A thermal dissociation laser-induced fluorescence instrument for in situ detection of NO<sub>2</sub>, peroxy nitrates, alkyl nitrates, and HNO<sub>3</sub>. *J. Geophys. Res.* 207, D6,4046, 2002.
- DiCarlo, P., Aruffo, E., Busilacchio, M., Giammaria, F., Dari-Salisburgo, C., Biancofiore, F., Visconti, G., Lee, J., Moller, S., Reeves, C.E., Bauguitte, S., Forster, G.,

Jones, R.L., Ouyang, B.: Aircraft based four-channel thermal dissociation laser induced fluorescence instrument for simultaneous measurements of NO<sub>2</sub>, total peroxy nitrate, total alkyl nitrate, and HNO<sub>3</sub>. *Atmos. Meas Tech. Discuss.*, 5, 8759-8787, 2012.

Dunlea, E.J., Herndon, S.C., Nelson, D.D., Volkamer, R.M., San Martini, F., Sheehy, P.M., Zahniser, M.S., Shorter, J.H., Wormhoudt, J.C., Lamb, B.K., Allwine, E.J., Gaffney, J.S., Marley, N.A., Grutter, M., Marquez, C., Blanco, S., Cardenas, B., Retama, A., Ramos Villegas, C.R., Kolb, C.E., Molina, L.T., Molina, M.J.: Evaluation of nitrogen dioxide chemiluminescence monitors in a polluted urban environment. *Atmos. Chem. Phys. Discuss.*, 7, 569-604, 2007.

Emmons, L.K., Carroll, M.A., Hauglustaine, D.A., Brasseur, G.P., Atherton, C., Penner, J., Sillman, S., Levy II, H., Rohrer, F., Wauben, W.M.F., Van Velthoven, P.F.J., Wang, Y., Jacob, D., Bakwin, P., Dickerson, R., Doddridge, B., Gerbig, C., Honrath, R., Hübler, G., Jaffe, D., Kondo, Y., Munger, J.W., Torres, A., Volz-Thomas, A.: Climatologies of NO<sub>x</sub> and NO<sub>y</sub>: A comparison of data and models. *Atmos. Environ.*, 31(12), 1851-1904, 1997.

EPA, Report No. EPA/600/R-05/0004aA, 2006.

Fehsenfeld, F.C., Dickerson, R.R., Hübler, G., Luke, W.T., Nunnermacker, L.J., Williams, E.J., Roberts, J.M., Calvert, J.G., Curran, C.M., Delany, A.C., Eubank, C.S., Fahey, D.W., Fried, A., Gandrud, B.W., Langford, A.O., Murphy, P.C., Norton, R.B., Pickering, K.E., Ridley, B.A.: A ground-based intercomparison of NO, NO<sub>x</sub>, and NO<sub>y</sub> measurement techniques. *J. Geophys. Res.*, 92 (D12), 14710-14722. 1987.

Fehsenfeld, F.C., Williams, E.J., Buhr, M.P., Hubler, G., Langford, A.O., Murphy, P.C., Parish, D.D., Norton, R.B., Fahey, D.W., Drummond, J.W., Mackay, G.I., Roychowdhury, U.K., Hovermale, C., Mohnen, V.A., Demerjian, K.L., Galvin, P.J., Calvert, J.G., Ridley, B.A., Grahek, F., Heikes, B.G., Kok, G.L., Shetter, J.D., Walega, J.G., Elsworth, C.M., Schiff, H.I.: Intercomparison of NO<sub>2</sub> measurement techniques. *J Geophys Resear.* 95(D4), 03579, 1990.

Finlayson-Pitts, B.J., Pitts Jr., J.N., 2000. *Chemistry of the Upper and Lower Atmosphere: Theory, Experiments, and Applications*. Academic Press, San Diego, CA, 4-8 pp.

Fried, A., Sams, R., Dorko, W., Elkins, J., Cai, Z-t.: Determination of nitrogen dioxide in air compressed gas mixtures by quantitative tunable diode laser absorption spectrometry and chemiluminescence detection. *Anal. Chem.* 60, 394-403, 1998.

Fuchs, H., Ball, S.M., Bohn, B., Brauers, T., Cohen, R.C., Dorn, H.-P., Dubé, W.P., Fry, J.L., Häsel, R., Heitmann, U., Jones, R.L., Kleffmann, J., Mentel, T.F., Müsgen, P., Rohrer, F., Rollins, A.W., Ruth, A.A., Kiendler-Scharr, A., Schlosser, E., Shillings, A.J.L., Tillmann, R., Varma, R.M., Venables, D.S., Villena Tapia, G., Wahner, A.,

- Wegener, R., Wooldridge, P.J., Brown, S.S.: Intercomparison of measurements of NO<sub>2</sub> concentrations in the atmosphere simulation chamber SAPHIR during the NO<sub>3</sub>Comp campaign. *Atmos. Meas. Tech.*, 3, 21-37, 2010.
- Halla, J.D., Wagner, T., Beirle, S., Brook, J.R., Hayden, K.L., O'Brien, J.M., Ng, A., Majonis, D., Wenig, M.O., McLaren, R.: Determination of tropospheric vertical columns of NO<sub>2</sub> and aerosol optical properties in a rural setting using MAX-DOAS. *Atmos. Chem. Phys.* 11, pp. 12475-12498, 2011.
- He, Hao., Loughner, C., Stehr, J., Arkinson, H., Brent, L., Follette-Cook, M., Thompson, A., Diskin, G., Anderson, B., Crawford, J., Weinheimer, A., Cohen, R.C., Lee, P., Hains, J., Dickerson, R., An elevated reservoir in a six-day pollution event over the Mid-Atlantic states: a case study from airborne measurements and numerical simulations. *In preparation*, 2013.
- He, H., Stehr, J., Hains, J., Krask, D., Doddridge, B., Vinnikov, K., Canty, T., Hosley, K., Salawitch, R., Worden, H., Dickerson, R.: Trends in emissions and concentrations of air pollutants in the lower troposphere in the Baltimore/Washington airshed from 1997 to 2011. *Atmos. Chem. Phys. Discuss.*, 13, 3135-3178, 2013.
- Hargrove J., Wang, L., Muyskens, K., Muyskens, M., Medina, D., Zaide, S., Zhang, J.: Cavity ring-down spectroscopy of ambient NO<sub>2</sub> with quantification and elimination of interferences. *Environ. Sci. Technol.*, (40), 7868-7873, 2006.
- Heland, J., Schlager, H., First comparison of tropospheric NO<sub>2</sub> column densities retrieved from GOME measurements and *In Situ* aircraft profile measurements. *Geophys. Res. Lett.*, 29(20), 2002.
- Herman, J., Cede, A., Spinei, E., Mount, G., Tzortziou, M., Abuhassan, N.: NO<sub>2</sub> column amounts from ground-based Pandora and MFDOAS spectrometers using the direct-sun DOAS technique: Intercomparisons and application to OMI validation. *J. Geophys. Res.* 14, D13307, 2009.
- Jacob, D.J., Heikes, B.G., Fan, S.-M., Logan, J.A., Mauzerall, D.L., Bradshaw, J.D., Singh, H.B., Gregory, G.L., Talbot, R.W., Blake, D.R., Sachse, G.W.: Origin of ozone and NO<sub>x</sub> in the tropical troposphere: A photochemical analysis of aircraft observations over the South Atlantic basin. *JGR.*, 10(D19), 24235-24250, 1996.
- Jaeglé, L., Jacob, D.L., Wang, Y., Weinheimer, A.J., Ridley, B.A., Campos, T.L., Sachse, G.W., Hagen, D.E.: Sources and chemistry of NO<sub>x</sub> in the upper troposphere over the United States. *Geo. Phys. Res. Lett.*, 25 (10), 1705-1708, 1998.
- Kebabian, P.L., Robinson, W.A., Freedman, A.: Optical extinction monitor using cw cavity detection. *Rev Sci Inst.*, 78, p063102.9, 2007.

Kebabian, P.L., Wood, E.C., Herndon, S.C., Freedman, A.: A practical alternative to chemiluminescence-based detection of nitrogen dioxide: Cavity attenuated phase shift spectroscopy. *Environ. Sci. Technol.*, 42, 6040-6045, 2008.

Kim, S.-W., Heckel, A., Frost, G.J., Richter, A., Gleason, J., Burrows, J.P., McKeen, S., Hsie, E.-Y., Cranier, C., Trainer, M.: NO<sub>2</sub> columns in the western United States observed from space and simulated by a regional chemistry model and their implications for NO<sub>x</sub> emissions. *J. Geophys. Res.* 114, D11301, 2009.

Kleinman, L.I., Lee, Y-N., Springston, S.R., Nunnermacker, L., Zhou, X., Brown, R., Hallock, K., Klotz, P., Leahy, D., Lee, J.H., Newman, L.: Ozone formation at a rural site in the southeastern United States. *J. Geophys. Resear.*, 99(D2), 3469-6482, 1994.

Lehmann, K., Berden, G., Engeln, R., An introduction to cavity ring-down spectroscopy. In *Cavity Ring-Down Spectroscopy*; Ed. Berden G., Engeln, R., Wiley, Chichester, United Kingdom, 2009; 6-10.

Leue, C., Wenig, M., Wagner, T., Klimm, O., Platt, U., Jähne, B.: Quantitative analysis of NO<sub>x</sub> emissions from Global Ozone Monitoring experiment satellite image sequences. *J. Geophys. Res.* 106, D6, 5493-5505.

Logan, J.A.: Ozone in rural areas of the United States, *J. Geophys. Res.* 94, D6, 8511-8532, 1989.

Luke, W.T., Dickerson, R.R., Ryan, W.F., Pickering, K.E., Nunnermacker, L.J.: Tropospheric chemistry over the lower great plains of the United States. 2. Trace gas profiles and distributions. *J. Geophys. Res.* 97, D18, 20647-20670, 1992.

Luke, W.T., Arnold, J.R., Gunter, R.L., Watson, T.B., Wellman, D.L., Dasgupta, P.K., Li, J., Riemer, D., Tate, P.: The NOAA Twin Otter and its role in BRACE: platform description, *Atmos. Environ.*, 41, 4177-4189, 2007.

Napelenok, S.L., Pinder, R.W., Gilliland, A.B., Martin, R.V.: A method for evaluating spatially-resolved NO<sub>x</sub> emissions using Kalman filter inversion, direct sensitivities, and space-based NO<sub>2</sub> observations. *Atmos. Chem. and Phys*, 8, 5603-5614, 2008.

Neuman, J.A., Gao, R.S., Fahey, D.W., Holecek, J.S., Ridley, B.A., Walega, J.G., Grahek, F.E., Richard, E.C., McElroy, C.T., Thompson, T.L., Elkins, J.W., Moore, F.L., Ray, E.A.: *In Situ* measurements of HNO<sub>3</sub>, NO<sub>y</sub>, NO and O<sub>3</sub> in the lower stratosphere and upper troposphere. *Atmos. Environ.*, 35(33), 5789-5797, 2001.

Ordóñez, C., Tichter, A., Steinbacher, M., Zellweger, C., Nüss, H., Burrows, J.P., Pérvôt, A.S.H.: Comparison of 7 years of satellite-borne and ground-based tropospheric NO<sub>2</sub> measurements around Milan, Italy, *J. Geophys. Res.* 111(D5), D05310, 2006.



Pollack, I.B., Lerner, B.M., Ryerson, T.B.: Evaluation of ultraviolet light-emitting diodes for detection of atmospheric NO<sub>2</sub> by photolysis-chemiluminescence. *J. Atmos. Chem.*, 65(2), 111-125, 2011.

Ryerson, T.B., Williams, E.J., Fehsenfeld, F.C.: An efficient photolysis system for fast-response NO<sub>2</sub> measurements. *JGR*, 105 (D21), 26,447-26,461, 2000.

Schaub, D., Boersma, K.F., Kaiser, J.W., Weiss, A.K., Folini, D., Eskes, H.J., Buchmann, B.: Comparison of GOME tropospheric NO<sub>2</sub> columns with NO<sub>2</sub> profiles deduced from ground-based *In Situ* measurements. *J. Atmos. Chem. Phys.*, 6, 3211-3229, 2006.

Schwartz, J., Zeger, S.: Passive smoking, air pollution, and acute respiratory symptoms in a diary study of student nurses. *Am. J. Respir. Crit. Care Med.*, 1(141), 62-67, 1990.

Skoog, D.A., Holer, F.J., Nieman, T.A.: Principles of Instrumental Analysis. Thomas Learning, Inc., Toronto, Ontario, 14 ppm, 1998.

Suzuki, H., Miyao, Y., Nakayama, T., Pearce, J.K., Matsumi, Y., Takahashi, K., Kita, K., Tonokura, K., Comparison of laser-induced fluorescence and chemiluminescence measurements of NO<sub>2</sub> at an urban site. *Atmos. Environ.*, 45, 6233-6240, 2011.

Thorn, W. J.: "Preparation and Analysis of NO and NO<sub>2</sub> Gas Standard Reference Materials In Aluminum Cylinders, hh"; Poster with Extended Abstract #2010-A-900-AWMA; presented at A&WMA's 103<sup>rd</sup> Annual Conference & Exhibition June 23, 2010, Calgary, Alberta, Canada

Thornton, J.A., P. J. Wooldridge, R. C. Cohen.: Atmospheric NO<sub>2</sub>: *In Situ* laser- induced fluorescence detection at parts per trillion mixing ratios. *Anal. Chem.* 72, 528, 2000.

Trainer, M., Parish, D.D., Buhr, M.P., Norton, R.B., Fehsenfeld, R.C., Anlauf, K.G., Bottenheim, J.W., Tang, Y.Z., Wiebe, H.A., Roberts, J.M., Tanner, R.L., Newman, L., Bowersox, V.C., Meagher, J.F., Olszyna, K.J., Rodgers, M.O., Wang, T., Berresheim, H., Demerjian, K.L., Roychowdhury, U.K.: Correlation of ozone with NO<sub>y</sub> in photochemically aged air, *J. Geophys. Res.*, 98, 2917-2925, 1993.

United States Environmental Protection Agency, Office of Air and Radiation, Sources of Bias in the Gas Analyzer. In An Operator's guide to eliminating bias in CEM systems, United States Environmental Protection Agency, 1994.  
<http://www.epa.gov/airmarkets/emissions/bias.html>.

Wagner, N., Dubé, W., Washenfelder, R., Young, C., Pollack, I., Ryerson, T., Brown, S.: Diode laser-based cavity ring-down instrument for NO<sub>3</sub>, N<sub>2</sub>O<sub>5</sub>, NO, NO<sub>2</sub> and O<sub>3</sub> from aircraft, *Atmos. Meas. Tech.*, 4, 1227-1240, 2011, 2011.

Wooldridge, P.J., Perring, A.E., Bertram, T.H., Flocke, F.M., Roberts, J.M., Singh, H.B., Huey, L.G., Thornton, J.A., Wolfe, G.M., Murphy, J.G., Fry, J.L., Rollins, A.W., LaFranchi, B.W., Cohen, R.C.: Total peroxy nitrates ( $\Sigma$ PNs) in the atmosphere: the thermal dissociation –laser induced fluorescence (TD-LIF) technique and comparisons to speciated PAN measurements. *Atmos. Meas. Tech.* 3, 593-607, 2010.

Anderson, T. L., et al. (1996), Performance characteristics of a high-sensitivity, three-wavelength, total scatter/backscatter nephelometer, *Journal of Atmospheric and Oceanic Technology*, 13(5), 967-986.

Anderson, T. L., S. J. Masonis, D. S. Covert, N. C. Ahlquist, S. G. Howell, A. D. Clarke, and C. S. McNaughton, Variability of aerosol optical properties derived from in situ aircraft measurements during ACE-Asia, *J. Geophys. Res.*, 108(D23), 8674, 2003.

Anderson, T. L., and J. A. Ogren, Determining aerosol radiative properties using the TSI 3563 integrating nephelometer, *Aerosol Sci. & Technol.*, 29(1), 57-69, 1998.

Andrea, M. O., Berresheim, H., Andreae, T.W., Kritz, M.A., Bates, T.S., Merrill, J.T., Vertical distribution of dimethylsulfide, sulfur dioxide, aerosol ions and radon over the northeast Pacific Ocean, *J. Atmos. Chem.*, 6, 149-173, 1998.

Arkinson, H. L., Stehr, J. W., Brent, L. C., Hao, H., Dickerson R.R., DISCOVER-AQ Documentation and Raw Data, Cessna 402B Aircraft Measurements, Trace Gases and AerosolsRep., 1-98 pp, University of Maryland, Internal Report, 2012.

Bahreini, R., J. L. Jimenez, J. Wang, R. C. Flagan, J. H. Seinfeld, J. T. Jayne, and D. R. Worsnop, Aircraft-based aerosol size and composition measurements during ACE-Asia using an Aerodyne aerosol mass spectrometer, *J. Geophys. Res.*, 108(D23), 8645, 2003.

Balducci, C., Cecinato, A., Particulate organic acids in the atmosphere of Italian cities: Are they environmentally relevant?, *Atmos. Environ.*, 44, 652-659, 2010.

Baron, P., Willeke (2005), John Wiley & Sons, New Jersey.

Bateman, A. P., S. A. Nizkorodov, J. Laskin, and A. Laskin, High-Resolution Electrospray Ionization Mass Spectrometry Analysis of Water-Soluble Organic Aerosols Collected with a Particle into Liquid Sampler, *Anal. Chem.*, 82(19), 8010-8016, 2010.

Bates, T. S., B. J. Huebert, J. L. Gras, F. B. Griffiths, and P. A. Durkee (1998), International Global Atmospheric Chemistry (IGAC) project's first aerosol characterization experiment (ACE 1): Overview, *J. Geophys. Res.*, 103(D13), 16297-16318.

Blando, J. D., R. J. Porcja, T. H. Li, D. Bowman, P. J. Liroy, and B. J. Turpin (1998), Secondary formation and the Smoky Mountain organic aerosol: An examination of

aerosol polarity and functional group composition during SEAVS, *Environ. Sci. Technol.*, 32(5), 604-613.

Blomquist, B. W., B. J. Huebert, S. G. Howell, M. R. Litchy, C. H. Twohy, A. Schanot, D. Baumgardner, B. Lafleur, R. Seebauch, and M. L. Laucks (2001), An evaluation of the community aerosol inlet for the NCAR C-130 research aircraft, *J Atmos Ocean Tech*, 18(8), 1387-1397.

Brent, L. C., J. W. Stehr, H. He, H. L. Arkinson, and R. R. Dickerson (2013a), Evaluation of the use of a commercially available cavity ringdown absorption spectrometer for measuring NO<sub>2</sub> in flight, and observations over the Mid Atlantic States during DISCOVER-AQ, *J. Atmos. Chem.*.

Brent, L. C., et al. (2013b), Evaluation of the use of a commercially available cavity ringdown absorption spectrometer for measuring NO<sub>2</sub> in flight, and observations over the Mid-Atlantic States, during DISCOVER-AQ, *J. Atmos. Chem.*.

Brook, R. D., et al. (2010), Particulate matter air pollution and cardiovascular disease: An update to the scientific statement from the American Heart Association, *Circulation*, 121(21), 2331-2378.

Carlton, A. G., B. J. Turpin, K. E. Altieri, S. Seitzinger, A. Reff, H. J. Lim, and B. Ervens (2007), Atmospheric oxalic acid and SOA production from glyoxal: Results of aqueous photooxidation experiments, *Atmos. Environ.*, 41(35), 7588-7602.

Carlton, A. G., B. J. Turpin, K. E. Altieri, S. P. Seitzinger, R. Mathur, S. J. Roselle, and R. J. Weber (2008), CMAQ Model Performance Enhanced When In-Cloud Secondary Organic Aerosol is Included: Comparisons of Organic Carbon Predictions with Measurements, *Environ. Sci. Technol.*, 42(23), 8798-8802.

Carvalho, A., C. Pio, and C. Santos (2003), Water-soluble hydroxylated organic compounds in German and Finnish aerosols, *Atmos. Environ.*, 37(13), 1775-1783.

Castellanos, P., Ehrman, S.H., Dickerson, R.R., Stehr, J.W. (2009), The sensitivity of modeled ozone to the temporal distribution of point, area, and mobile emissions in the eastern U.S., *Atmos. Environ.*, 43, 4603-4611.

Castellanos, P., L. T. Marufu, B. G. Doddridge, B. F. Taubman, J. J. Schwab, J. C. Hains, S. H. Ehrman, and R. R. Dickerson (2011), Ozone, oxides of nitrogen, and carbon monoxide during pollution events over the eastern United States: An evaluation of emissions and vertical mixing, *Journal of Geophysical Research-Atmospheres*, 116.

Chang, H. (2005), On the use of anion exchange chromatography for the characterization of water soluble organic carbon, *Geophys. Res. Lett.*, 32(1), 101810.

- Chebbi, A., and P. Carlier (1996), Carboxylic acids in the troposphere, occurrence, sources, and sinks: A review, *Atmos. Environ.*, *30*(24), 4233-4249.
- Claeys, M., Graham, B., Vas, G., Wang, W., Vermeylen, R., Pashynska, V., Cafmeyer, J., Guyon, P., Andreae, M., Artaxo, P., Maenhaut, W. (2004), Formation of secondary organic aerosols through the photooxidation of isoprene., *Science*, *303*, 1173-1176.
- Clarisse, L., P. F. Coheur, F. Prata, J. Hadji-Lazaro, D. Hurtmans, and C. Clerbaux (2013), A unified approach to infrared aerosol remote sensing and type specification, *Atmos Chem and Phys*, *13*(4), 2195-2221, doi:DOI 10.5194/acp-13-2195-2013.
- Clean Air Act, U. S. C. S. e. s. (1970), The Public Health and Welfare, ch 85 Air pollution and prevention and control, in *42*, edited by U. S. Code, U.S. Government Printing Office.
- Covert, D. S., Charlson, R.J., Ahlquist, N.C. (1972), A study of the relationship of chemical composition and humidity to light scattering by aerosols., *J. Appl. Meteor*, *11*, 968-972.
- DeCarlo, P. F., et al. (2006), Field-deployable, high-resolution, time-of-flight aerosol mass spectrometer, *Anal. Chem.*, *78*(24), 8281-8289, doi:10.1021/ac061249n.
- Decesari, S., M. C. Facchini, S. Fuzzi, and E. Tagliavini (2000), Characterization of water-soluble organic compounds in atmospheric aerosol: A new approach, *J. Geophys. Res.*, *105*(D1), 1481-1489, doi:Doi 10.1029/1999jd900950.
- Decesari, S., M. C. Facchini, E. Matta, F. Lettini, M. Mircea, S. Fuzzi, E. Tagliavini, and J. P. Putaud (2001), Chemical features and seasonal variation of fine aerosol water-soluble organic compounds in the Po Valley, Italy, *Atmos. Environ.*, *35*(21), 3691-3699, doi:Doi 10.1016/S1352-2310(00)00509-4.
- Ding, J., and R. J. Anderegg (1995), Specific and nonspecific dimer formation in the electrospray ionization mass spectrometry of oligonucleotides, *Journal of the American Society for Mass Spectrometry*, *6*(3), 159-164, doi:10.1016/1044-0305(94)00102-6.
- Domingos, J. S., A. C. Regis, J. V. Santos, J. B. de Andrade, and G. O. da Rocha (2012), A comprehensive and suitable method for determining major ions from atmospheric particulate matter matrices, *Journal of chromatography. A*, *1266*, 17-23, doi:10.1016/j.chroma.2012.08.074.
- Donahue, N. M., W. Chuang, S. A. Epstein, J. H. Kroll, D. R. Worsnop, A. L. Robinson, P. J. Adams, and S. N. Pandis (2013), Why do organic aerosols exist? Understanding aerosol lifetimes using the two-dimensional volatility basis set, *Environ. Chem*, *10*, 151-157, doi:10.107/En13022.

Edney, E. O., T. E. Kleindienst, T. S. Conner, C. D. McIver, E. W. Corse, and W. S. Weathers (2003), Polar organic oxygenates in PM<sub>2.5</sub> at a southeastern site in the United States, *Atmos. Environ.*, *37*(28), 3947-3965, doi:Doi 10.1016/S1352-2310(03)00461-8.

EPA (2006), Air Quality Criteria for Ozone and Related Photochemical Oxidants *Rep. EPA/600/R-05/0004aA*.

EPA (2013), Integrated Science Assessment for Ozone and Related Photochemical Oxidants *Rep. EPA 600/R-10/076F*.

Fisseha, R., J. Dommen, M. Sax, D. Paulsen, M. Kalberer, R. Maurer, F. Hofler, E. Weingartner, and U. Baltensperger (2004), Identification of organic acids in secondary organic aerosol and the corresponding gas phase from chamber experiments, *Anal Chem*, *76*(22), 6535-6540, doi:10.1021/ac048975f.

Forstner, H. J. L., R. C. Flagan, and J. H. Seinfeld (1997), Secondary organic aerosol from the photooxidation of aromatic hydrocarbons: Molecular composition, *Env. Sci. Technol.*, *31*(5), 1345-1358, doi:Doi 10.1021/Es9605376.

Fuchs, N. A. (1975), Sampling of Aerosols, *Atmos. Environ.*, *9*(8), 697-707, doi:Doi 10.1016/0004-6981(75)90156-0.

Gao, S., D. A. Hegg, P. V. Hobbs, T. W. Kirchstetter, B. I. Magi, and M. Sadilek (2003), Water-soluble organic components in aerosols associated with savanna fires in southern Africa: Identification, evolution, and distribution, *J. Geophys. Res.*, *108*(D13), doi:Artn 8491 Doi 10.1029/2002jd002324.

Gao, S., J. D. Surratt, E. M. Knipping, E. S. Edgerton, M. Shahgholi, and J. H. Seinfeld (2006), Characterization of polar organic components in fine aerosols in the southeastern United States: Identity, origin, and evolution, *J. Geophys. Res.*, *111*(D14), D14314, doi:Artn D14314 Doi 10.1029/2005jd006601.

Gassó, S., Hegg, D.A., Covert, D.S., Collins, D., Noone, K.J., Öström, E., Schmid, B., Russell, P.B., Livingston, J.M., Durkee, P.A., Jonsson, H. (2000), Influence of humidity on the aerosol scattering coefficient and its effect on the upwelling radiance during ACE-2, *Tellus*, *52B*, 546-567.

Generation, E. P. A. v. E. H. c. (TBD), edited.

Glausius, M., Duane, M., Larsen, B. R. (1999), Determination of polar terpene oxidation products in aerosols by liquid chromatography-ion trap mass spectrometry, *J. Chromatog. A.*, *833*, 121-135.

- Hains, J. C., L. W. A. Chen, B. F. Taubman, B. G. Doddridge, and R. R. Dickerson (2007), A side-by-side comparison of filter-based PM<sub>2.5</sub> measurements at a suburban site: A closure study, *Atmospheric Environment*, 41(29), 6167-6184.
- Hains, J. C., B. F. Taubman, A. M. Thompson, J. W. Stehr, L. T. Marufu, B. G. Doddridge, and R. R. Dickerson (2008a), Origins of chemical pollution derived from Mid-Atlantic aircraft profiles using a clustering technique, *Atmospheric Environment*, 42(8), 1727-1741.
- Hains, J. C., B. F. Taubman, A. M. Thompson, J. W. Stehr, L. T. Marufu, B. G. Doddridge, and R. R. Dickerson (2008b), Origins of chemical pollution derived from Mid-Atlantic aircraft profiles using a clustering technique, *Atmos. Environ.*, 42(8), 1727-1741, doi:DOI 10.1016/j.atmosenv.2007.11.052.
- Hamilton, J. F., A. C. Lewis, T. J. Carey, and J. C. Wenger (2008), Characterization of polar compounds and oligomers in secondary organic aerosol using liquid chromatography coupled to mass spectrometry, *Anal. Chem.*, 80(2), 474-480, doi:10.1021/ac701852t.
- Hänel, G. (1976), The properties of atmospheric particles as function of the relative humidity at thermodynamic equilibrium with the surrounding air, *Advances in geophysics*, 11, 968-976.
- Hansen, J. E., and M. Sato (2001), Trends of measured climate forcing agents, *Proceedings of the National Academy of Sciences of the United States of America*, 98(26), 14778-14783, doi:10.1073/pnas.261553698.
- He, H., et al. (2013a), An elevated reservoir in a six-day pollution event over the Mid-Atlantic states: a case study from airborne measurements and numerical simulations, *Atmos. Chem. Phys.*, 85, 18-30.
- He, H., et al. (2013b), Trends in emissions and concentrations of air pollutants in the lower troposphere in the Baltimore/Washington airshed from 1997 to 2011, *Atmos. Chem. Phys.*, 13(15), 7859-7874, doi:DOI 10.5194/acp-13-7859-2013.
- Heald, C. L., Coe, H., Jimenez, J.L., Weber, R.J., Bahreini, R., Middlebrook, A.M., Russell, L.M., Jolleys, M., Fu, T.-M., Allan, J.D., Bower, K.N., Capes, G., Crosier, J., Morgan, W.T., Robinson, N.H., Williams, P.I., Cubison, M.J., DeCarlo, P.F., Dunlea, E. J. (2011), Exploring the vertical profile of atmospheric organic aerosol: comparing 17 aircraft field campaigns with a global model, *atmos. Chem. Phys. Discuss.*, 11, 12673-12696, doi:10.5194/acp-11-12673-2011.
- Healy, R. M., et al. (2013), Quantitative determination of carbonaceous particle mixing state in Paris using single-particle mass spectrometer and aerosol mass spectrometer

measurements, *Atmos. Chem. Phys.*, 13(18), 9479-9496, doi:DOI 10.5194/acp-13-9479-2013.

Hegg, D. A., D. S. Covert, H. Jonsson, and P. A. Covert (2005), Determination of the transmission efficiency of an aircraft aerosol inlet, *Aerosol Sci & Technol.*, 39(10), 966-971, doi:Doi 10.1080/02786820500377814.

Hegg, D. A., R. J. Ferek, and P. V. Hobbs (1993), Light-Scattering and Cloud Condensation Nucleus Activity of Sulfate Aerosol Measured over the Northeast Atlantic-Ocean, *J. Geophys. Res.*, 98(D8), 14887-14894, doi:Doi 10.1029/93jd01615.

Heintzenberg, J., Wiedensohler, A., Tuch, T.M., Covert, D.S., Sheridan, P., Ogren, J.A., Gras, J., Nessler, R., Kleefeld, C., Kalivitis, N., Aaltonen, V., Wilhelm, R.-T., Havlicek, M. (2006), Intercomparison and aerosol calibrations of 12 commercial integrating nephelometers of three manufacturers, *J. Atmos. Ocean. Technol.*, 23, 902-914.

Henze, D. K., and J. H. Seinfeld (2006), Global secondary organic aerosol from isoprene oxidation, *Geophys. Res. Lett.*, 33(9), doi:ArtN L09812Doi 10.1029/2006gl025976.

Hinckley, D. A., T. F. Bidleman, and C. P. Rice (1991), Atmospheric Organochlorine Pollutants and Air-Sea Exchange of Hexachlorocyclohexane in the Bering and Chukchi Seas, *J. Geophys. Res.*, 96(C4), 7201-7213, doi:Doi 10.1029/90jc02642.

Hinds, W. C. (1999), *Aerosol Technology; Properties, behavior, and measurements of airborne particles*, John Wiley & Sons, NY, NY.

Hoff, R. M., Christopher, S.A. (2009), Remote sensing of particulate pollution from space: Have we reached the promised land?, *J. Air Waste Manage. Assoc.*, 59, 645-675.

Hsieh, L.-Y., Kuo, S-C, Chen, C-L, Tsai, Y. I. (2009), Size distributions of nano/micron dicarboxylic acids in inorganic ions in suburban PM episodes and non-episodic aerosol, *Atmos. Environ.*, 43, 4396-4406.

Hubertz, E. J. (2013), Brief of Amici Curiae atmospheric scientists and air quality modeling experts in support of petitioners, in *12-1182, -1183*, edited by I. E. Clinic.

Huebert, B. J., et al. (2004), PELTI: Measuring the passing efficiency of an airborne low turbulence aerosol inlet, *Aerosol Sci & Technol.*, 38(8), 803-826, doi:Doi 10.1080/027868290500823.

Huebert, B. J., G. Lee, and W. L. Warren (1990), Airborne Aerosol Inlet Passing Efficiency Measurement, *J. Geophys. Res.*, 95(D10), 16369-16381, doi:Doi 10.1029/Jd095id10p16369.

Linuma, Y., Boge, O., Gnauk, T., Herrmann, H. (2004), Aerosol-chamber study of the  $\alpha$ -pinene/O<sub>3</sub> reaction: influence of particle acidity on aerosol yields and products, *Atmos. Environ.*, 38, 761-773.

Jacobson, M. C., H. C. Hansson, K. J. Noone, and R. J. Charlson (2000), Organic atmospheric aerosols: Review and state of the science, *Rev Geophys*, 38(2), 267-294, doi:Doi 10.1029/1998rg000045.

Jimenez, J. L., et al. (2009), Evolution of organic aerosols in the atmosphere, *Science*, 326(5959), 1525-1529, doi:10.1126/science.1180353.

John, W., S. M. Wall, J. L. Ondo, and W. Winklmayr (1990), Modes in the Size Distributions of Atmospheric Inorganic Aerosol, *Atmos. Environ.*, 24(9), 2349-2359, doi:Doi 10.1016/0960-1686(90)90327-J.

Jonsson, H. H., et al (1995), Performance of a focused cavity aerosol spectrometer for measurements in the stratosphere of particle size in the 0.06 – 2.0 micrometer diameter range, *J. Atmos. Ocean. Technol.*, 12, 115-129.

Kawamura, K., L. L. Ng, and I. R. Kaplan (1985), Determination of organic acids (C<sub>1</sub>-C<sub>10</sub>) in the atmosphere, motor exhausts, and engine oils, *Environmental science & technology*, 19(11), 1082-1086, doi:10.1021/es00141a010.

Kawamura, K., K. Ono, E. Tachibana, B. Charrière, and R. Sempéré (2012), Distributions of low molecular weight dicarboxylic acids, ketoacids and  $\alpha$ -dicarbonyls in the marine aerosols collected over the Arctic Ocean during late summer, *Biogeosciences*, 9(11), 4725-4737, doi:10.5194/bg-9-4725-2012.

Kleindienst, T. E., M. Lewandowski, J. H. Offenberg, M. Jaoui, and E. O. Edney (2009), The formation of secondary organic aerosol from the isoprene plus OH reaction in the absence of NO<sub>x</sub>, *Atmos. Chem. Phys.*, 9(17), 6541-6558, doi:10.5194/acp-9-6541-2009.

Levy, R. C., S. Mattoo, L. A. Munchak, L. A. Remer, A. M. Sayer, F. Patadia, and N. C. Hsu (2013), The Collection 6 MODIS aerosol products over land and ocean, *Atmos Meas Tech*, 6(11), 2989-3034, doi:DOI 10.5194/amt-6-2989-2013.

Levy, R. C., L. A. Remer, J. V. Martins, Y. J. Kaufman, A. Plana-Fattori, J. Redemann, and B. Wenny (2005), Evaluation of the MODIS aerosol retrievals over ocean and land during CLAMS, *J. Atmos. Sci.*, 62(4), 974-992, doi:Doi 10.1175/Jas3391.1.

Librando, V., and G. Tringali (2005), Atmospheric fate of OH initiated oxidation of terpenes. Reaction mechanism of alpha-pinene degradation and secondary organic aerosol formation, *Journal of environmental management*, 75(3), 275-282, doi:10.1016/j.jenvman.2005.01.001.



- Maria, S. F., L. M. Russell, M. K. Gilles, and S. C. B. Myneni (2004), Organic aerosol growth mechanisms and their climate-forcing implications, *Science*, *306*(5703), 1921-1924, doi:DOI 10.1126/science.1103491.
- Marufu, L. T., B. F. Taubman, B. Bloomer, C. A. Piety, B. G. Doddridge, J. W. Stehr, and R. R. Dickerson (2004), The 2003 North American electrical blackout: An accidental experiment in atmospheric chemistry, *Geophysical Research Letters*, *31*(13).
- Marufu, L. T., B. F. Taubman, B. Bloomer, C. A. Piety, B. G. Doddridge, J. W. Stehr, and R. R. Dickerson (2005), Reply to comment by D. A. Hansen et al. on "The 2003 North American electrical blackout: An accidental experiment in atmospheric chemistry", *Geophysical Research Letters*, *32*(10).
- Matta, E., M. C. Facchini, S. Decesari, M. Mircea, F. Cavalli, S. Fuzzi, J. P. Putaud, and A. Dell'Acqua (2003), Mass closure on the chemical species in size-segregated atmospheric aerosol collected in an urban area of the Po Valley, Italy, *Atmos. Chem. Phys.*, *3*, 623-637.
- May, W. E., and S. A. Wise (1984), Liquid-Chromatographic Determination of Polycyclic Aromatic-Hydrocarbons in Air Particulate Extracts, *Anal. Chem.*, *56*(2), 225-232, doi:Doi 10.1021/Ac00266a024.
- Mayol-Bracero, O. L., P. Guyon, B. Graham, G. Roberts, M. O. Andreae, S. Decesari, M. C. Facchini, S. Fuzzi, and P. Artaxo (2002), Water-soluble organic compounds in biomass burning aerosols over Amazonia - 2. Apportionment of the chemical composition and importance of the polyacidic fraction, *J. Geophys. Res.*, *107*(D20), LBA 59-51 – LBA 59-15, Doi 10.1029/2001jd000522.
- McFarland, A. R., C. A. Ortiz, M. E. Moore, R. E. Deotte, and S. Somasundaram (1989), A Shrouded Aerosol Sampling Probe, *Env. Sci., Technol.*, *23*(12), 1487-1492, doi:Doi 10.1021/Es00070a006.
- McNaughton, C. S., et al. (2007), Results from the DC-8 Inlet Characterization Experiment (DICE): Airborne versus surface sampling of mineral dust and sea salt aerosols, *Aerosol Sci & Technol.*, *41*(2), 136-159, Doi 10.1080/02786820601118406.
- Meng, Z. Y., and J. H. Seinfeld (1994), On the Source of the Submicrometer Droplet Mode of Urban and Regional Aerosols, *Aerosol Science and Technology*, *20*(3), 253-265, Doi 10.1080/02786829408959681.
- Nocun, M. S., and M. M. Schantz (2013), Determination of selected oxygenated polycyclic aromatic hydrocarbons (oxy-PAHs) in diesel and air particulate matter standard reference materials (SRMs), *Analytical and bioanalytical chemistry*, *405*(16), 5583-5593, Doi 10.1007/s00216-013-6957-3.

- Novakov, T., D. A. Hegg, and P. V. Hobbs (1997), Airborne measurements of carbonaceous aerosols on the East Coast of the United States, *J. Geophys. Res.*, *102*(D25), 30023-30030, Doi 10.1029/97jd02793.
- Novakov, T., and J. E. Penner (1993), Large Contribution of Organic Aerosols to Cloud-Condensation-Nuclei Concentrations, *Nature*, *365*(6449), 823-826, Doi 10.1038/365823a0.
- Odum, J. R., T. P. Jungkamp, R. J. Griffin, R. C. Flagan, and J. H. Seinfeld (1997), The atmospheric aerosol-forming potential of whole gasoline vapor, *Science*, *276*(5309), 96-99.
- Öström, E., Noone, K.J. (2000), Vertical profiles of aerosol scattering and absorption measured in situ during the North Atlantic Aerosol Characterization Experiment (ACE-2), *Tellus*, *52b*, 526-545.
- Pan, H. (2008), A non-covalent dimer formed in electrospray ionisation mass spectrometry behaving as a precursor for fragmentations, *Rapid Comm. Mass Spectrom.*, *22*, 3555-3560.
- Pandis, S. N. W., A.S., Seinfeld, J.H. (1993), Secondary Organic Aerosol Formation and Transport. II. Predicting the Ambient Secondary Aerosol Size Distribution, *Atmos. Environ.*, *27*, 2403-2416.
- Patton, G. W., M. D. Walla, T. F. Bidleman, and L. A. Barrie (1991), Polycyclic Aromatic and Organochlorine Compounds in the Atmosphere of Northern Ellesmere-Island, Canada, *J. Geophys. Res.*, *96*(D6), 10867-10877, doi:Doi 10.1029/91jd00010.
- Petzold, A., M. Fiebig, H. Flentje, A. Keil, U. Leiterer, F. Schroder, A. Stifter, M. Wendisch, and P. Wendling (2002), Vertical variability of aerosol properties observed at a continental site during the Lindenberg Aerosol Characterization Experiment (LACE 98), *J. Geophys. Res.*, *107*(D21), 8128,
- Pope, C. A., Burnett, R., Thun, M., Calle, E., Krewski, D., Ito, K., Thurston, G. (2002), Lung cancer, cardiopulmonary mortality, and long-term exposure to fine particulate air pollution, *JAMA*, *287*, 1132-1143.
- Pope, C. A., M. J. Thun, M. M. Namboodiri, D. W. Dockery, J. S. Evans, F. E. Speizer, and C. W. Heath (1995), Particulate Air-Pollution as a Predictor of Mortality in a Prospective-Study of Us Adults, *Am. J. Resp. Crit. Care. Med.*, *151*(3), 669-674.
- Remer, L. A., et al. (2005), The MODIS aerosol algorithm, products, and validation, *J Atmos Sci*, *62*(4), 947-973, doi:Doi 10.1175/Jas3385.1.
- Robinson, A. L., N. M. Donahue, M. K. Shrivastava, E. A. Weitkamp, A. M. Sage, A. P. Grieshop, T. E. Lane, J. R. Pierce, and S. N. Pandis (2007), Rethinking organic aerosols:

semivolatile emissions and photochemical aging, *Science*, 315(5816), 1259-1262, doi:10.1126/science.1133061.

Rogge, W. F., M. A. Mazurek, L. M. Hildemann, G. R. Cass, and B. R. T. Simoneit (1993), Quantification of Urban Organic Aerosols at a Molecular-Level - Identification, Abundance and Seasonal-Variation, *Atmos. Environ.*, 27(8), 1309-1330, doi:10.1016/0960-1686(93)90257-Y.

Rohrl, A., and G. Lammel (2002), Determination of malic acid and other C4 dicarboxylic acids in atmospheric aerosol samples, *Chemosphere*, 46(8), 1195-1199.

Rudel, R. A., Camann, D.E., Spengler, J.D., Korn, L.R., Brody, J.G. (2003), Phthalates, Alkylphenols, Pesticides, Polybrominated Diphenyl Ethers, and other Endocrine-disruptin compounds in indoor air and dust, *Environmental science & technology*, 37, 4543-4553, doi:10.1021/es0264596.

Russell, L. M., R. Bahadur, and P. J. Ziemann (2011), Identifying organic aerosol sources by comparing functional group composition in chamber and atmospheric particles, *Proceedings of the National Academy of Sciences of the United States of America*, 108(9), 3516-3521, doi:10.1073/pnas.1006461108.

Samet, J. M., Zeger, S.L., Dominici, F., Curriero, F., Coursac, I., Dockery, D.W., Schwartz, J., Zanobetti, A. (2000), The national morbidity, mortality, and air pollution study. Part II: Morbidity and mortality from air pollution in the United States. *Rep.*, Health Effects Institute.

Schantz, M. M., E. McGaw, and S. A. Wise (2012), Pressurized liquid extraction of diesel and air particulate standard reference materials: effect of extraction temperature and pressure, *Anal. Chem.*, 84(19), 8222-8231, doi:10.1021/ac301443v.

Schuetzle, D., D Cronn, and A. L. Crittenden (1975), Molecular composition of secondary aerosol and its possible origin, *Environ.Sci.Technol* 9(9), 838-845.

Seinfeld, J., H., Pandis, Spyros, N. (2006), *Atmospheric Chemistry and Physics*, 2nd ed., Wiley & Sons, New Jersey.

Sheridan, J. Z., W.H. (1989), Elemental composition of particulate material sampled from teh arctic haze aerosol, *J. atmos. Chem.*, 9, 363-381.

Sheridan, P. J., E. Andrews, J. A. Ogren, J. L. Tackett, and D. M. Winker (2012), Vertical profiles of aerosol optical properties over central Illinois and comparison with surface and satellite measurements, *Atmos. Chem. Phys.*, 12(23), 11695-11721, doi:DOI 10.5194/acp-12-11695-2012.

Sheridan, P. J., and W. H. Zoller (1989), Elemental Composition of Particulate Material Sampled from the Arctic Haze Aerosol, *J. Atmos. Chem.*, 9(1-3), 363-381, doi:Doi 10.1007/Bf00052843.

Smith, K. R. (2000), National burden of disease in India from indoor air pollution, *Proceedings of the National Academy of Sciences of the United States of America*, 97(24), 13286-13293, doi:10.1073/pnas.97.24.13286.

Sorooshian, A., N. L. Ng, A. W. H. Chan, G. Feingold, R. C. Flagan, and J. H. Seinfeld (2007), Particulate organic acids and overall water-soluble aerosol composition measurements from the 2006 Gulf of Mexico Atmospheric Composition and Climate Study (GoMACCS), *J Geophys Res-Atmos*, 112(D13), D13201,

Surratt, J. D., et al. (2007), Evidence for organosulfates in secondary organic aerosol, *Environ. Sci. Technol.*, 41(2), 517-527.

Talbot, R. W., A. S. Vijgen, and R. C. Harriss (1992), Soluble Species in the Arctic Summer Troposphere - Acidic Gases, Aerosols, and Precipitation, *J. Geophys. Res.*, 97(D15), 16531-16543.

Taubman B.F., M., L.T., Piety, C.A., Doddridge, B.G., Stehr, J.W., Dickerson, R.R. (2004), Airborne characterization of the chemical, optical, and meteorological properties, and origins of a combined ozone-haze episode over the eastern United States., *J. Atmos. Sci.*, 61, 1781-1793.

Taubman, B. F. (2004), Airborne Characterization of Regional Aerosol Origins and Optical Properties, 242 pp, The University of Maryland, College Park.

Taubman, B. F., J. C. Hains, A. M. Thompson, L. T. Marufu, B. G. Doddridge, J. W. Stehr, C. A. Piety, and R. R. Dickerson (2006), Aircraft vertical profiles of trace gas and aerosol pollution over the mid-Atlantic United States: Statistics and meteorological cluster analysis, *Journal of Geophysical Research-Atmospheres*, 111(D10), doi:10.1029/2005JD006196.

Taubman, B. F., L. T. Marufu, C. A. Piety, B. G. Doddridge, J. W. Stehr, and R. R. Dickerson (2004a), Airborne characterization of the chemical, optical, and meteorological properties, and origins of a combined ozone-haze episode over the eastern United States, *Journal of the Atmospheric Sciences*, 61(14), 1781-1793.

Taubman, B. F., L. T. Marufu, B. L. Vant-Hull, C. A. Piety, B. G. Doddridge, R. R. Dickerson, and Z. Q. Li (2004b), Smoke over haze: Aircraft observations of chemical and optical properties and the effects on heating rates and stability, *Journal of Geophysical Research-Atmospheres*, 109(D2).

- Thompson, A. M., et al. (2007), Intercontinental Chemical Transport Experiment Ozonesonde Network Study (IONS) 2004: 1. Summertime upper troposphere/lower stratosphere ozone over northeastern North America, *Journal of Geophysical Research-Atmospheres*, 112(D12).
- Topping D., C., H., McFiggans, G., Burgess, R., Allan, J., Alfarra, M., Bower, K., Choularton, T., Decesari, S., Facchini, M. (2004), Aerosol chemical characteristics from sampling conducted on the Island of Jeju, Korea during ACE Asia, *Atmos. Environ.*, 38, 2111-2123.
- Torgeson, W. L. a. S. C. S. (1996), An aircraft impactor for determining the size of distributions of tropospheric aerosols, *J.Appl.Meteorol*, 5, 205-210.
- Tsai, Y. I., Hsieh, L-Y., Weng, T-H., Ma, Y-C., Kuo, S-C. (2008), A novel method for determination of low molecular weight dicarboxylic acids in background atmospheric aerosol using ion chromatograph, *Anal. Chim. Acta*, 626(1), 78-88.
- Turpin, B. J., P. Saxena, and E. Andrews (2000), Measuring and simulating particulate organics in the atmosphere: problems and prospects, *Atmos. Environ.*, 34(18), 2983-3013, doi:Doi 10.1016/S1352-2310(99)00501-4.
- Vant-Hull, B., Z. Q. Li, B. F. Taubman, R. Levy, L. Marufu, F. L. Chang, B. G. Doddridge, and R. R. Dickerson (2005), Smoke over haze: Comparative analysis of satellite, surface radiometer, and airborne in situ measurements of aerosol optical properties and radiative forcing over the eastern United States, *Journal of Geophysical Research-Atmospheres*, 110(D10).
- Wang, G. H., L. M. Huang, S. X. Gao, S. T. Gao, and L. S. Wang (2002), Characterization of water-soluble species of PM10 and PM2.5 aerosols in urban area in Nanjing, China, *Atmos. Environ.*, 36(8), 1299-1307, doi:Pii S1352-2310(01)00550-7 Doi 10.1016/S1352-2310(01)00550-7.
- Wilson, J. C., B. G. Lafleur, H. Hilbert, W. R. Seebaugh, J. Fox, D. W. Gesler, C. A. Brock, B. J. Huebert, and J. Mullen (2004), Function and performance of a low turbulence inlet for sampling supermicron particles from aircraft platforms, *Aerosol Sci. & Technol.*, 38(8), 790-802, doi:Doi 10.1080/027868290500841.
- Winterhalter, R., Van Dingenen, R., Larsen, B.R., Jensen, N.r., Hjorth, J. (2003), LC-MS analysis of aerosol particles from the oxidation of  $\alpha$ -pinene by ozone and OH-radicals, *Atmos. Chem. Phys.*, 3, 1-39.
- Wise, S., Sander, L., Schantz, M., Hays, M., Benner, B. (2000), Recertification of standard reference material (SRM) 1649, Urban Dust, for the determination of polycyclic aromatic hydrocarbons (PAHs), *Polycyclic Aromat. Compd.*, 13, 419-456.

Wozniak, A. S., J. E. Bauer, R. L. Sleighter, R. M. Dickhut, and P. G. Hatcher (2008), Technical Note: Molecular characterization of aerosol-derived water soluble organic carbon using ultrahigh resolution electrospray ionization Fourier transform ion cyclotron resonance mass spectrometry, *Atmos. Chem. Phys.*, 8(17), 5099-5111.

Yoon, J., W. von Hoyningen-Huene, A. A. Kokhanovsky, M. Vountas, and J. P. Burrows (2012), Trend analysis of aerosol optical thickness and Angstrom exponent derived from the global AERONET spectral observations, *Atmospheric measurement techniques*, 5, 1271-1299.

